6335

405056

SPACE POWER AND PROPULSION SECTION

405056

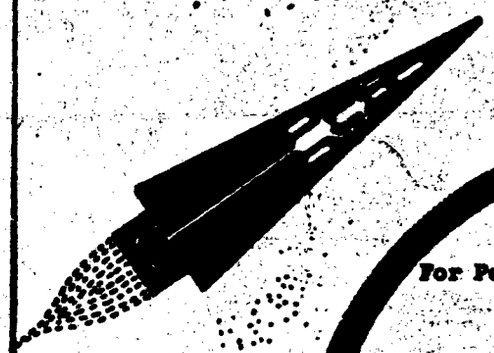

QUARTERLY REPORT #4

For Period Ending April 15, 1963

DYNAMIC SHAFT SEALS IN SPACE

Under Contract #AF33(657)8459

For

Aeronautical Systems Division

Wright Patterson Air Force Base, Ohio

MISSILE and SPACE DIVISION

GENERAL ELECTRIC

CINCINNATI, OHIO

SPACE POWER AND PROPULSION SECTION

QUARTERLY PROJECT STATUS REPORT

APRIL 15, 1963

DYNAMIC SHAFT SEALS IN SPACE

Under Contract #AF 33(657)-8459

RE-ENTRY SYSTEMS DEPARTMENT
MISSILE AND SPACE DIVISION
GENERAL ELECTRIC COMPANY
CINCINNATI 15, OHIO

SUMMARY

The Space Power and Propulsion Section of the General Electric Company has been under contract to the Aeronautical Systems Division, Wright Patterson Air Force Base, Ohio, since April 15, 1962 for the development of dynamic shaft seals for space applications. The objective of this program is to acquire the techniques for sealing high speed rotating shafts under the operating conditions of high temperature liquid metals and vapors, the near-vacuum environments of space, and to provide long seal life.

A. The contract specifies the following requirements:

1. The fluid to be sealed shall be potassium.
2. The seals shall be operative at fluid temperatures from the melting point of the fluid selected to 1400°F.
3. The pressure on the fluid side of the seal shall be 15 psi and the external pressure shall be 10^{-6} mm Hg.
4. The speed of the rotating shaft shall be a maximum of 36,000 rpm.
5. The seal, or seal combinations, shall be designed for 10,000 hours of maintenance-free life.
6. The working fluid, potassium, shall be used as the seal lubricant.
7. The seal, or seal combinations, shall be capable of maintaining zero leakage - in the technical sense - under all conditions of operation.
8. The seals shall be designed for a 1.0 inch diameter shaft.

9. The seals shall be capable of operating in a zero "g" environment.

B. The seal evaluation shall consist of:

1. Preliminary experiments with water.
2. 100-hour operational screening test with liquid metal.
3. Thermal-cycling test with liquid metal.
4. 3000-hour life test with liquid metal.

This report covers progress during the quarter ending April 15, 1962. The main events of this reporting period are:

1. First phase evaluation of screw seals using water and silicone fluids has been completed. The results of screw seal analysis and experiments have been summarized and are being published as a complete report in this progress report.

Other activities have been:

2. Experimental studies of inlet and outlet configurations of the rotating housing seal have been completed.
3. Evaluation of test data from the squeeze seal and the double disk seal continued.
4. Investigation of the sputter phenomena observed during the operation of rotating fluid ring seals continues. Various means to suppress the loss of liquid have been designed and tested. Considerable efforts have been expanded to obtain a physical understanding of the sputter phenomena. Additional work in design and testing continues.

5. Design of the seal test rig has been completed. All specifications have been prepared and the drawings have been released for quoting.

6. An IBM program has been set up for the analysis of the test rig's argon gas bearing. Gas bearing operation has been analytically investigated. Temperature distribution on gas bearing shaft and housing have been recalculated, using an existing in-house program.

7. Procurement of hardware for the liquid metal seal test facility continued.

TABLE OF CONTENTS

NOMENCLATURE

A	Area of wetted seal or constant in turbulent flow equation
B	Dimensionless pressure
C	Cavitation number or constant in turbulent flow equation
D	Shaft diameter
e	Land width along axis
E	Eccentricity correction factor
f	Friction factor
F	Force or Froude number
G	Zotov's sealing coefficient
h	Groove depth
k	Constant in turbulent flow equation
K	Function of β, $K = E\beta^3/[\gamma(1-\gamma)]$
K_1	Constant in equation 51
K_2	Constant in equation 51
K_{1_h}	Sealing coefficient constant based on groove depth
K_{2_h}	Sealing coefficient constant based on groove depth
K_1	Sealing coefficient constant based on clearance
K_2	Sealing coefficient constant based on clearance
ℓ	Leakage path length
L	Length of wetted portion of seal
n	Number of threads or power of Reynolds number
N	Shaft angular velocity
p	pressure
p_v	Vapor pressure
Δp	Pressure drop across seal
P	Power
Q	Volume flow

r	Radius
Re_h	Reynolds number $\quad Re_h = \frac{Uh}{\nu}$
Re	Reynolds number $\quad Re_\delta = \frac{U\delta}{\nu}$
t	Thread pitch, $t = \pi D \tan \phi$
t^*	t/n
u	Velocity along groove axis
U	Shaft surface velocity
V	Component of shaft surface velocity along groove
w	Width of channel
w'	Width of land
W	Weber number $\quad W = \frac{U^2 \delta \rho}{\sigma}$ or cooling water flow rate
x	Coordinate along shaft axis
y	Coordinate in radial direction
α	Aspect ratio $\alpha = h/w$ or coefficient of expansion
β	Ratio of clearance to groove depth, $\beta = \delta/h$
γ	$w/(w + w')$
δ	Radial clearance
μ	Absolute viscosity
ν	Kinematic viscosity
ρ	Fluid density
σ	Fluid surface tension
ϕ	Helix angle
τ	Shear stress
ξ	Coordinate along groove axis
η	Coordinate along perpendicular to groove axis

SUBSCRIPTS

c	couette flow value
cr	critical
d	drag
h	based on screw depth

j.b.	journal bearing
l	laminar
L	leakage
m	mean value
max	maximum
opt	optimum value
p	pressure flow value
sl	sleeve
ss	screw seal
t	turbulent

SUBSCRIPTS

'	fluctuating value
-	time averaged value

FIGURES

TABLES

Dynamic Seal Work Schedule

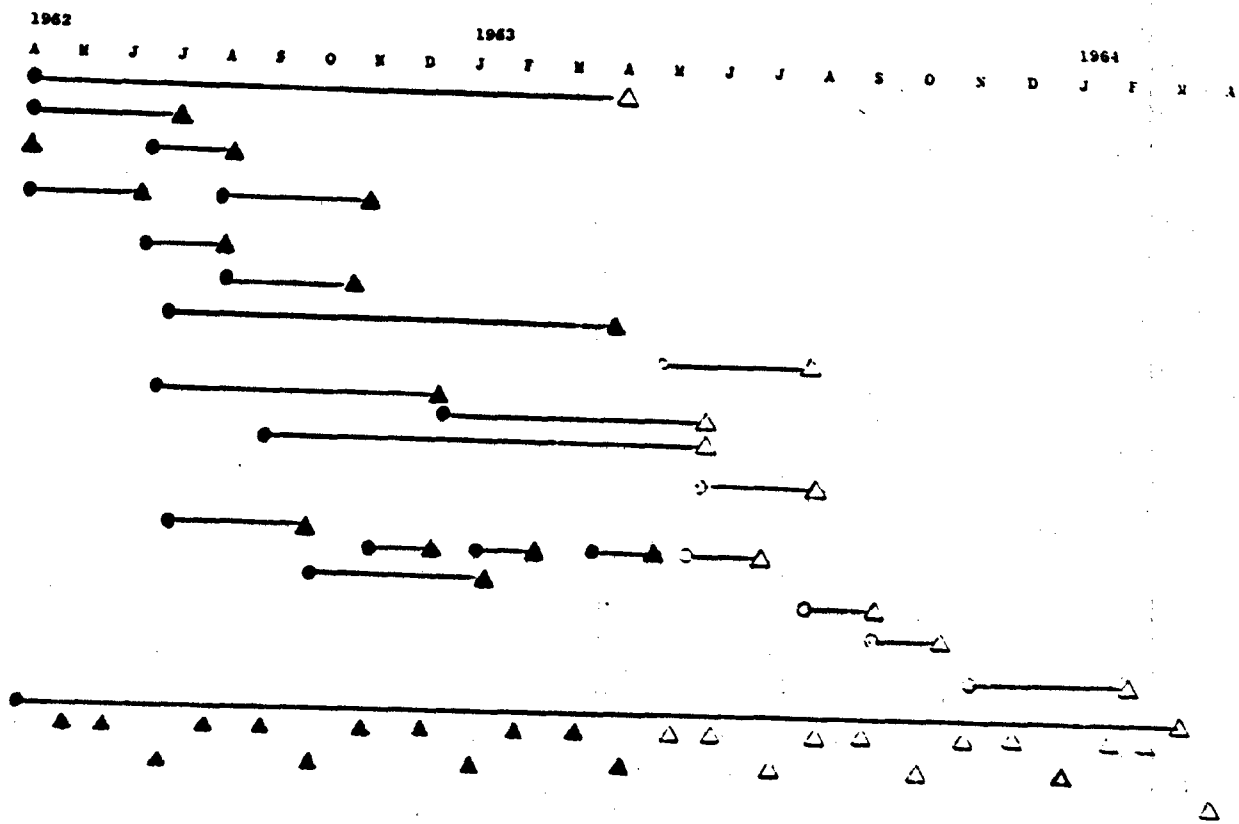

I. INTRODUCTION

One of the most basic engineering problems facing the machine designer is that of providing adequate dynamic seals for rotating shafts. The problem has become more acute in recent years for several reasons. There has been a trend toward increased speeds to reduce size and weight of machinery packages which, in turn, requires an extrapolation of existing seal performance; the consequence of a leaking seal has become more critical, for example, in nuclear applications; the need for maintenance-free operation has become greater, for example, in space vehicle applications.

Non-contacting seals are desirable since the separation of solid surfaces by a fluid film promises low wear rate and long life. Most such seals, however, require a small but finite leakage flow. In contrast, the screw seal offers both the possibility of contact-free surfaces and zero leakage. There has therefore been a resurgence of interest in the screw seal within the past few years. Results of analyses and experiments for laminar screw seal operation have recently appeared in the technical literature of England, Russia, Germany, Japan and Holland.

This report is part of contract AF-33(657)-8459. The prime objective of this contract is the development of leak-free dynamic seals for rotating shafts exposed to vacuum of space. The work reported here has been prepared by the Advanced Technology Laboratory, which was sub-contracted by the Space Power and Propulsion Section to evaluate screw seal performance using so-called "easy" fluids such as distilled water and silicones.

In the following, the various scatter analyses of laminar screw seal operation are evaluated in comparison with one another and with a simplified flow model; the basic equations are extended to cover turbulent flow; experiments are described in which the screw seal was tested in both laminar and turbulent regimes and results compared with the theoretical expectations; finally, the breakdown of sealing capability under certain conditions is examined and reasons postulated for its behavior.

II. THEORY OF SCREW SEAL OPERATION

Two fundamentally different patterns of flow, laminar and turbulent, exist for the flow of fluids through and around hydraulic devices such as pipes, valves, bearings, spheres, plates, etc. The observed velocity distributions, pressure drops, and friction losses are substantially different for the two patterns of flow, and as a result, two separate sets of laws are needed to predict the flow patterns for laminar and turbulent flows.

In early applications of the screw seal, the conditions of operation, low speed and high viscosity, were favorable for laminar flow. Laws were deduced for describing the laminar operation of screw seals, but experience with other fluid devices gives us no reason to assume that these same laws will predict the performance of screw seal operation in turbulent flow. The basic purpose of this study then is to answer two questions:

1. What are the laws of screw seal operation in turbulent flow?
2. What is the value of the critical Reynolds number for which transition from laminar to turbulent operation takes place?

In this section a simplified theory of laminar screw seal operation is derived. Following this an analysis is presented for predicting the sealing equation for turbulent flow, without land leakage.

A. Laminar Flow Case

1. Laminar Flow Sealing Equation

The screw seal is essentially a screw pump operating at zero flow. Therefore, the discussion which follows will concern the screw pump,

since the analysis includes the screw seal as a special case.

The screw pump consists of a threaded shaft rotating in a fixed cylinder or sleeve. The screw channel is constantly changing its position relative to sleeve and the advance of the fluid through the sleeve of the pump follows a helical path which is a mirror image of the helix on the screw. It has been shown, both analytically and experimentally in reference 7, the end results would be the same if the screw were held stationary and the sleeve rotated in a direction opposite to the actual rotation of the screw, since the relative velocities of the screw and the barrel are unaltered. But in this case, the liquid moves along the helical path defined by the screw channel. Because the channel walls are attached to the screw, it is far easier to visualize and discuss the case in which the sleeve rotates. For this reason, the screw is usually taken as the frame of reference.

Figure 1 shows a portion of a screw pump in which the rotational speed of the sleeve is U. The component V tends to drag the fluid in the direction of the channel. The T component induces a transverse flow. This transverse flow is neglected in the analysis.

If part of the screw channel is isolated as shown in Figure 2, the flow in the screw pump can be considered as a special case of couette flow in an arbitrarily shaped channel against a pressure gradient. This assumption is valid since in most applications the radius of the sleeve or rotor is usually much larger than the screw depth.

The differential equations governing this type of flow are the Navier Stokes equations. As shown in Reference 1, these equations, after simplification, appear as

$$\frac{dp}{d\xi} = \mu \frac{\partial^2 u}{\partial y^2} \qquad (1)$$

for incompressible laminar flow between two parallel plates.

A very simple solution of equation (1) is obtained for the case of steady flow between two parallel flat walls one of which is moving with a velocity V. (Figure 26). The boundary conditions are:

$$y = o;\ u = o$$

$$y = h;\ u = \frac{V}{1+\beta}$$

For the sake of brevity the parameters used to define the screw geometry are shortened to:

$$\alpha = \frac{h}{w}$$

$$\beta = \frac{\delta}{h}$$

$$y = \frac{w}{w'+w} = \frac{t^*-e}{t^*}$$

The solution is

$$u = \frac{y}{h} \frac{V}{(1+\beta)} - \frac{h^2}{2\mu} \frac{dp}{d\xi} \frac{y}{h} \left(1 - \frac{y}{h}\right) \qquad (2)$$

The flow through a channel of width w

$$Q = w \int_o^h u\,dy \qquad (3)$$

$$Q = \frac{Vwh}{2(1+\beta)} - \frac{bh^3}{12\mu} \frac{dp}{d\xi} \tag{4}$$

or

$$\frac{Q}{Vwh} = \frac{1}{2(1+\beta)} - \frac{1}{12} \left[\frac{h^2}{\mu V} \frac{dp}{d\xi} \right] \tag{5}$$

In addition to the flow given by equation (4), there is a leakage through the clearance space δ. This is analyzed by assuming the flow is isothermal, laminar pressure flow through a narrow slot or

$$Q_L = E \frac{\pi D \delta^3}{12\mu} \frac{dp}{d\ell} \tag{6}$$

where ℓ is distance along the leakage path.

The factor E is a correction for possible eccentricity of the screw in the sleeve. It varies from 1 for a perfectly centered screw to 2.5 for a screw with maximum eccentricity.

The total leakage flow can be obtained by calculating the leakage across a length of thread equal to one turn of the helix. If it is assumed that the fluid pressure along the length of the clearance varies linearly, then the pressure drop between adjacent grooves is

$$\Delta p_1 = \frac{\Delta p}{(L/t^*)} \tag{7}$$

The leakage path is e. The leakage flow becomes

$$Q_h = \frac{E\pi D\delta^3}{12\mu e} \frac{\Delta p}{(L/t^*)} \tag{8}$$

Reference to Figure 1 reveals

$$V = U \cos \phi = \pi D N \cos \phi \tag{9}$$

$$d\xi = dx / \sin \phi \tag{10}$$

$$t = nt^* = \pi D \tan \phi \tag{11}$$

$$w = (t^* - e) \cos \phi \tag{12}$$

Substitution of the above into equation 8 gives

$$Q_h = \frac{E \pi D t \delta^3 \Delta p}{12 \mu n e L} \tag{13}$$

or

$$Q_L = \frac{E \pi^2 D^2 \delta^3 \tan \phi}{12 \, n e w h^3 \sin} \left(\frac{h^2}{\mu V} \frac{dp}{d\xi} \right) \tag{14}$$

or

$$\frac{Q_L}{Vwh} = E \Gamma \left(\frac{h^2}{\mu V} \frac{dp}{d\xi} \right) \tag{15}$$

where

$$\Gamma = \frac{\pi^2 D^2 \delta^3 \tan \phi}{12 \, n e w h^3 \sin \phi} \tag{16}$$

The first term of equation (4) is the drag flow. The second term represents the backward flow along the channel due to the negative pressure gradient. The total flow can be viewed as a drag flow minus a pressure flow and a leakage flow or:

$$Q = Q_d - Q_p - Q_L \tag{17}$$

By combining equations (5) and (15), the total flow in dimensionless terms becomes

$$\frac{Q}{Vwh} = \frac{1}{2(1+\beta)} + \frac{B}{12} + E\Gamma B \tag{18}$$

where

$$B = -\frac{h^2}{\mu V}\frac{dp}{d\xi}$$

If Q/(Vwh) is plotted versus B a straight line results with a negative slope as shown in Figure 3. Data for a given geometry of screw pump should all fall on one straight line independent of speed when plotted in the above dimensionless form.

For seal operation, the shut off pressure coefficient is of interest. For Q=0, this becomes for the theoretical case,

$$\frac{h^2}{\mu V}\frac{dp}{d\xi} = \frac{1}{2(1+\beta)(E\Gamma + 1/12)} \tag{19}$$

Equation 19 is written with reference to a coordinate system along the groove. It is more convenient in practice to use a coordinate system along the axis of the screw.

The drag flow term is

$$Q_d = \frac{Vwh}{2(1+\beta)} \tag{20}$$

or substituting equations 9 and 12

$$Q_d = \frac{nU(t^* - e)\cos^2\phi h}{2(1+\beta)} \tag{21}$$

where the factor n is added to account for multiple thread screws. The pressure flow term

$$Q_p = \frac{wh^3}{12\mu} \frac{dp}{d\xi} \tag{22}$$

becomes after substituting equations 10 and 12

$$Q_p = \frac{nh^3(t^*-e)\sin\phi\cos\phi}{12\mu} \frac{\Delta p}{L} \tag{23}$$

The total discharge delivered by the screw is then

$$Q = Q_d - Q_p - Q_h$$

$$Q = \frac{nhU(t^*-e)\cos^2\phi}{2} - \frac{nh^3(t^*-e)\sin\phi\cos\Delta p}{12\mu L} - \frac{E\pi Dt\delta^3\Delta p}{12\mu neL} \tag{24}$$

For operation as a seal we desire Q = 0, or

$$\frac{h^2\Delta_p}{\mu UL} = \frac{6n(t^*-e)\cos^2\phi(1+\beta)^{-1}}{\left[n(t^*-e)\sin\phi\cos\phi + \frac{E\pi Dt\beta^3}{ne}\right]} \tag{25}$$

or

$$\frac{h^2\Delta p}{\mu UL} = \frac{6(1+\beta)^{-1}}{\tan\phi\left[1 + \frac{Et^2\beta^3}{n^2(t^*-e)e\sin^2\phi}\right]} \tag{26}$$

or

$$\frac{h^2}{\mu U}\frac{\Delta p}{L} = \frac{6(1+\beta)^{-1}}{\tan\phi\left[1 + \frac{E\beta^3}{\gamma(1-\gamma)\sin^2\phi}\right]} \tag{27}$$

The dimensionless coefficient $\frac{h^2\Delta p}{\mu UL}$ we will designate as the sealing coefficient ψ_h. It is seen in equation 27 to be a function of geometry alone.

It is also of interest to consider another coefficient denoted ψ_δ which is defined as

$$\psi_\delta = \frac{\delta^2\Delta p}{\mu UL} = \frac{6\beta^2(1+\beta)^{-1}}{\tan\phi\left(1+\frac{E\beta^3}{\gamma(1-\gamma)\sin^2\phi}\right)} = K_{1\delta} \tag{28}$$

The coefficient $K_{1\delta}$ is also a function of geometry alone. The relation between ψ_h and ψ_δ is simply

$$\psi_\delta = \beta^2\psi_h \tag{29}$$

With no leakage ($Q_L = 0$) equations 27 and 28 become

$$\psi_h = \frac{6}{\tan\phi} \tag{30}$$

and

$$\psi_\delta = \frac{6\beta^2}{\tan\phi} \tag{31}$$

2. Effect of Eccentricity on Sealing Capability

Equation 19 reveals that the leakage flow over the screw lands is strongly influenced by the position of the shaft in the sleeve. The sealing coefficient ψ_δ, is a function of eccentricity due to the factor E which varies from a value of 1.0 to 2.5 as the eccentricity varies. The

geometrical factor Γ also varies since δ/h changes along the circumstance, but this does not appreciably affect the sealing coefficient.

If we ignore the circumferential variation of δ/h, we can calculate a maximum and minimum value of ψ_δ corresponding to minimum and maximum eccentricity, respectively. This is shown in Figure 4. The cross hatched area between the extreme values of the sealing coefficient define the laminar working characteristic of the seal. The large variation possible explains in part the differences in measured sealing coefficients shown in Table II.

Since it is very difficult to control eccentricity in a close clearance seal, it is best practice to design the seal for maximum eccentricity.

3. Laminar Flow Power Loss Equation

The simplest method for estimating the power loss in a screw seal is to treat the loss as frictional dissipation by viscous shear in an annulus which has a clearance δ over part of its area and a clearance h for the remaining part. The force exerted on the shaft is simply

$$F = \frac{\mu U}{\delta} A_l + \frac{\mu U}{(\delta+h)} A_g \qquad (32)$$

and the power is

$$P = FxU$$

By observing that

$$\gamma = \frac{A_g}{A_l + A_g}$$

$$\text{and } \beta = \frac{\delta}{h},\ A = A_l + A_g$$

the expression for power becomes

$$P = \frac{\mu U^2 A}{6600\,\delta}\left[\frac{\gamma\beta}{\beta+1} + (1-\gamma)\right] \qquad (33)$$

Substituting in equation (33) from equation (28)

$$\frac{\mu UL}{\delta} = \frac{\Delta p \delta}{K_{1\delta}}$$

and rearranging equation (33)

$$\frac{P}{(\pi 6600)\ U\Delta p} = \frac{\delta D}{K_{1_\delta}} \left[\frac{\gamma \beta}{\beta + 1} + (1 - \gamma)\right] \tag{34}$$

We see that the right hand side is a function of geometry alone. Hence, in laminar flow for a given speed and required sealing pressure, power is independent of fluid viscosity.

In bearing practice, it is often convenient to present power loss data in terms of a friction factor f, defined as

$$f = \frac{F/A}{\frac{\rho U^2}{2g}} \tag{35}$$

where F is given by equation 32. Equation 35 can be rewritten as

$$f = \frac{2}{Re_h} \left[\frac{1 - \gamma}{\beta} + \frac{\gamma}{\beta + 1}\right] \tag{36}$$

where

$$Re_h = \frac{Vh}{\nu}$$

The friction factor can also be written in terms of a Reynolds number based on the clearance rather than the groove depth.

$$f = \frac{2}{Re_\delta} \left[\frac{\gamma \beta}{\beta + 1} + (1 + \gamma)\right] \tag{37}$$

where

$$Re_\delta = \frac{U\delta}{\nu}$$

The previous analysis of bearing loss has included only Couette or drag flow. In addition there is a Poissuelle or pressure flow within the groove which also contributes to the power loss. Boon and Tal[5] performed an analysis in which this additional factor was considered. They found that the energy dissipated in laminar operation of a screw seal is given by

$$P = \frac{\mu U^2 A}{\delta} \left[1 - \gamma + \frac{\gamma}{v} + \frac{3t^3 \gamma (1-\gamma)(v-1)^2 (1-\gamma+v^3)}{(1+t^2) v^3 + t^2 \gamma (1-\gamma)(v^3-1)^2} \right] \quad (38)$$

where

$$t = \tan \phi \text{ and } \quad v = 1 + \frac{1}{\beta} = \frac{\delta + h}{\delta}$$

In the above expression $(1 - \gamma + \frac{\gamma}{v})$ is the power loss due to the Couette portion of the flow, the remainder being the loss contributed by the Poisseuille portion of the flow. If the geometrical parameters γ, ϕ, and v are so chosen that the Poisseuille flow term is zero, equation reduces to equation 33.

It is of interest to determine the relative order of magnitude of the Couette and Poisseuille flow terms in the power loss equation. For values of the geometrical parameters of

$$t = .2586$$
$$\gamma = .63$$
$$v = 3.86$$

the expression for the power loss is

$$P = \frac{\mu U^2 A}{\delta} (.533 + .014)$$

where the terms in the bracket are values of the drag and pressure terms respectively. According to equation 38 the power loss due to the pressure flow is about 1-1/2% of the drag flow power loss for the chosen geometry.

Measured powers by Hughes[3] and Boon and Tal[5] were greater than that calculated from either equation 33 or 38.

4. Optimization for Maximum Sealing Capability

(a) Optimization of Simplified Sealing Equation

The sealing coefficient ψ_h can be maximized by taking the partial derivatives of ψ_h with respect to β, γ, and ϕ, and setting these partial derivatives

equal to zero. A system of 3 equations is obtained which yield values of β, γ, and ϕ for which ψ_h is a maximum

$$\frac{\partial \psi h}{\partial \beta} = 0 = \frac{\delta}{h} \tag{39a}$$

$$\frac{\partial \psi h}{\partial \gamma} = 0 = 2\gamma - 1 \tag{39b}$$

$$\frac{\partial \psi_h}{\partial \phi} = 0 = K - \sin^2 \phi \ (1 + 2K) \tag{39c}$$

This leads to the conclusion that the sealing coefficient $\psi_h \rightarrow \infty$ for

$$\phi = 0$$
$$\beta = 0$$
$$\gamma = .5$$

The above conditions in effect say that the clearance should be zero and that for zero clearance the groove path should be made as long as possible; (i.e. $\phi = 0$).

In any practical seal, however, there is a finite clearance, and in order to optimize the seal geometry for a given finite clearance it is necessary to consider the sealing coefficient ψ_δ.

The coefficient ψ_δ is given by

$$\psi_\delta = \frac{6(1+\beta)^{-1}\beta^2}{\tan\phi \left[1 + \frac{K}{\sin^2\phi}\right]} \tag{28}$$

where $K = \frac{E\beta^3}{\gamma(1-\gamma)}$

Again the partial derivatives of equation 28 can be obtained and set equal to zero. This leads to

$$\frac{\partial \psi \delta}{\partial \phi} = 0 = K - \sin^2 \phi \ (1 + 2K) \tag{40a}$$

$$\frac{\partial \psi_\delta}{\partial \gamma} = 0 = 2\gamma - 1 \qquad (40b)$$

$$\frac{\partial \psi_\delta}{\partial \beta} = = \frac{8\beta^4}{\sin^2 \phi} + \frac{4\beta^3}{\sin^2 \phi} - \beta - 2 \qquad (40c)$$

The simultaneous solution of the above equations gives

$$\phi = 21.6^\circ$$

$$\beta = .36$$

$$\gamma = .5$$

The value of ψ_δ for these conditions is

$$\psi_\delta = .61$$

Optimization of the sealing coefficient based on the clearance gives the added information that there is an optimum groove depth for a given clearance δ. For tight clearances, however, the optimum ratio of clearance to groove depth leads to very shallow grooves. For a 1/2 mil clearance, the optimum groove depth is only 1-1/2 mils. Such a groove is very difficult to machine. In order to estimate the sealing coefficient at other than optimum conditions, the following method can be used.

From equation 40 the condition, $\gamma = .5$, is an optimum condition independent of the value of ϕ and β. Substituting for γ in equation and letting $K_o = 4E\beta^3$ for $\gamma = .5$, we obtain

$$\sin^2 \phi_o = \frac{K_o}{2K_o + 1} \qquad (30a)$$

or

$$\phi_o = \sin^{-1}\left[\frac{K_o}{2K_o + 1}\right] \qquad (30b)$$

Then

$$\psi_{\delta_o} = \frac{6(1+\beta)^{-1}\ \beta^2}{\tan\phi\left[1 + \dfrac{K_o}{\sin^2\phi}\right]} \tag{31}$$

and since

$$\sin^2\phi + \cos^2\phi = 1 \tag{32}$$

$$\cos^2\phi = \frac{K_o + 1}{2K_o + 1}$$

we can write

$$\psi_{\delta_o} = \frac{6\,(1+\beta)^{-1}\beta^2}{2\left[K_o\,(1+K_o)\right]^{1/2}}$$

or

$$\psi_{\delta_o} = \frac{3\,(1+\beta)^{-1}\beta^2}{2\left[E\beta^3\,(1+4E\beta^3)\right]^{1/2}}$$

This is plotted in Figure 10.

For any value of β with $\gamma = .5$, an optimum value of ψ_{δ_o} can be read from Figure 10. The helix angle required to attain this value of ψ_δ is calculated from equation 30b or read from Figure 11.

In Figure 10, it is seen that eccentricity markedly reduces the sealing coefficient but hardly changes the value of ψ_δ where the sealing curve reaches a maximum. In Table II, the values of required for maximum sealing coefficient as reported in several different references range from .2 to .38. Figure 10 indicates that in this range of β, the sealing coefficient changes little and that any of these "optima" would give good sealing capability.

For values of β below .2, however, the curve drops off sharply, and for a given clearance, a considerable penalty in reduced sealing capability is paid for by using small values of β.

Figure 11 provides the value of helix angle required to attain the sealing coefficients given in Figure 10 as a function of β. The effect of eccentricity is to increase the helix angle required to obtain maximum sealing for any given β.

The previous analysis was based on a simplified model of the screw seal in that the edge effects of the channel were neglected. The analysis is therefore limited to channels which are much wider than they are deep or h/w, the aspect ratio, is small.

If end effects are considered, more complicated expressions for the sealing equation are found with different geometrical optima. Several different investigators have included aspect ratio and other effects and maximized the laminar sealing coefficient. The sealing coefficient is then a function of four variables.

$$\psi_\delta = f(\alpha, \beta, \gamma, \emptyset)$$

Optimizing this equation leads to a set of four equations.
The simultaneous solution of this set of equations gives two real solutions which correspond to the maximum and minimum values of the function ψ_δ. All the investigators who have optimized screw seal geometry have done essentially the above, but due to different starting assumptions and slightly different techniques they did not all arrive at exactly the same result. The various optimizations are discussed below.

b. Optimization of Zotov

In Reference 6, Zotov presents the sealing effect of the screw seal in terms of:

$$\frac{\Delta p}{\mu N} = \frac{6\pi(h/L)}{(\delta/D)^2 G} \qquad (41a)$$

on in different nomenclature

$$\psi_\delta = \frac{\delta^2}{\mu U}\frac{dp}{dx} = \frac{6}{G} = K_{1\delta} \qquad (41b)$$

The quantity G depends on the four geometrical parameters α, β, γ, and ϕ. Zotov found analytically that G was a minimum for the following values of the above geometrical parameters

$\alpha = .08$ $\qquad$ $\beta = .32$

$\gamma = .63$ $\qquad$ $\phi = 14.5^\circ$

In the above case

$$\left(\frac{1}{G}\right)_{max} = .116$$

$$\left(K_{1_\delta}\right)_{max} = .116 \times 6 = .696$$

His measured values were less than this, however, and ranged from .5 down to .37. He attributed the lower measured sealing coefficients to imperfect alignment.

c. Optimization of Asanuma

Asanuma in Reference 7 describes the results of extensive tests of various thread forms. The sealing equation employed by Asanuma can be expressed as

$$\psi_\delta = \frac{\delta^2}{\mu U}\frac{dp}{dx} = 6S = K_{1_\delta} \qquad (42)$$

The quantity S, he terms the sealing characteristic factor which like Zotov's G is a function of screw geometry. In order to obtain maximum sealing performance, Asanuma found that the pertinent geometrical parameters should have the following values:

$\alpha = .05 \sim .2$ $\qquad$ $\beta = \delta/h = .2$

$\gamma = .5$ $\qquad$ $\phi = 10^\circ \sim 11^\circ$

The above optimized parameters are close to what Zotov found. For rectangular threads of optimum geometry, Asaruma found that

$$\left(K_{1_\delta}\right)_{max} = .45 \text{ (theoretical value)}$$

For a screw of optimum geometry, he actually measured values of K_{1_δ} ranging from .36 to .33.

d. Optimization of Boon and Tal

In Reference 5, Boon and Tal presented a comprehensive theoretical study of screw seal operation. Their sealing equation can also be expressed in the form of equation 41b. Their maximum theoretical sealing coefficient K_{1_δ} was $K_{1_\delta} = .55$ and occurred at

$$\beta = .422 \qquad \gamma = .5$$
$$\phi = 15.8^{o}$$

Boon and Tal performed some measurements but unfortunately did not publish their results. They merely state that their measured values were below the theoretical value.

e. Optimization of Frössel

Frössel in Reference 8 also performed considerable research on screw seals. Frössel's sealing equation can also be expressed in the form of equation 41b. Like the other investigators, Frössel found that K_{1_δ} was dependent on geometry alone. The data presented by Frössel modified to match the nomenclature used here is given on the following page:

TABLE I

Sealing Coefficient K_{1_δ}

(Adapted from Reference 8)

	Helix Angle							
	0	5	10	12	15	20	25	0
Metric Thread t = 1mm, h = 0.7 mm h/δ = 14	0	.0175	.127	.138	.123	.0815	.056	0
Metric Thread t = .5mm, h = .3mm h/δ = 6	0	.0835	.139	.167	.195	.195	.167	0

Frössel's data reaches a maximum at about $\phi = 15^{o}$. His data is limited however, in that he did not locate an optimum for δ/h or h/w.

f. Optimization of Whipple

In connection with the development of thrust bearings pressurized by the viscous pumping action of grooves, Whipple at. al.[9-13] developed an equation for the pressure developed similar to equation 41b. They found that in order to maximize ψ_δ, the conditions required were

$$K_{1_\delta} = .55 \quad \gamma = .5 \quad \phi = 13.8^{o} \quad \beta = .38$$

The above conditions are similar to those found by the previously discussed investigators.

Whipple did not perform any experiments to check his theory, but D. P. Hughes in Reference 3 designed a screw seal using Whipple's methods. Hughes actually measured sealing coefficients 14% below the theoretical value of $K_{1\delta}$ or $\left(K_{1_\delta}\right)_{meas} = .49$.

g. Comparisons of the Various Optimizations

Table II is a summary of the various screw seal optimizations for

SUMMARY OF OPTIMUM GEOMETRY FOR LAMINAR SCREW SEAL OPERATION

	$(K_1)_{theor}$	$(K_1)_{meas}$	ϕ	δ/h	$\gamma = \frac{w}{w' + w}$	h/w	Test Regimes
1. Zotov - Reference 6	.69	.37-.69	14.5	.32	.63	.08	Lam. and Turb. $Re_{h_{cr}} = 1300$
2. Asanuma - Reference 7	.45	.33-.36	10°~11°	.2	.5	.05~.2	Lam.
3. Boon and Tal - Ref. 5	.55	-----	15.8°	.38	.5	----	Lam.
4. Frössel - Ref. 8	----	.122*	12°	.007*	------	----	Lam.
		.18*	15°~20°	.16*	------	----	Lam.
5. Whipple et. al. Ref. 9-13	.55	-----	13.8°	.38	.5	----	Lam.
6. Hughes, Ref. 3	.55	.47	13.8	.38	.5	.055	Lam.
7. Simplified Model	.61	-----	21.6	.36	.5	-----	Lam.

*Not optimum value

TABLE II

laminar operation. The optimum geometries found by the various investigators for maximum sealing capability are similar, but not exactly the same. The table does, however, give a range of values of the geometrical parameters for which reasonable sealing coefficients can be expected. The measured sealing coefficients, where available, were usually lower than theoretical values and exhibited a considerable amount of scatter. This was in general attributed to two causes by the various authors.

1. The difficulty in knowing the amount of shaft eccentricity, the effect of which was discussed previously.
2. The fact that recorded sealing fluid temperatures are generally lower than the actual fluid film temperature. The sealing pressure varies directly as the viscosity, and most liquids have a fairly large viscosity change with temperature. Thus one of the most difficult factors to measure and control in seal operation is the fluid viscosity.

The simplified model analysis gives results which are close to those given by the more complicated analyses. The optimizations which include aspect ratio effects arrive at a low aspect ratio for optimum sealing. Since this is a basic assumption of the simplified approach, it is not unusual that the two approaches should give comparable results. The largest discrepancy between the simplified analysis and the other optimizations in Table II is in the helix angle required for maximum sealing. The simplified approach gives angles from 7-10^{o} larger than the other methods.

5. Optimization for Minimum Power Dissipation

In practice it sometimes is more desirable to optimize for minimum power dissipation rather than maximum sealing capability. Equation 38 from Reference 5 expresses the power loss. Boon and Tal[5] attempted to find the values of the shape parameters which minimize the power loss by taking the partial derivatives of P with respect μL, $1 + 1/\beta$, $\tan \phi$ and γ. They found that P approached a minimum as $\gamma \to 1$ and $(1 + 1/\beta) \to \infty$. The asymptotic limiting value of P was found to be

$$P_{min} = \frac{\pi}{2} \Delta p \omega D^2 \delta \qquad (43a)$$

For the combination of shape parameters for which Δp is a maximum

$$P = 1.3581 P_{min} \qquad (43b)$$

which shows that the optimum geometry for maximum sealing does not give minimum power consumption.

Even though the geometry required for minimum power loss is not practical, the power can be kept low by appropriate choice of shape parameters. Table III was prepared by Boon and Tal to aid in this selection of shape parameters. If a constant value of δ/h is selected, the table gives the value of γ, ϕ, and K_{1_δ} for minimum power dissipation. The power dissipated for any of these conditions can be calculated from equation 38.

6. Sealing Coefficients with Other Thread Shapes

Frössel[8] and Asanuma[7] performed experiments with thread shapes other than rectangular ones. Frössel tested with rectangular, trapezoidal and triangular grooves. His results indicated that the triangular

TABLE III

FORM PARAMETERS FOR MINIMUM POWER LOSS
ADAPTED FROM BOON & TAL, REFERENCE 5

$1 + 1/\beta$	β	γ	$\tan \phi$	ϕ	K_{1_δ}
2	1	.59	.564	$29^{o}26'$	.525
3	.5	.65	.318	$17^{o}38'$	.499
4	.33	.70	.211	$11^{o}55'$	.482
5	.25	.74	.155	$8^{o}50'$	.445
6	.2	.77	.122	$6^{o}57'$	.408
7	.167	.79	.099	$5^{o}40'$	.377
8	.143	.81	.084	$4^{o}27'$	.346
9	.125	.83	.073	$4^{o}9'$	.317
10	.1	.84	.064	$3^{o}38'$	.398

groove seal produced higher sealing coefficients than the rectangular or trapezoidal varieties.

Asanuma's results showed that the triangular shape produced higher sealing pressures than either semi-circular or rectangular ones. Thus the rectangular groove does not appear to be the optimum shape. However, for this study, a rectangular groove was selected since more information is available about this geometry and the turbulent flow equations are easier to apply to a rectangular geometry.

B. Turbulent Flow Case

In the previous section the laminar theory of screw seal operation was reviewed. As screw seals are operated at higher Reynolds numbers, the laminar motion develops into a turbulent one. The analysis must then be extended to cover turbulent flow.

In Reference 14, a study is made of the turbulent hydrodynamic motion in a lubricant layer. The results of this study have direct application to the screw seal or pump operated in the turbulent regime.

In order to describe turbulent flow in mathematical terms, it is convenient to separate it into a mean motion, $\bar{u}$, and a fluctuating motion u'.

The velocity and pressure components then become

$$u = \bar{u} + u' \qquad v = \bar{v} + v' \qquad w = \bar{w} + w' \qquad p = \bar{p} + p'$$

If the above are substituted in the Navier Stokes equations and a time average made, the following equations result for the physical situation of Figure 2b.

$$\frac{d\bar{p}}{\partial \xi} = \mu \frac{\partial^2 \bar{u}}{\partial y^2} + \frac{\partial}{\partial y} \left(-\overline{\rho u' v'}\right) \tag{44}$$

$$\frac{\partial \bar{p}}{\partial y} = \frac{\partial}{\partial y} \left(-\rho \overline{v'^2}\right)$$

Upon comparison with equation (1), it is noticed that equations 44 contain an additional term, the so-called turbulent stress $\overline{u' v'}$. Further, there is a variation in pressure across the lubricant layer.

In order to integrate equation 44, it is necessary to know the turbulent stress $\overline{u'v'}$ beforehand. Constantinescu does this in Reference 14 by introducing Prandtl's mixing length, l, where

$$-\rho \overline{u'v'} = \rho l^2 \frac{\partial \bar{u}}{\partial y} \left| \frac{\partial \bar{u}}{\partial y} \right| \tag{45}$$

The mixing length l may be defined as

$$l = k y \qquad 0 \leq y \leq \frac{h}{2}$$

$$l = k(h-y) \qquad \frac{h}{2} \leq y \leq h$$

where k is an empirical factor that must be determined by experiment. This has been done by measuring the fully developed turbulent velocity profile in a pipe. Measurements of this type yield values of $k = .04$.

After substituting equation 45 in equation 44 and simplifying, he arrives at

$$A\bar{y}^2 \frac{\partial \bar{u}}{\partial \bar{y}} \frac{\partial \bar{u}}{\partial \bar{y}} + \frac{\partial \bar{u}}{\partial \bar{y}} + B\bar{y} - C = 0 \qquad (46)$$

where

$$A = k^2 Re \qquad B = -\frac{h^2}{\mu V} \frac{\partial p}{\partial \xi}$$

$$\bar{y} = y/h \qquad Re = \frac{\rho V h}{\mu}$$

Solution of equation 46 yields the velocity profile for various pressure coefficients and Reynolds numbers. It is instructive to compare the velocity profiles predicted by the laminar and turbulent theories. These are shown in Figure 5. The differences are very great. For the same pressure (B parameter) more flow will be delivered in turbulent flow than in laminar.

If the couette flow velocity profile is plotted for various Reynolds numbers, Figure 6 results. The Reynolds number has substantial influence upon the velocity profile; when $Re \to 0$ the velocity profile tends towards the laminar one and when $Re \to \infty$ the velocity distribution tends to become constant with respect to y. It is more important to note that the area under the velocity distribution curve is independent of Reynolds number. This means that the drag flow term, $Q_d = \frac{Vhw}{2}$, in equation 4 is also independent of Reynolds number.

Now if velocity is plotted for a constant value of pressure coefficient $B = -20$, the influence of Reynolds number is clearly seen. This is shown in Figure 7.

The mean velocity in the screw channel can be thought of as consisting of two parts.

$$u_m = u_{m_c} + u_{m_p} \tag{47}$$

where u_{m_c} = mean couette velocity

u_{m_p} = mean pressure velocity

Figure 6 shows that u_{m_c} is independent of Reynolds number. The mean velocity is then

$$u_m = \frac{V}{2} + u_{m_p} \tag{48}$$

For laminar flow, neglecting internal seal leakage, this becomes

$$\frac{u_m}{V} = \frac{1}{2} + \frac{B}{12} \tag{49}$$

For turbulent flow, u_{m_p} is a function of Reynolds number. Mean velocity for various Reynolds numbers and various B parameters were calculated in Reference 14. This is shown in Figure 6 for the pertinent range of values. The pressure coefficient is almost linear for all Reynolds numbers. This can be expressed analytically as

$$B = k'\left(\frac{u_{m_p}}{V}\right)^n \tag{50}$$

where $k' = 12$ for $Re = 0$ and $k' = \infty$ for $Re \rightarrow \infty$.

This variation can be expressed as

$$k' = K_1 + K_2\, Re^n$$
$$= 12 + 0.14\, Re^{0.725} \tag{51}$$

Substituting for u_{m_p} in equation 48, we obtain

$$\frac{Q}{Vwh} = \frac{u_m}{V} = \frac{1}{2} + \frac{B}{[K_1 + K_2\, Re^{0.725}]} \tag{52}$$

$$\frac{Q}{Vwh} = \frac{u_m}{V} = \frac{1}{2} + \frac{B}{[\,12 + 0.14\,Re^{0.725}\,]} \qquad (53)$$

For Reynolds number = 0, this reduces to the laminar case with no leakage as shown in Equation 30. The dimensionless pressure coefficient versus the dimensionless flow coefficient is plotted in Figure 9.

It is interesting to compare the theoretical screw pump characteristics with a typical measured characteristic of Frössel[15] in Figure 10. If the flow in the pump were laminar and isothermal all of the data points would lie on one straight line when the dimensionless pressure coefficient was plotted against dimensionless flow coefficient. This held true at low rotational speeds, but at higher speeds a fan shaped family of characteristics was obtained. Since the pumps tested by Frössel were not cooled, the temperature of the oil increased as it passed through the pump with an attendant decrease in viscosity and increase in Reynolds Number. The effect is a minimum at high flows since the temperature rise is smaller due to the higher mass rate. At low flows and high speeds the temperature rise is greater giving a larger negative slope to the characteristic. For this reason, along any speed line, the slope of the characteristic becomes steeper as the pump operating point moves to lower flows. The dip on the characteristic lines at high rotational speeds is most likely a result of the flow changing from laminar to turbulent conditions. The above theoretical analysis predicts the same shape of characteristic as was experimentally observed by Frössel[15].

When the screw pump is adapted for use as a seal, the important point on the characteristic is the shut off pressure, i.e., the value of pressure

coefficient at zero flow.

From equation 53, the shut off value is given by

$$\frac{dp}{d\xi}\ \frac{h^2}{uV} = \frac{1}{2}\ \left[12 + 0.14\ Re^{0.725}\right] \tag{54}$$

The constants in the above equation are the theoretical values. It was shown for the laminar case that the experimentally determined constant was considerably lower than the theoretical maximum. A similar discrepancy between the theoretical and actual would be expected in the turbulent case. Thus we would expect an expression for the turbulent sealing pressure to be of the form

$$\Delta p = \left[K_{1_h} + K_{2_h} Re^{n}\right] \left(\frac{\mu UL}{h^2}\right) \tag{55}$$

where the constants in the equation will be a function of the screw geometry. or

$$\psi_h = \frac{\Delta p h^2}{\mu UL} = K_{1_h} + K_{2_h} Re_h^{\,n} \tag{56}$$

By multiplying the sealing equation by $\left(\frac{\delta}{h}\right)^2$, we can write it as

$$\psi_\delta = \frac{\Delta p \delta^2}{\mu UL} = K_{1_\delta} + K_{2_\delta} Re_h^{\,n} \tag{57}$$

where

$$K_{1_\delta} = K_{1_h} \left(\frac{\delta}{h}\right)^2 \tag{58a}$$

$$K_{2_\delta} = K_{2_h} \left(\frac{\delta}{h}\right)^2 \tag{58b}$$

The primed constants still remain a function of geometry alone. The approach here has been to demonstrate the form of the turbulent sealing equation, and then to evaluate the constants in the equation experimentally.

III. TEST APPARATUS

A. Floating Sleeve Arrangement

A test apparatus was designed and built in order to supply data necessary to determine the constants in the turbulent sealing equation and to verify its form. The first configuration of the test apparatus employed a free floating sleeve. Boon (5) had suggested that the screw seal had self-centering tendency. Wigg and Battelle (16) were issued a patent incorporating this self-aligning feature of screw seals. One of the important concepts proposed in their patent is that the seal sleeve surrounding the grooved shaft is free to move and because of this feature the sleeve is self aligning.

If the test sleeve could be made to be self-centering, the scatter in the test data due to eccentricity effects reported by earlier experimenters could be reduced. For this reason the test apparatus was designed with a free floating sleeve.

Figure 13 shows a layout drawing of the screw seal test rig with floating sleeve. The drive motor is a 3 h.p., 2500 rpm D.C. motor with "Thymatrol" speed control. An intermediate speed spindle is belt driven by the motor. The intermediate speed spindle in turn drives a high speed spindle.

The intermediate speed spindle is a standard B-251C Whitnon grease lubricated spindle rated at 15,000 rpm. The high speed spindle is an oil mist lubricated Whitnon B-257D spindle which has been modified for operation to 35,000 rpm.

The high speed spindle is equipped with an internal taper at one end. Special tapered quills on which the test screw threads are cut fit into the internal taper of the high speed spindle. This arrangement permits easy interchange of quills with different screw thread geometry.

The free floating sleeve fits over the test quill. Rotation of the sleeve is prevented by rods protruding from the sides of the sleeve. These rods fit against strain gage beams which are used for measuring torque.

The thrust load on the sleeve is taken by the bracket above the sleeve. A spherical indentation on the sleeve fits over a ball of slightly smaller diameter on the bracket. The difference in diameters is large enough to allow the sleeve to center itself around the quill due to the hydrodynamic force created by the fluid in the clearance space between sleeve and quill.

The screw seal test rig consumes about 1/2 h.p. due to viscous shear when operating at maximum speed. In order to carry away the heat generated without raising the sleeve temperature to unreasonably high values, it is necessary to cool the sleeve. Since the Reynolds number is an important test parameter, it is important that the fluid temperature and thus its viscosity be controlled. By varying the flow of cooling water through the sleeve, control over the fluid viscosity is attained.

A free cutting brass was selected for the sleeve material. It has a high conductivity $K = 67$ Btu/ (hr-ft-F°) and a coefficient of thermal expansion ($\alpha = 11.4 \times 10^{-6}\ {}^{\circ}F^{-1}$) which is close to that of the shaft material (304SS, $\alpha = 9.6 \times 10^{-6}\ {}^{\circ}F^{-1}$).

Figure 14 is a print of the free floating sleeve, and Figure 15, a picture of the sleeve in place over the test quill.

B. Fixed Sleeve Arrangement

During test the free floating sleeve proved to be unstable in the turbulent flow regime. To correct this, the sleeve was mounted in ball bearings as shown in Figures 16 and 17.

The free floating sleeve was bored out and a shaft press fitted into it. The ball bearings are mounted on one end of the press fitted shaft. The housing which holds the bearing and the shaft sleeve combination is mounted on three lips protruding from the housing on a plate above the screw. Shim stock placed beneath the three lips is used to align the sleeve with the screw. The remainder of the test rig was unchanged.

C. Test Loop and Instrumentation

A sketch of the layout of the test rig and instrumentation is presented

in Figure 18. Figures 19 and 20 are pictures of the test rig and its associated instrumentation.

1. Test Loop

The loop is designed so that the threaded shaft can be tested either as a pump or seal. When operated as a pump, the working fluid, silicone fluid or water, enters the inlet groove of the sleeve from a sump. The fluid is then pumped through the screw and discharged from the sleeve. A 1/4 inch needle valve is used to throttle the flow. The flow then passes through a rotameter, a Sendure heat exchanger, and then is dumped back into the sump.

For operation as a seal, pressurized fluid is introduced at the top of the sleeve. The fluid is pressurized in a reservoir by imposing pressurized nitrogen over the surface of the fluid. The nitrogen pressure is controlled by a gas bottle regulator. The fluid which leaks through the thread shaft was collected in the shield shown in Figure 13.

2. Test Instrumentation

a. Temperature Measurement

Since screw pump operation is dependent on Reynolds number, which is dependent on viscosity, the measurement of fluid temperature is very important. Thermocouples imbedded at 1/2 inch intervals along the sleeve are used to measure the axial temperature profile. The temperature of the fluid entering and leaving the test apparatus when used as a pump; the temperature entering the test apparatus when used as a seal; and the cooling water inlet and discharge temperatures are also measured with thermocouples.

Figure 14 shows the four copper-constantan thermocouples embedded in the seal sleeve. The location of thermocouples at the inlet and discharge of the screw seal, and the cooling coil are shown in Figure 15.

The emf output from all of the thermocouples are recorded on a Brown Electronik recorder.

b. Pressure Measurements

Static pressure taps at 1/2 inch intervals along the inner sleeve give the axial pressure distribution. In addition, the inlet and discharge pressure are also measured. Bourden type pressure gages are used to indicate pressure.

The axial pressure distribution is also used to determine the axial location of the fluid-air interface as shown in Figure 18. At design pressure the fluid theoretically fills the entire seal length which is 4 inches in this case. At lower pressures the fluid-air interface moves in. The distance "b" is filled with fluid and distance "a" is filled with ambient air. By measuring the axial pressure distribution, the location of the interface can be located by plotting pressure versus length and extrapolating to ambient pressure.

The location of the four static pressure taps along the test sleeve are shown in Figure 14.

c. Torque Measurements

The torque exerted on the sleeve was measured with strain gage beams. Two rods mounted on the sleeve are restrained from rotating by two spring steel beams as shown in Figure 13. It is possible to vary the moment arm of the rods and thus the strain measured in the strain gage beams. This feature makes it possible to increase or decrease the maximum value of torque that can be measured.

d. Flow Measurements

A two gpm rotameter indicated cooling water flow rate. Although the test screw was not operated as a pump in the tests described here, there is a rotameter available for measuring test fluid flow rate. The location of both meters is shown in Figure 18.

e. Speed Measurements

Three magnetic pick-up pins are mounted on the drive pulley of the high speed spindle. These pins excite a magnetic pickup. The resulting pulses are counted on an electronic counter to indicate rotational speed.

D. Test Screw Geometry

There are an infinite number of possible screw geometries. Thus, the selection of which geometry to test is a difficult problem. For laminar flow, several investigators (See Table II) have proposed optimum geometries for maximum sealing performance. Since at the present time an optimized geometry for turbulent screw seal operation is not available, the screw tested in the series of tests described here was based on the laminar optimization of Zotov described in Section II-A-4-a. A print of the test quill is shown in Figure 22, and a photograph in Figure 23. Figure 24 is a picture of the screw quill in place in the high speed spindle with the sleeve removed.

E. Selection of Test Fluids

In order to achieve operation in the turbulent range, it is necessary to run with a fluid of low viscosity. It is also desirable to use a fluid whose viscosity is insensitive to changes in temperature. This minimizes any Reynolds number effects due to temperature dependent viscosity changes.

Silicone fluids are available in low viscosities and have a relatively flat viscosity-temperature relationship. They can also be blended to produce intermediate viscosities. This property provides another method, other than changes in geometry and shaft speed, to control the operating Reynolds number. For these reasons they are good fluids for testing screw seals.

Water, although it has a relatively steep viscosity-temperature curve, is a cheap low viscosity test fluid. Data taken with water as a test fluid also provides a check on the data taken with a silicone fluid of the same viscosity. Comparisons of such data may point out properties other than viscosity, such as vapor pressure which may have an effect on screw seal performance. The kinematic viscosity of several grades of silicone oil and water is shown in Figure 25.

For most fluids in ordinary technical applications, the inception of

cavitation occurs at pressures of the order of the vapor pressure. Therefore in evaluating the cavitation performance of a screw seal, it is necessary to know the vapor pressure. The vapor pressures of several grades of silicone oil and water are presented in Figure 26.

Surface tension can also be an important physical property in evaluating the performance of seals and bearings. The surface tensions for the test fluids in contact with air are shown in Figure 27.

Some other data of interest is included in Table IV below:

Fluid	Specific Gravity 77°F	Thermal Conductivity at 150°F Btu/hr ft°F	Specific Heat at 77°F Btu/lb. °F
Water	.997	.378	1.0
SF96-(0.65)	.759	.057	.36
SF96-2	.873	--	.36
SF96-5	.916	.067	.36

Table IV

PROPERTIES OF TEST FLUIDS

IV. TEST PROCEDURE

The test procedure followed in obtaining the test data was as follows:

1. The electronic indicating and recording equipment were turned on and allowed to warm up for about one hour. They were then zeroed.
2. The drive motor was turned and its speed set at the desired operating speed.
3. As the motor was turned on test fluid was introduced into the seal and the fluid pressure adjusted until the fluid-gas interface moved to a point about 3 inches from the top of the sleeve.
4. The cooling water through the sleeve was set at about 1.4 lb/min. The seal was then run under these conditions until temperature equilibrium was reached. This took from 5 to 15 minutes.
5. The test data was then recorded. The type and amount of data is described in section III-C-2.
6. After the data was recorded, the valve between the seal and the pressure accumulator was closed. If the seal maintained pressure, it was noted on the data sheet. If the seal did not maintain pressure, the amount of pressure drop off during the five minute period was recorded. Any leakage was also noted on the data sheet.

V. TEST RESULTS

A. Summary of Tests

Tests were run with two different test rig configurations and four different test fluids. Only one screw geometry was tested. A brief summary of the range of sealing pressures, rotational speeds, and measured powers is presented in Figure 29. The maximum speed reached was 35,000 rpm.

B. Free Floating Sleeve Test Results

Data points 1-1 through 1-19 were taken with the free floating sleeve. With the low viscosity fluid, SF 96-0.65, the sleeve was very unstable resulting in sleeve wear. Figure 30 shows the variation of sleeve diameter versus sleeve length before and after tests with the SF 96-0.65 fluid. The pattern of sleeve wear indicates that the sleeve instability was primarily a rocking type vibration about the sleeve center. The effect of the sleeve instability and wear was to change the screw seal geometry during the tests. This has been compensated for in presenting the test data by assuming uniform wear with time during testing. The estimated radial clearances calculated on this basis are shown for each test point in Figure 29 .

The sealing coefficient ψ_δ is plotted against Reynolds number in Figure 31. Discussion of these results will be given in the next section.

Due to the fact that rubbing occurred during the free floating sleeve tests, the measured values of torque were unusually high. Thus the power and friction factor data for these tests have been omitted.

C. Fixed Sleeve Test Results

As described in section III-B, the test rig was modified after it was

realized that the free floating sleeve arrangement was unstable. The fixed sleeve arrangement proved successful and operation to 35,000 rpm was possible.

The measured sealing coefficients for fixed sleeve operation are shown in Figure 31 as a function of Reynolds number. The sealing coefficient curve is similar to those observed in other fluid systems, with a laminar, a transition, and a turbulent regime. The measured sealing coefficients for fixed sleeve operation approximate those with the floating sleeve in the turbulent regime. The laminar sealing coefficient, however, approached a lower value ψ_δ for fixed sleeve operation than for the free floating sleeve. This is not unexpected as the leakage flow term in the laminar sealing equation 28, is a function of eccentricity. Since the free floating sleeve tended to center itself in the laminar flow regime, the leakage back over the lands was a minimum. With the fixed sleeve, it is very difficult to exactly center the shaft. Any slight eccentricity will increase the land leakage flow and thus lower the sealing coefficient.

It was shown in Section II that in laminar flow the sealing coefficient can be expressed as

$$\psi_\delta = K_{1_\delta} \tag{28}$$

and in turbulent flow

$$\psi_\delta = K_{1_\delta} + K_{2_\delta} \, Re_h^{\,n} \tag{57}$$

where the K's are functions of geometry alone. Reference to Figure 31 shows that test data verifies the form of the sealing equation predicted in the previous analytical studies. In the laminar regime the curve flattens and approaches a

constant value independent of Reynolds number. In the turbulent regime the sealing coefficient increases with Reynolds number.

If all of the measured values of K_{1_h} below $Re_h = 300$ are averaged, a value of

$$K_{1_\delta} = .313 \tag{59}$$

is obtained. This result is lower than the values measured or predicted in the other studies reported in Table II. The results are, however, fairly close to those measured by Asanuma, the second entry in the table. The discrepancies are felt to be the result of eccentricity.

In order to determine the constants in equation, it is necessary to rewrite the equation in the following form:

$$\psi_\delta - K_{1_\delta} = Re_h^{\,n} \tag{60}$$

or

$$\ln (\psi_\delta - K_{1_\delta}) = n \ln Re_h \tag{60a}$$

If $(\psi_\delta - K_{1_\delta})$ is plotted versus Re_h on log-log paper, it should give a straight line of slope n. Using a value of $K_{1_\delta} = .313$, this has been done in Figure 32, for values of Re_h above 550. The data closely approximates a straight line at high Reynolds numbers. The method of least squares was used to fit a curve to the data.

The value of the fitted equation is

$$\psi_\delta = .313 + 1.31 \times 10^{-4} Re_h^{\,1.044} \tag{61}$$

where the mean error on $(\psi_\delta - K_{1_\delta})$ is 0.1.

The data taken yields three important conclusions:

1. A laminar sealing coefficient has been obtained which approximately verifies previously determined values.

2. The theoretically derived form of the turbulent sealing equation has been verified.

3. Values of the constants in the turbulent sealing equation have been experimentally determined for one geometry of screw.

D. Power Measurements

The energy dissipated in a screw seal, ignoring the pressure flow terms, has been shown in Section II-A-3 to be given by the following expression:

$$P = \frac{\mu U^2 A}{66000\delta}\left[\frac{\gamma\beta}{\beta+1} + (1-\gamma)\right] \qquad (33)$$

The term $\frac{\gamma\beta}{\beta+1} = .1525$ represents the portion of power dissipated in the groove and the term $(1-\gamma) = .37$ represents the portion dissipated over the land. For this test geometry then, about 70% of the total loss occurs over the land. Therefore, it is more appropriate to present the frictional characteristics of the screw seal in terms of a Reynolds number based on the clearance between the land and sleeve, rather than in terms of a Reynolds number based on the groove depth as was done in presenting the sealing coefficient data.

The screw seal friction factor in the laminar flow regime is given by

$$f = \frac{2}{Re_\delta}\left[\frac{\gamma\beta}{\beta+1} + (1-\gamma)\right] \qquad (37)$$

For the case of $\gamma = 0$, equation reduces to the case of the unloaded journal bearing, that is

$$f = \frac{2}{Re_\delta}$$

or

$$f_{ss} = f_{jb}\left[\frac{\gamma\beta}{\beta+1} + (1-\gamma)\right] \qquad (62)$$

In Reference 17, the frictional characteristics of an unloaded journal bearing are presented in terms of a friction factor f. In this study the coefficient

of friction f was found in the laminar regime to be given by equation 62 and in the turbulent regime by

$$f = \frac{.078}{Re_\delta^{0.43}} \tag{63}$$

The friction factor from Reference 17 multiplied by $\left[\frac{\gamma\beta}{\beta+1} + (1-\gamma)\right]$ is shown in Figure 33 along with the measured screw seal friction factors. It is seen that the measured screw seal friction factors run about 3 times higher than the theoretical value. This indicates that the simple model on which the analysis is based is not adequate, and further work should be done in this area to develop analytical techniques for predicting friction loss.

The data as a whole can be approximated by a line of slope 1. However, for any one fluid, the data exhibits a slightly higher negative slope. This peculiarity of the data may be a result of eccentricity. From Reference 17, it is known that the laminar frictional torque of a bearing increases with eccentricity ratio. If the screw quill is eccentric in the sleeve, the hydrodynamic forces will tend to center the quill, and the higher the speed the larger the hydrodynamic forces tending to center the quill. If the quill is originally misaligned, as the speed increases the eccentricity ratio will decrease and consequently the friction torque. This effect is such as to cause the higher slope.

The scatter in the friction data is considerable. The reason for this is that the torques being measured were small, as low as 12 in-gms. The static friction in the ball bearings supporting the sleeve approached this value. In addition the numerous pressure lines and thermocouple wires attached to sleeve contributed additional error. The level of data points 1-98 through 1-118 were adjusted to match the other SF-96-5 data. This was required in order to correct

an error in the zero setting of the recording instrument for these runs.

The frictional characteristic of the screw seal retains its laminar character to values of Re_δ up to about 1000. This value is fairly close to the critical Reynolds number in the land clearance based on Taylors instability criterion which is

$$Re_{\delta_{cr}} = 41.1\sqrt{\frac{D}{2\delta}} = 700 \qquad (64)$$

In contrast the flow in the groove enters the transition range at Re ≈ 224 ($Re_h \approx 700$) as evidenced by the increase in the sealing coefficient at that point. The data indicates that Re_δ is the proper criterion for correlating the frictional characteristics of a screw seal since most of the loss occurs in the land clearance space. On the other hand, the Reynolds number, Re_h, is more suitable for correlating the sealing characteristic. Three separate modes of flow appear possible in the screw seal.

Nature of flow	In the Groove	Over the Land
	laminar	laminar
	turbulent	laminar
	turbulent	turbulent

At very low Reynolds numbers the flow is laminar in the groove and over the land. At $Re_h = 700$, the flow in the groove becomes turbulent. At this point the sealing coefficient starts increasing with Reynolds number while the friction factor retains its laminar character. When $Re_h \approx 3100$ corresponding to a $Re_\delta \approx 1000$, the friction factor curve loses its laminar character and enters the transition range indicating that the flow is now turbulent both in the groove and over the land.

E. Seal Breakdown

As the shaft speed is increased, a point is reached where the seal brcaks down. When this happens, the pressure profile along the sleeve still shows a zero pressure intercept well within the seal. This can be seen for instance in Figure 34 where for a Reynolds number of 11,700 the zero pressure intercept shows an active seal length of 2.8 inches, yet the seal was leaking.

The term seal breakdown, when used here, is defined by the condition when the seal will no longer maintain the seal pressure when the valve is closed between the seal and the pressure accumulator (See Figure 18). The seal breakdown is not a catastrophic type failure but amounts to about a drop of leakage every three minutes. Once breakdown has occurred, the seal pressure drops off at the rate of about 1 psi every 5 minutes after the valve between the seal and accumulator has been closed.

It is apparent that in order to use the screw seal in high speed applications, the designer must be able to predict when seal breakdown will occur. To do this requires knowledge of the mechanism of seal breakdown. In deriving the sealing coefficient equations, three types of fluid forces and seal geometry were included. The sealing coefficient can be thought of as the product of a pressure coefficient, a Reynolds number, and geometrical ratio, that is

$$\psi_\delta = \frac{\Delta p\, \delta^2}{\mu U L} = \frac{\Delta p}{\rho U^2} \times \frac{\rho U \delta}{\mu} \times \frac{\delta}{L} \qquad (65)$$

In the analysis it was shown that the above sealing coefficient was a function of the Reynolds number and seal geometry. Looking at it this way, we see that

only the following factors were included in the analysis:

Pressure forces
Viscous forces
Inertial forces
Geometry

Consideration of these factors alone does not permit prediction of seal breakdown, since seal breakdown occurs at both low and high Reynolds numbers. Therefore, we must look to the other fluid forces which were omitted from the analysis for an explanation of seal failure. There are several useful parameters which portray the relative importance of several factors, vapor pressure, gravitation, and surface tension which are of possible importance in this study. These are discussed below:

E-1 Cavitation

Cavitation is usually defined as the formation of the vapor phase of a liquid which has been subjected to reduced pressures. When the phase change is a result of pressure changes brought about by the motion of a liquid relative to a solid body, the two-phase flow is said to be a cavitating flow. Such a condition can exist in a screw seal where a liquid is contained in a clearance space between a sleeve and a high speed rotating shaft.

For most fluids in ordinary technical application, the inception of cavitation occurs at pressures of the order of the vapor pressure. The pressure at which it occurs however, is variable and depends upon the amount of entrained gas and foreign material in the fluid.

The parameter which is used to predict when cavitation will occur is called the cavitation number and is defined as

$$C = \frac{P_a - P_v}{1/2\rho U^2} \tag{66}$$

where p_a is the ambient static pressure, p_v is the vapor pressure at the operating temperature, and U is a reference velocity, characteristic of the flow. For application to the screw seal, it appears reasonable to take p_1 as the ambient pressure and U, the shaft speed, as characteristic flow velocity. Thus the cavitation number becomes

$$C = \frac{p_1 - p_v}{1/2\rho U^2} \tag{67}$$

According to the above equation, the lowest pressure in the seal is p_1, since at any point beyond this, the pressure should be higher due to the increasing pressure gradient. Measurements verify this in Figures 34 to 37. However, secondary flows may exist within the seal and lower pressures may exist permitting cavitation. Since it is not possible to predict the minimum pressures which may arise as a result of secondary flows, the cavitation parameter is expressed in terms of p_1, an easily measured quantity.

The magnitude of the cavitation number is an indication of the degree of cavitation or the tendency to cavitate. The value of of the cavitation number at which cavitation is first observed is the critical cavitation number. The cavitation number provides a means for predicting cavitation behavior on tests run with different geometries and different fluids.

If cavitation is the cause of seal breakdown, the inception of seal breakdown should always occur at the same cavitation number, and it should be possible to operate at higher shaft speeds with low vapor pressure fluids than with high vapor pressure fluids. In Table VI, the cavitation numbers at

seal breakdown for the four test fluids is shown. From first appearance there seems to be no one critical cavitation number which corresponds to seal breakdown. Before reaching any conclusions it is important to note that the actual film temperature is higher than the measured sleeve temperature. This means that the vapor pressure corresponding to the sleeve temperature may be considerably lower than the vapor pressure actually existing in the fluid film.

To gain some appreciation of the magnitude of the difference between the measured sleeve temperature and actual film temperature, Couette flow between two flat plates is considered. Since most of the power loss in the seal occurs over the lands (See Equation 33) and the eccentricity is assumed zero, the flow in the clearance space over the lands can be approximated by Couette flow with no pressure gradient.

If the shaft clearance space is approximately two parallel flat plates, from Reference 1, the governing equations are

$$\frac{\partial^2 u}{\partial y^2} = \frac{\partial p}{\partial x} \tag{68}$$

$$k \frac{d^2 T}{dy^2} = -\mu\left(\frac{\partial u}{\partial y}\right)^2 = \mu\left(\frac{U}{\delta}\right)^2 \tag{69}$$

The boundary conditions are:

$$y = 0,\ u = U,\ \frac{dT}{dy} = 0$$

$$y = \delta,\ u = 0\quad T_f = T_{sl}$$

The boundary condition at y = o assumes that no heat is conducted away through the shaft.

This is a conservative assumption, as some heat will be removed through

the shaft and the calculated temperatures with no heat removal through the shaft will be higher than with heat removal through the shaft.

The solution of equation is

$$T(y) - T_{sl} = \frac{\mu U^2}{2k}\left[1 - (y/\delta)^2\right] \tag{70}$$

and for $y = \delta$

$$\left(T_f - T_{sl}\right)_{max} = \frac{\mu U^2}{2k} \tag{71}$$

Now consider operating conditions with water and SF 96-0.65 fluid at 35,000 rpm. The Reynolds number for this condition is Re = 6,260 for the SF 96-0.65, and 4960 for water. This flow is in the turbulent regime and losses would be higher than laminar theory would predict.

TABLE V

Fluid	$\frac{\text{lb-sec}}{\text{in}^2}$	$\frac{k}{\frac{\text{lb}}{\text{sec.}^{\circ}\text{R}}}$	$\frac{(T_f - T_{sl})_{max}}{^{\circ}\text{F}}$
Water	1.29×10^{-7}	.0815	2.65
SF96-0.65	$.725 \times 10^{-7}$	.0123	9.87

Even at this high speed, the temperature differences are not large enough to appreciably affect the vapor pressure. Yet in Table VI it is seen that it is possible to run the seal with water at speeds of twice that possible with SF 96-0.65 fluid at the same sleeve temperature. Since both fluids have about the same vapor pressure and their differences in conductivity are not large enough to cause a large difference between film and sleeve temperature, it appears that cavitation was not a cause of the observed seal breakdown.

E-2 Gravitational Effects

Whenever devices operate with free liquid surfaces, such as the

gas-fluid interface in a screw seal, the Froude number may be important in determining the nature of the flow. It is the ratio of inertial forces to gravitational forces and is given by

$$F = \frac{U^2}{gl} \tag{72}$$

where U and l are a velocity and length characteristic of the flow. The appropriate velocity and length for the screw seal appear to be U and δ. The Froude number is then expressed as

$$F = \frac{U^2}{g\delta} \tag{73}$$

This parameter is also shown in Table VI. If seal breakdown were a function of Froude number alone, then the critical shaft velocity would be the same for all fluids since the geometry was the same for all tests.

E-3 Surface Tension Effects

In deriving the sealing equation, the boundary condition at the gas-liquid interface was not considered. Through the action of surface tension between the liquid and the adjoining gas a pressure difference arises according to the equation

$$p_l = p_g + \frac{\sigma}{R} \tag{74}$$

where p_l is the liquid pressure and p_g is the gas pressure and R is the principal radius of curvature of the gas-liquid surface in the clearance space. If the liquid being sealed wets the shaft and sleeve material, the liquid pressure is less than the gas pressure. If it does not, the gas pressure is greater than the liquid pressure. In addition the value of the surface tension depends upon the gas in which the surface tension of the liquid is measured. Thus if surface tension

forces are of importance, the liquid, the gas and the seal material must be considered in the seal design.

A mechanism comparable to the atomization of a liquid jet may occur at the gas-liquid interface of the screw seal. As the shaft speed is increased, the inertial forces of the liquid may overcome the surface tension forces causing liquid particles to leave the surface and drop, as observed, from the seal.

In studies of this type, the ratio of surface tension forces to inertial forces, called the Weber number, is an important parameter. It is defined as

$$W = \frac{U^2 l \rho}{\sigma} \tag{75}$$

where

σ = surface tension
ρ = density
l = characteristic length
U = characteristic velocity

In applying it to a screw seal, we choose U and δ as the characteristic velocity and dimension. The expression then becomes

$$W = \frac{U^2 \delta \rho}{\sigma} \tag{76}$$

This parameter is also presented in Table VI for conditions at which seal breakdown occurred.

4. Comparison of Possible Mechanisms of Seal Breakdown

Table VI is a summary of the previously discussed dimensionless parameters which are ratios of fluid forces which may contribute to seal breakdown. Cavitation does not seem to be a cause of seal breakdown since

it was possible to run with water at values of cavitation number far below 1.0. If gravitational forces were important, the Froude number would indicate that seal breakdown would always occur at the same shaft speed, and this was not the case. Reynolds number alone will not account for it, since the water and SF 96-0.65 data indicates breakdown in the turbulent range, the SF 96-2 data in the transition range, and SF 96-5 data in the laminar range.

The Weber number data however, presents a more consistent pattern in that for 3 of the 4 test fluids seal breakdown occurred in the range of Weber number from 80 to 110. The performance of the SF 96-2 fluid was not as good with breakdown occurring at a value of W = 22. Water with a value of σ/ρ about three times larger than the σ/ρ for all three silicone fluids was the fluid for which breakdown was postponed to higher speeds. It appears that fluids with high values of σ/ρ can be operated in screw seals at higher shaft surface velocities than fluids with lower values of σ/ρ, and this property ratio should be considered when considering screw seals for sealing application.

Other fluid properties which are conducive to good screw seal operation are high conductivity and specific heat to keep film temperatures down and low vapor pressures to prevent cavitation, should this become a problem.

The fluid forces at seal breakdown have been presented in dimensionless form in Table VI in an effort to deduce logical groupings of variables involved in the mechanism of seal failure. This effort has resulted in the conclusion that surface tension forces appear to be a significant property in controlling seal failure. However, other dimensionless groupings may also be important and because of the limited test data, their affect on the pattern of the test data

DATA SUMMARY AT SEAL BREAKDOWN

Seal Breakdown Data Point	Fluid	Average Sleeve Temperature °F	U in/sec	Cavitation Number $\frac{P_1-P_v}{\rho U^2/2g}$	Froude Number $\frac{U^2}{g\delta}$	Weber Number $U^2\delta\rho/\sigma$	Reynolds Number Uh/ν	Sealing Coefficient $\Delta p\delta^2/\mu UL$
1-15	SF96-0.65	78.5	636	.95	29.8×10^4	112	6300	1.58
1-48	SF96-5	57.5	592	1.08	23.2×10^4	79.2	592	.428
1-73	Water	72	1163	.228	100×10^4	106	7805	1.983
1-77	SF96-2	71.5	290	4.25	6.2×10^4	22.1	973	.336

Table VI

could not be detected. To determine the actual mechanism of seal failure would require more extensive tests of fluids with more widely varying properties. Visual studies of seal operation through a transparent sleeve would also be helpful.

F. Pressure and Temperature Distribution Along the Sleeve

Figures 34 through 37 are sample plots of pressure and temperature measurements along the sleeve for all four test fluids. The distance x is measured from the edge of the groove where fluid is introduced into the sleeve. The first temperature measurement is actually above this point by 1/2 inch (i.e. $x = -.5$) but is plotted at $x = 0$.

The distance L for each test point was determined by drawing a straight line through the pressure points and extrapolating to zero gauge pressure. As can be seen from the plots the pressure distribution is linear, as theory predicts.

VI. CONCLUSIONS AND RECOMMENDATIONS

A. Conclusions

1. A simplified expression for the laminar sealing capability of a screw seal and a method of optimizing the screw geometry to obtain maximum sealing capability were derived. The results closely approximate the results of other published methods.
2. The analysis was extended to the turbulent flow case, and an expression for the turbulent sealing equation, not considering leakage effects, was derived.
3. An experimental investigation of the screw seal was also conducted using water and silicone fluids. The test program verified the form of, and evaluated the constants in, the derived turbulent sealing equation for one screw geometry.
4. Seal breakdown was observed in both laminar and turbulent flow. The test results indicate that the ratio of fluid surface tension to density is the most significant property controlling seal breakdown. The higher this ratio, the higher are the permissible shaft speeds before seal breakdown occurs.

B. Recommendations

The study and experiments reported here have shown that it is possible to seal low viscosity fluids with a screw seal. In order to extend the analysis of the screw seal to include a more comprehensive investigation of leakage effects, optimize the seal geometry for turbulent operation and to determine the exact mechanism of seal breakdown, the following additional

development work is recommended:

1. Derive, optimize and verify experimentally an analytical expression for turbulent screw seal operation including leakage effects. This phase would be divided into three separate tasks.

   A- Derive the turbulent sealing equation including leakage effects. This equation will yield a sealing coefficient which will be a function of Reynolds number and screw geometry. Due to the complexity of the problem, a semi-empirical approach will be required.

   B- Optimize the derived turbulent sealing coefficient with respect to the appropriate geometrical parameters. This will involve a numerical computer solution of a set of simultaneous equations.

   C- Verify experimentally the form of the equation derived in A and the optimum geometry found in B. It is estimated that about 30 different test geometries will be necessary to verify the analysis.

2. Investigation of heat generation (power loss) effects

   A- Develop a method for predicting the temperature distribution within the seal and evaluate the importance of several possible modes of heat removal, i.e., through the shaft, sealed fluid, or sleeve.

   B- Experimental verification of the analytical methods developed in IIA.

3. Investigation of the mechanism of seal breakdown (leakage). This phase would be primarily experimental and would involve testing

with fluids of widely varying properties in order to determine which fluid characteristics induce seal breakdown. Visual experiments would be performed using a transparent sleeve to observe the liquid-vapor interface. An attempt would be made to correlate the sealing coefficient at breakdown with Reynolds number, cavitation number, Froude number or other parameters that the investigation reveals to be most significant.

4. Investigate the screw seal characteristic at other than the shut off point, i.e., zero flow. This is desirable for applications where a screw seal would be used as a pressure dam. The finite flow through the seal helps to remove the heat generated within the seal.

C. REFERENCES

1. Schlichting, H., Boundary Layer Theory, Pergamon Press, New York, 1955.

2. Carley, J. F. and Strub, R.A., Industrial and Engineering Chemistry, Vol. 45, No. 5, May 1953.

3. Hughes, D.P., "Shaft Seal for High Gas Pressures," Paper C 1, April 17-19. 1961, International Conference on Fluid Sealing, BHRA, Harlow, Essex, England.

4. Stair, W.K., "The Visco Seal--A Survey," Univ. of Tennessee Engineering Experiment Report No. ME-5-62-2, March 1962.

5. Boon, E.F., S.E. Tal "Hydrodynamische Dichtung für rotierende Wellen," (Hydrodynamic Seal for Rotating Shafts), Chemie-Ing-Technik, Vol. 31, No. 3, January 31, 1959, pp. 202-12.

6. Zotov, V.A., "Research on Helical Groove Seals," Machine Design and Calculation (Russia) Issue No. 10.

7. Asanuma, T., "Studies on the Sealing Action of Viscous Fluids, "International Conference on Fluid Sealing, Paper A3, April 17-19, 1961 BHRA, Harlow Essex, England, 26 papers.

8. Frössel, W., Hydrodynamisch Wirkende Wellendichtung," Konstruktion, Vol. 8, No. 11, November 1956.

9. Whipple, R.T.P. "Herring-Bone Pattern Thrust Bearing, UKHEA, Atomic Energy Research Establishment, TIM-29, Aug. 24, 1949.

10. Whipple, R.T.P., "Theory of the Spiral Grooved Thrust Bearing with Liquid or Gas Lubricant," UKAEA, Atomic Energy Research Establishment, T/R 622, March 6, 1951.

11. Woodrow J., Viscosity-Plates Flow and Loading, "UKHEA, Atomic Energy Research Establishment, E/M 31, December 22, 1949.

12. Wordsworth, D.V., "The Viscosity Plate Thrust Bearing," UKAEA, Atomic Energy Research Establishment, E/R 2217, Oct. 1952.

13. Snell, L.N., "Theory of Viscosity Plate Thrust Bearing Based on Circular Geometry," UKAEA, Ministry of Supply, Div. of Atomic Energy (Production) 5181, Oct. 13, 1952.

14. Constantinescu, V.N., "On Turbulent Lubrication," Proc. Instn. Mech. Engrs., Vol. 173, No. 38, 1959.

15. Frössel, W., "Hochtourige Schmierölpumpe," Konstrucktion, Vol. 12, No. 5, 1960, pp. 195-203.

16. Wigg, R.E., N. Battle, "Improvements in or Relating to Sealing Means," Great Britain Patent 834,923, May 11, 1960.

17. M.I. Smith and D.D. Fuller, "Journal Bearing Operation at Super Laminar Speeds," Trans. of ASME, Vol. 78, 1956.

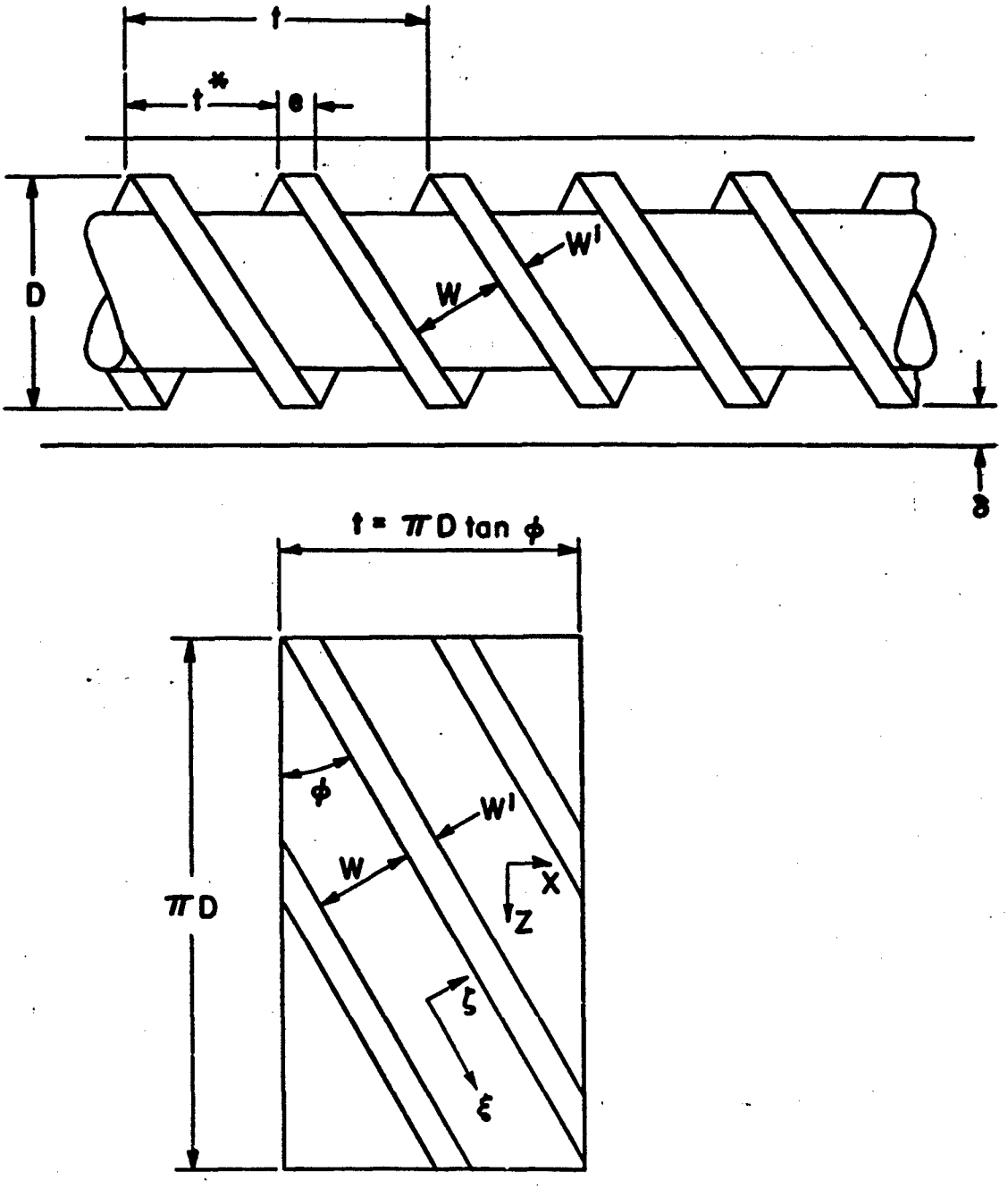

Figure 1

Screw Geometry

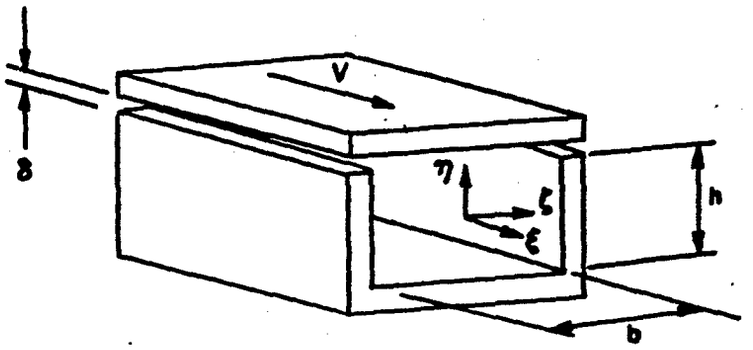

Figure 2a. Portion of Screw Pump Channel

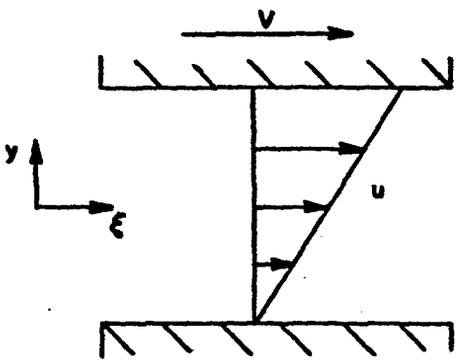

Figure 2b. Couette Flow Approximation to Flow in Screw Pump Channel.

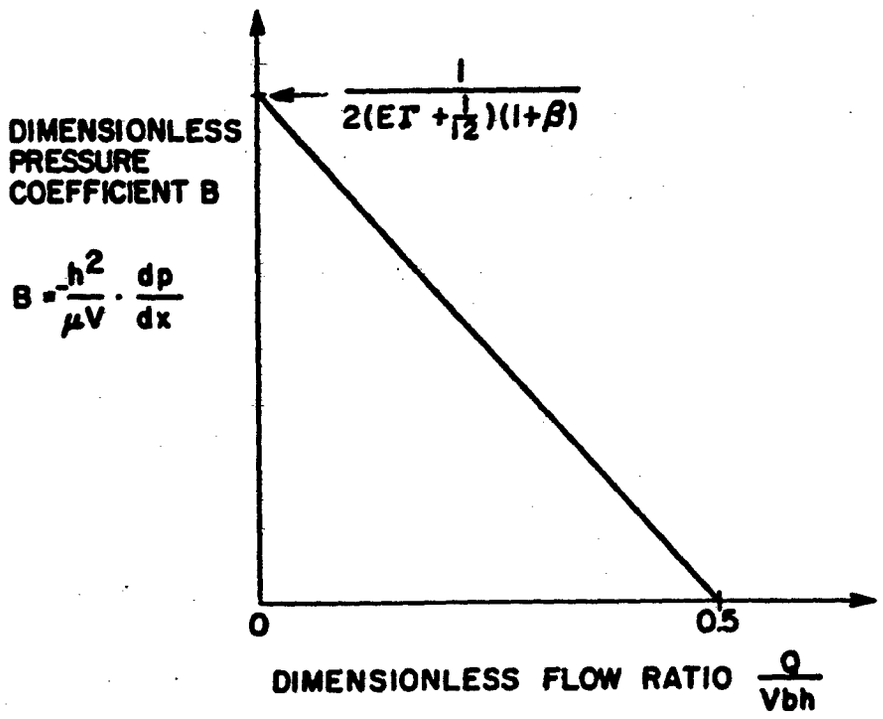

Figure 3

Theoretical Screw Pump Characteristic for Isothermal, Laminar Flow.

100 x 140 7/100 In. Div.

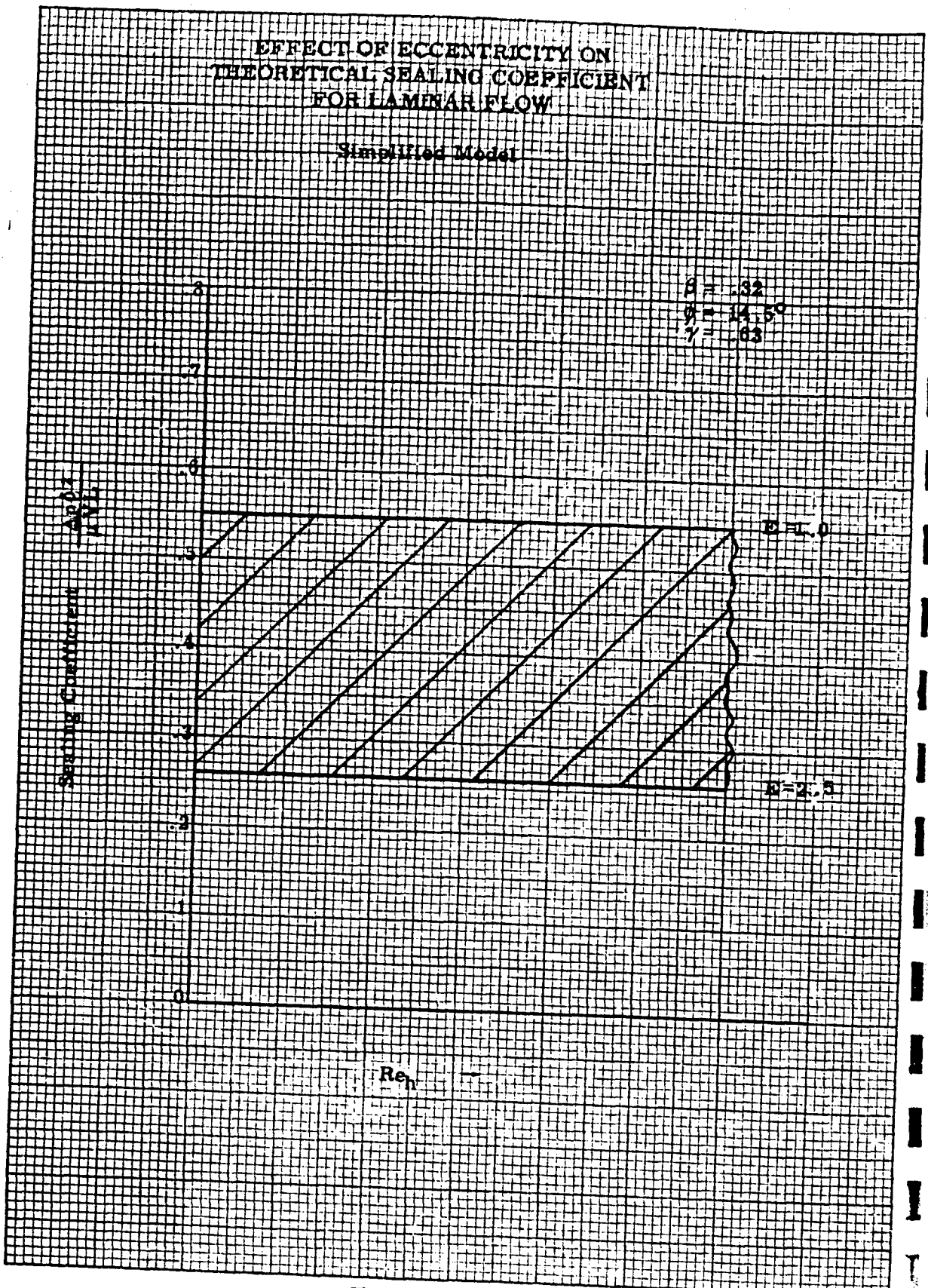

Figure 4

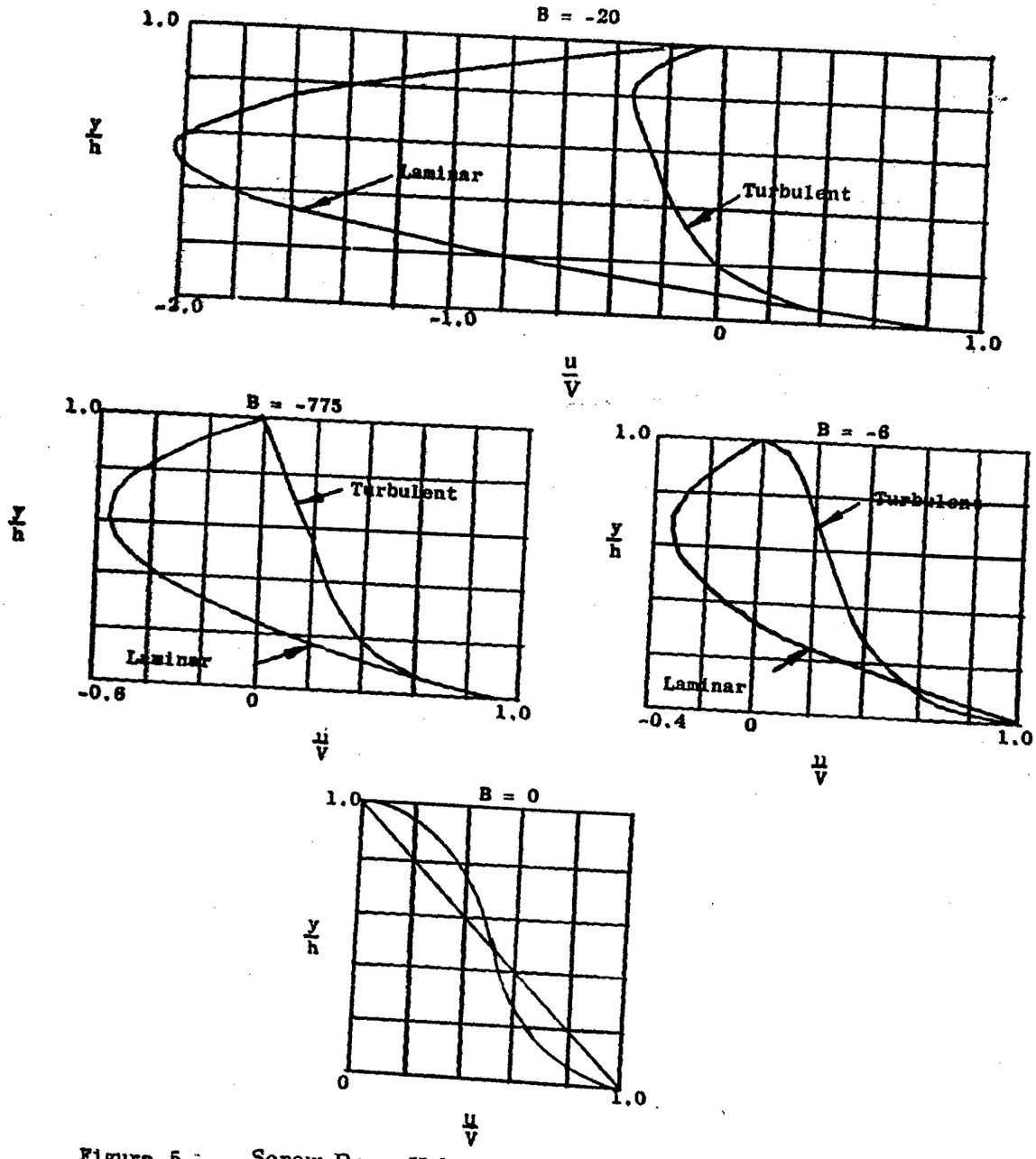

Figure 5. Screw Pump Velocity Profiles

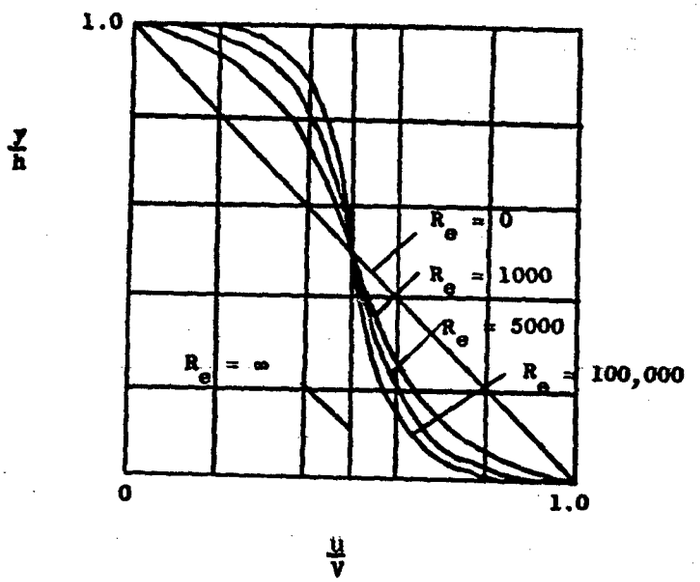

From Reference 14

Figure 6. Couette Flow Velocity Profiles for Various Reynolds Numbers

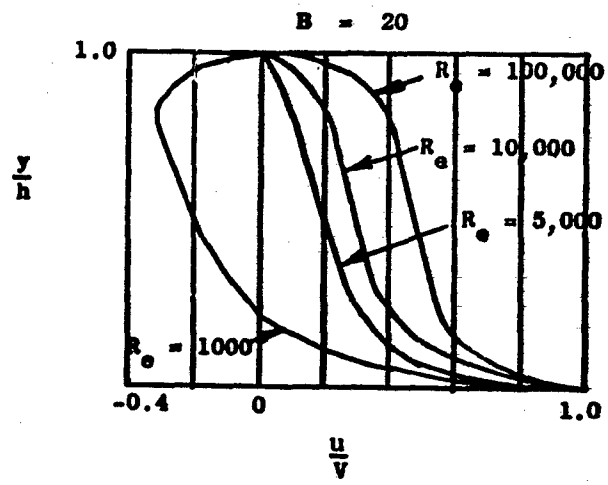

From Reference 14

Figure 7.. Screw Pump Velocity Profiles.

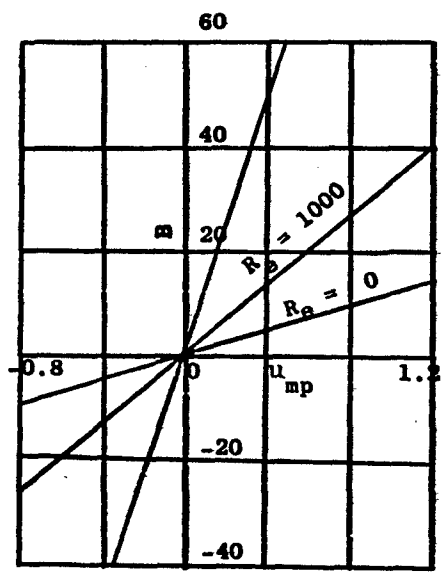

Figure 8.. Screw Pump Pressure Coefficient.

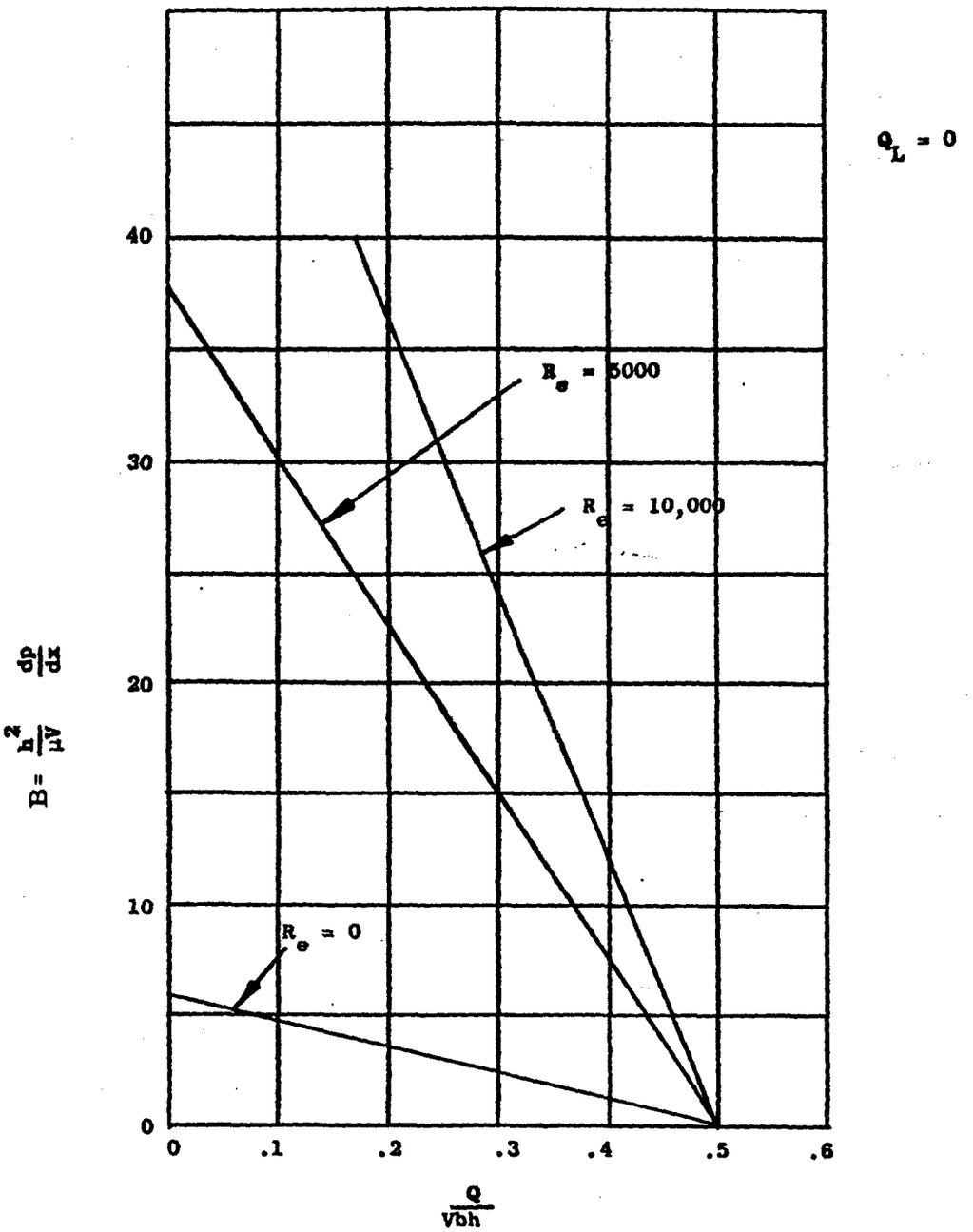

Figure 9. Screw Pump Theoretical Characteristics.

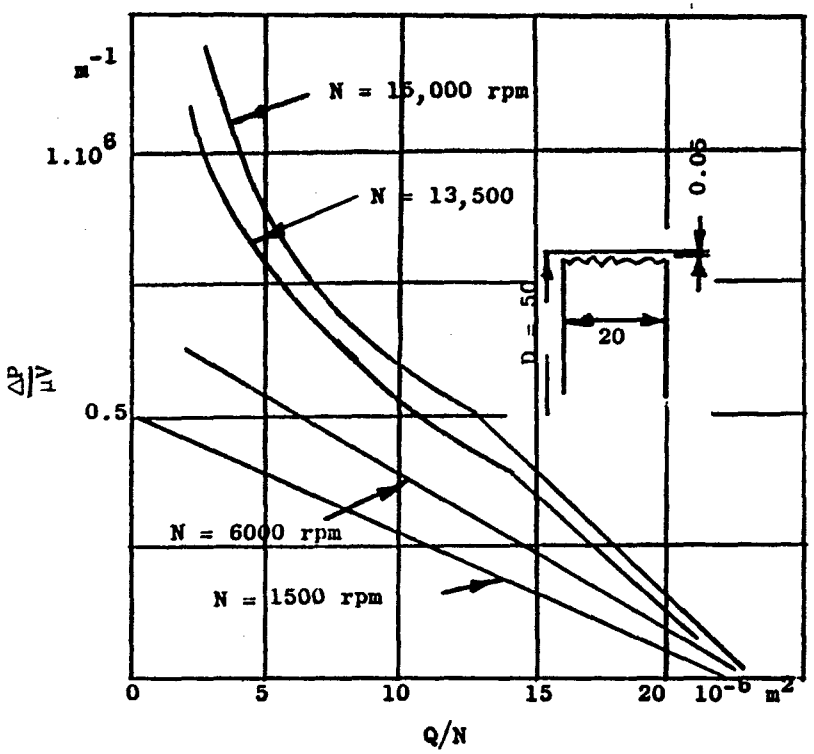

Figure 10a.

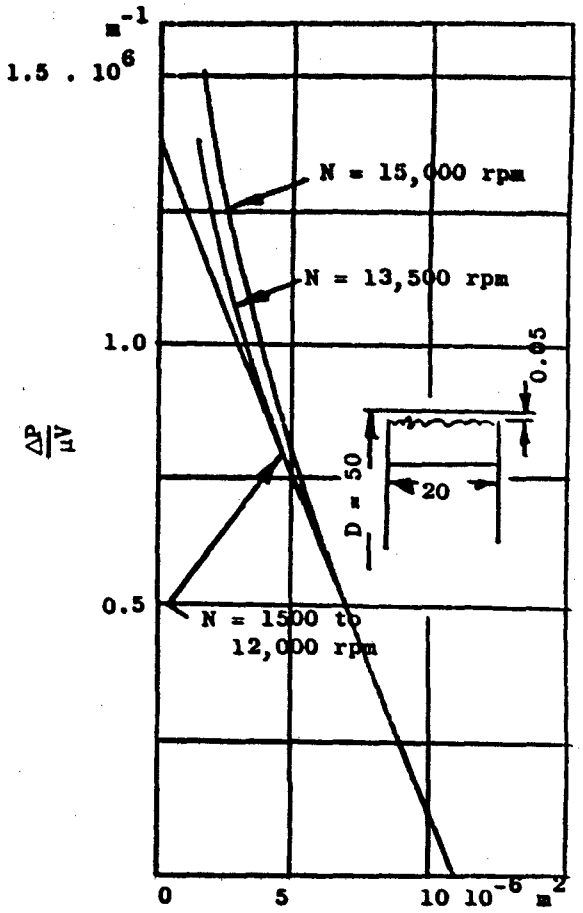

Figure 10b.

Screw Pump Pressure Characteristics

Typical Data of Frossel (Reference 8)

100 x 140 7/100 In. Div.

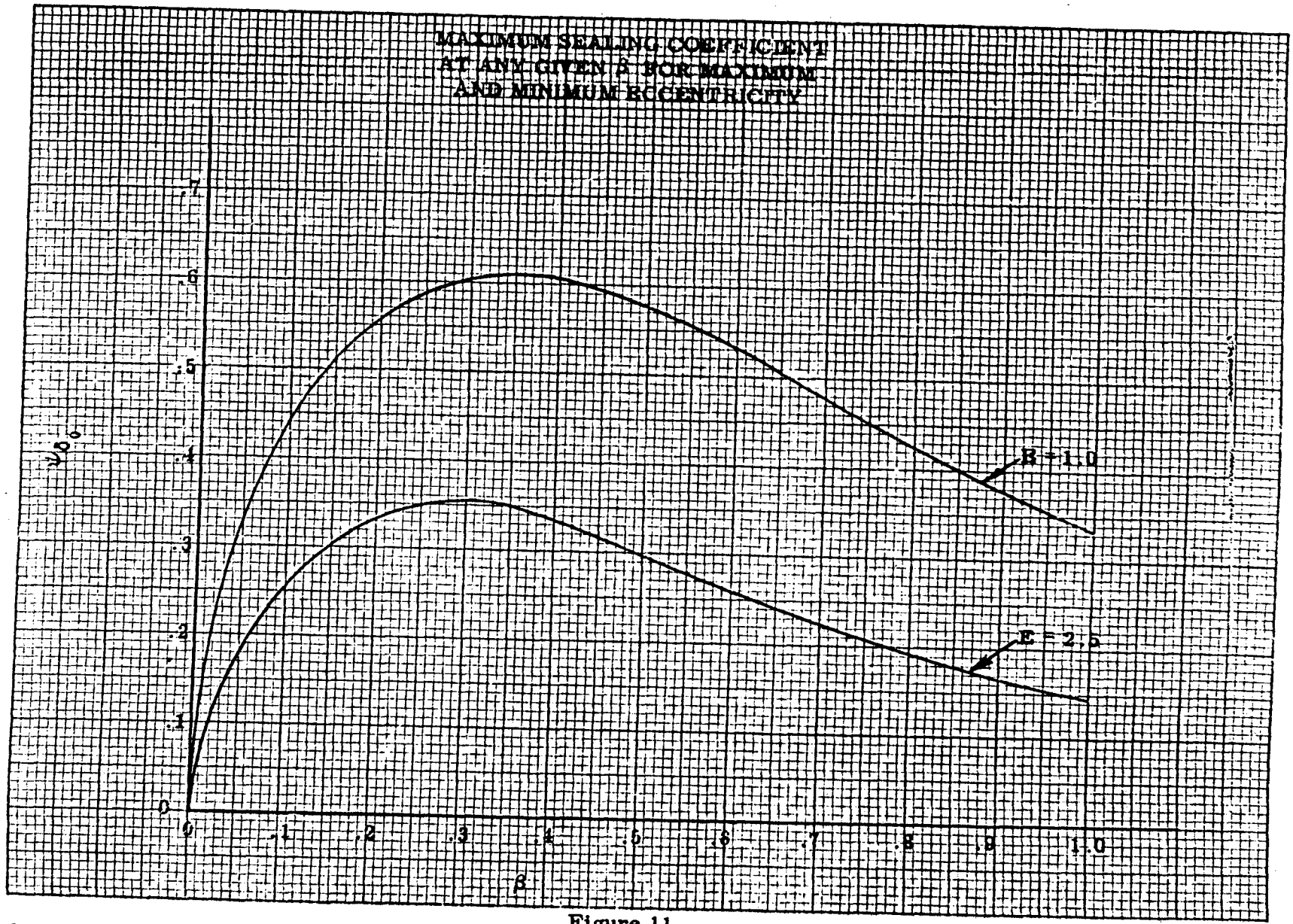

Figure 11

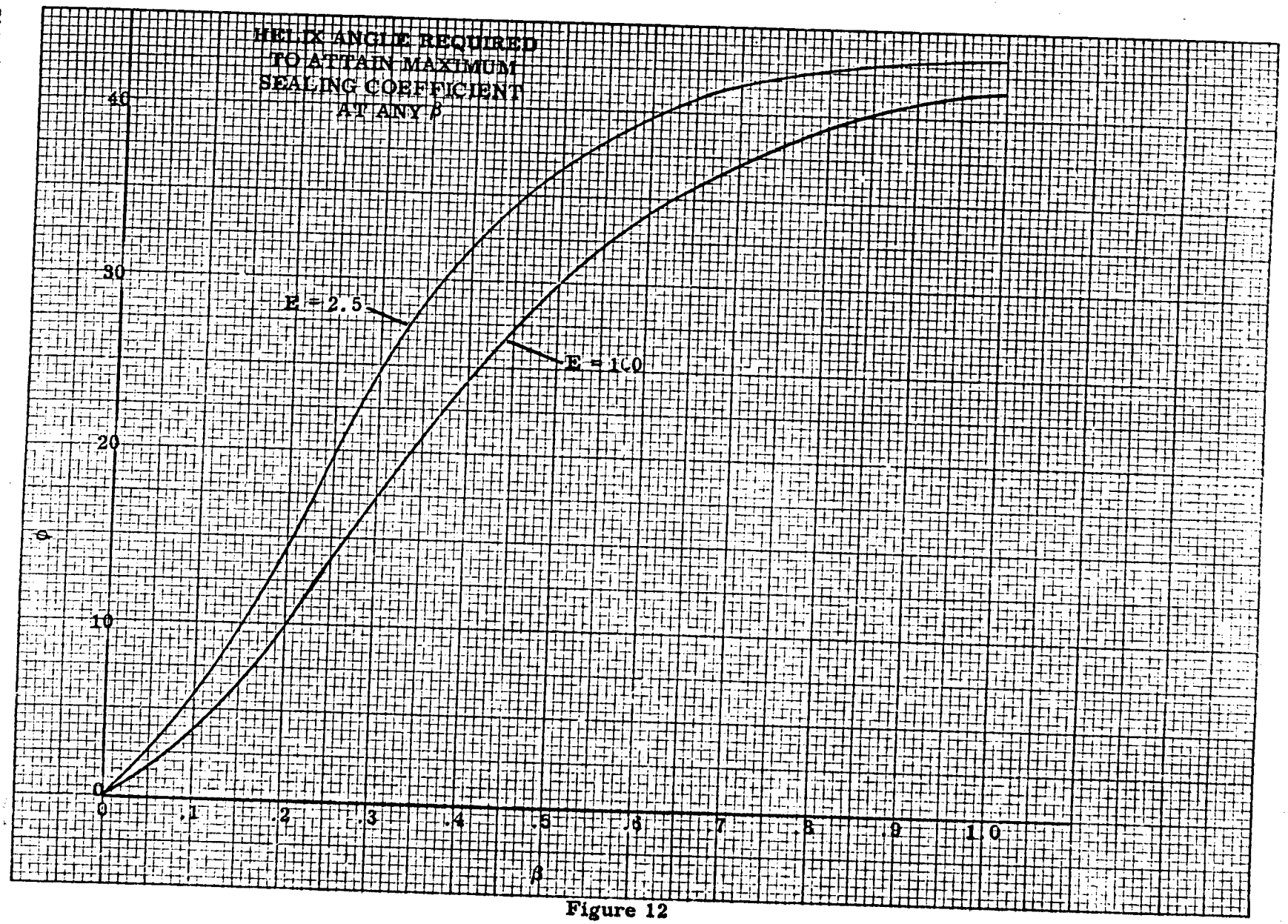
HELIX ANGLE REQUIRED
TO ATTAIN MAXIMUM
SEALING COEFFICIENT
AT ANY β
40
30
20
10
0
φ
E = 2.5
E = 10.0
0
.1
.2
.3
.4
.5
.6
.7
.8
.9
1.0
β

Figure 12

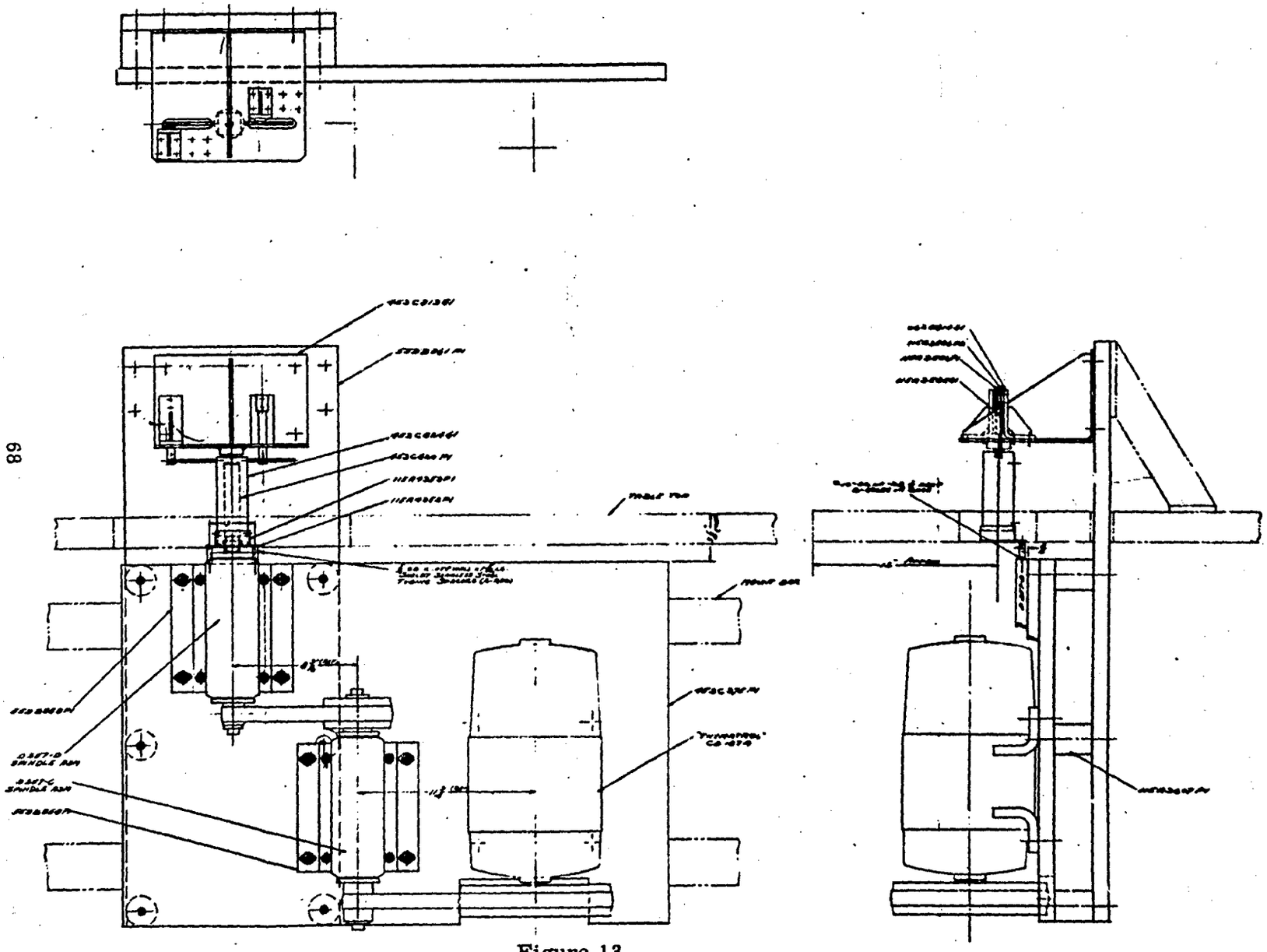

Figure 13

Layout of Screw Seal Test Rig

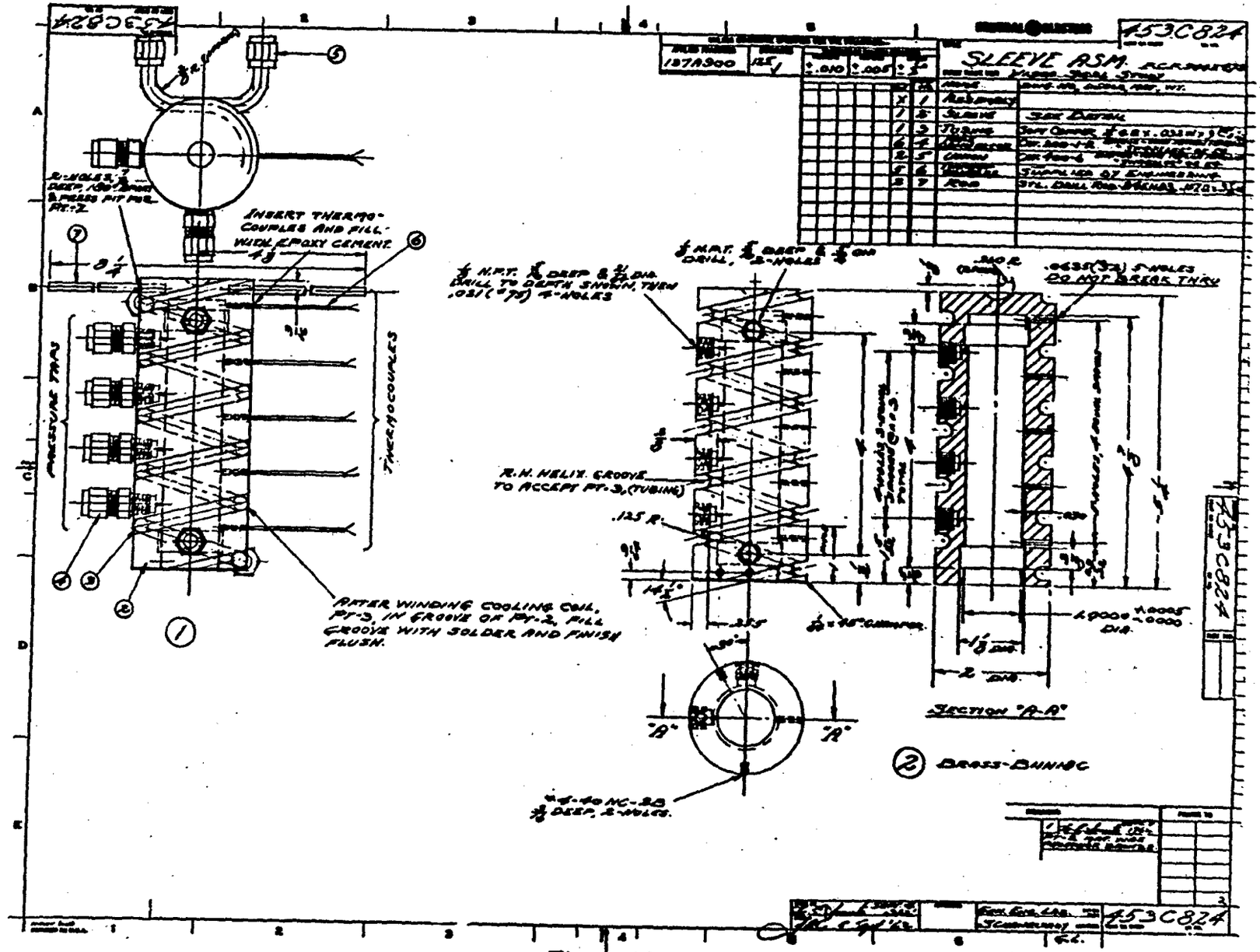
453C824
SLEEVE ASM.
INSERT THERMO-COUPLES AND FILL WITH EPOXY CEMENT
PRESSURE TAPS
THERMOCOUPLES
R.H. HELIX GROOVE TO ACCEPT PT-3, (TUBING)
WATER WINDING COOLING COIL, PT-3, IN GROOVE OF PT-2, FILL GROOVE WITH SOLDER AND FINISH FLUSH.
SECTION "A-A"
BRASS-BUNABC

Figure 14

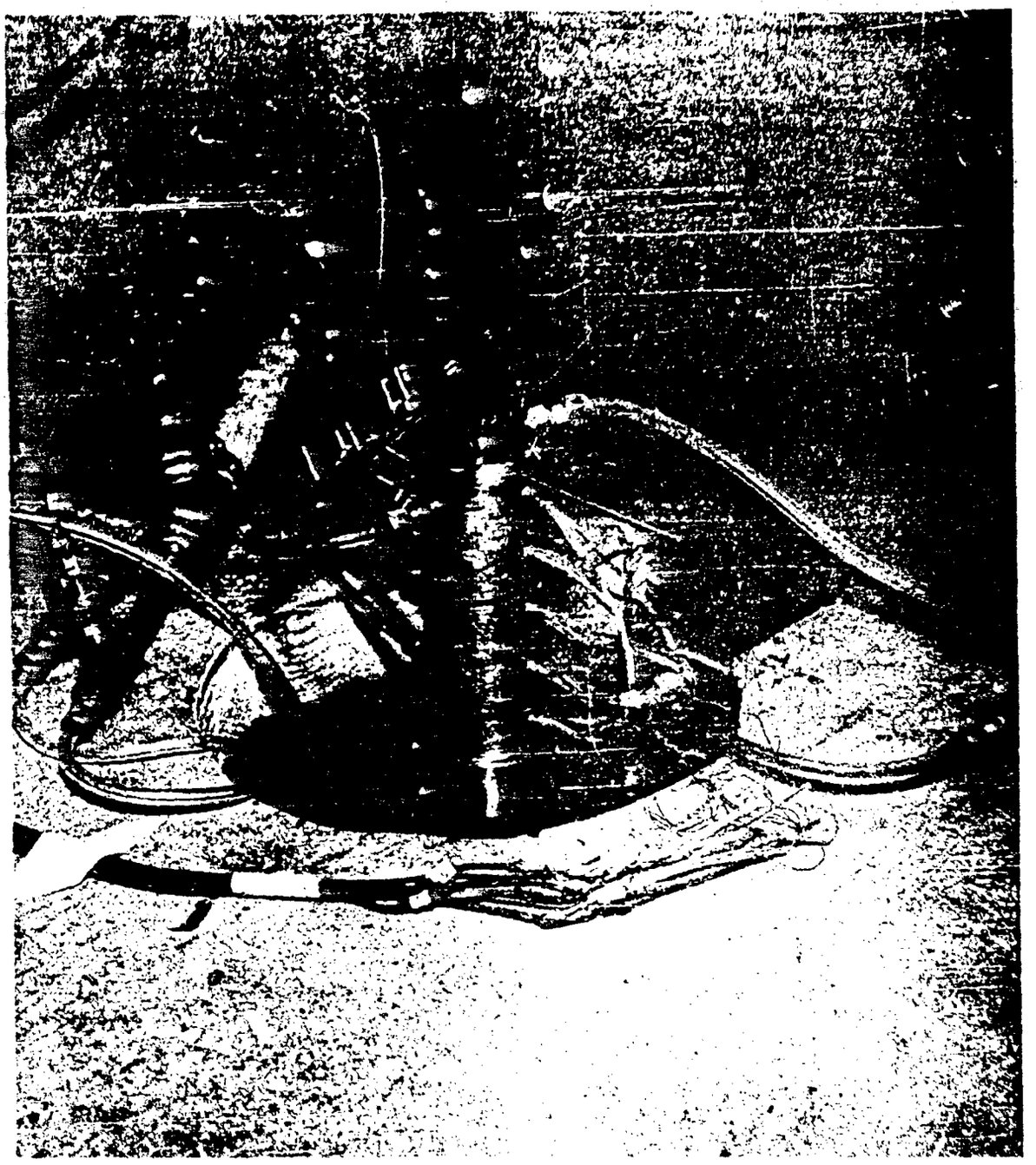

Figure 15. Picture of Free Floating Sleeve

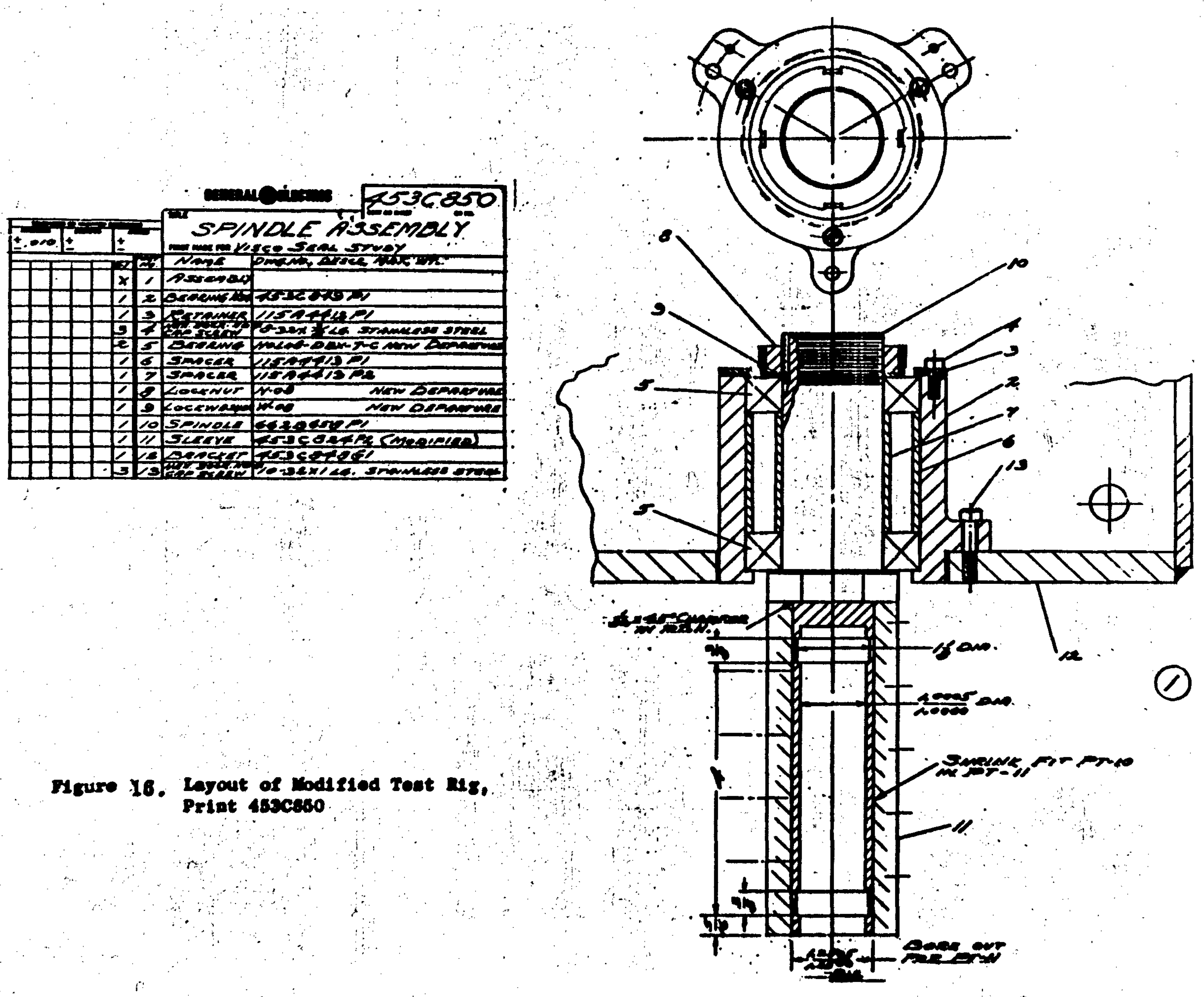

Figure 16. Layout of Modified Test Rig,
Print 453C850

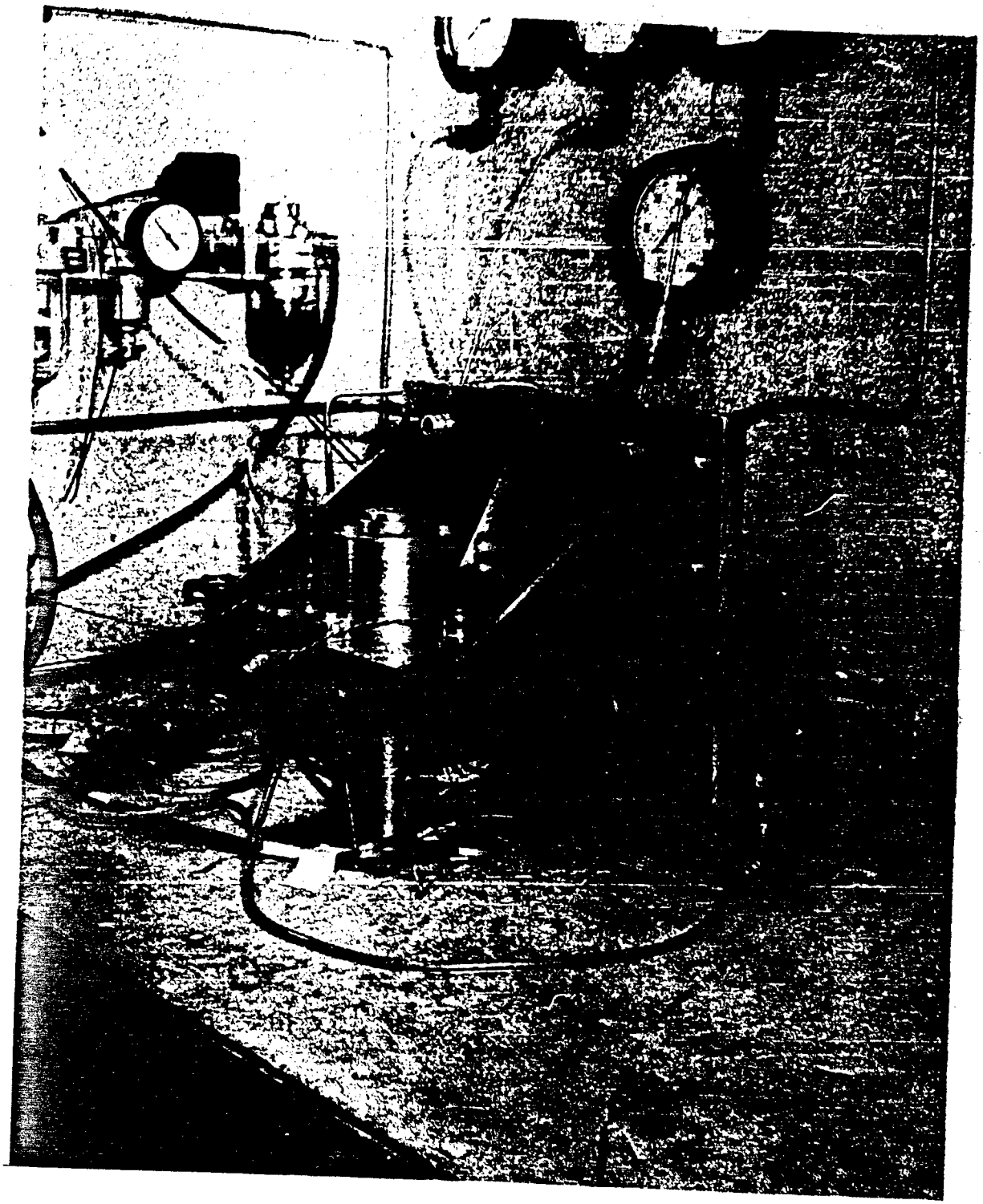

Figure 17. Picture of Fixed Sleeve

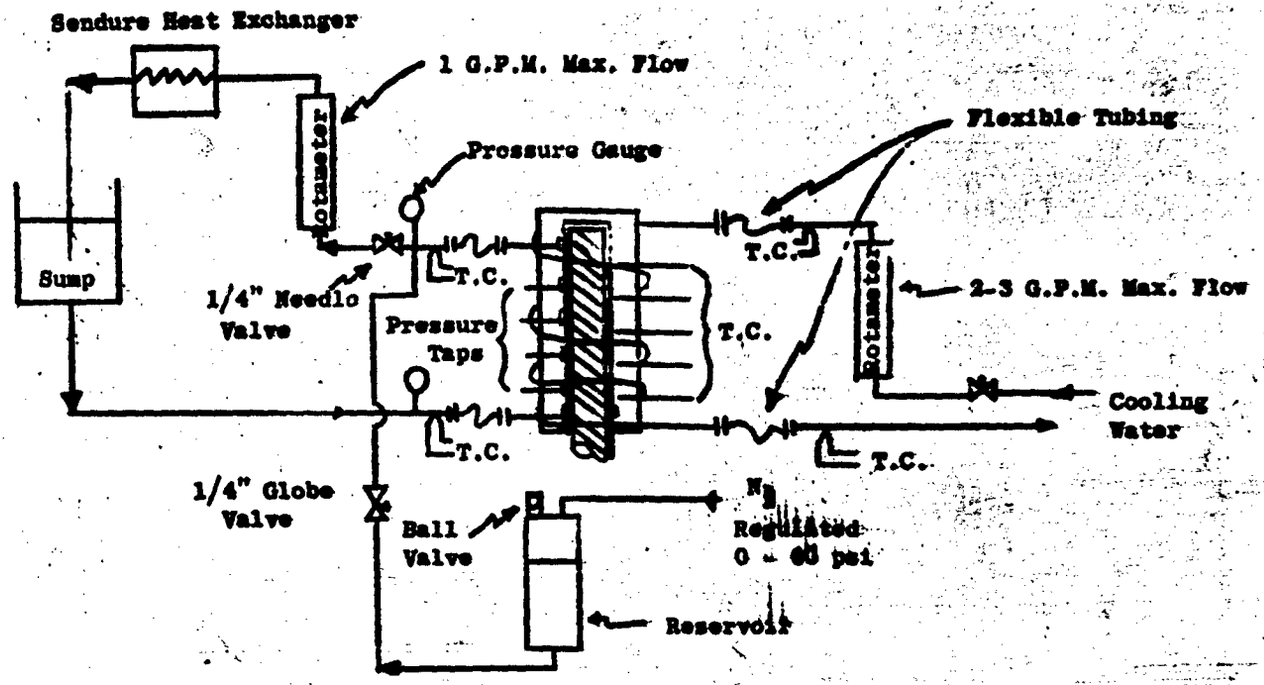

Figure 18. Test Loop and Instrumentation for Screw Seal Test.

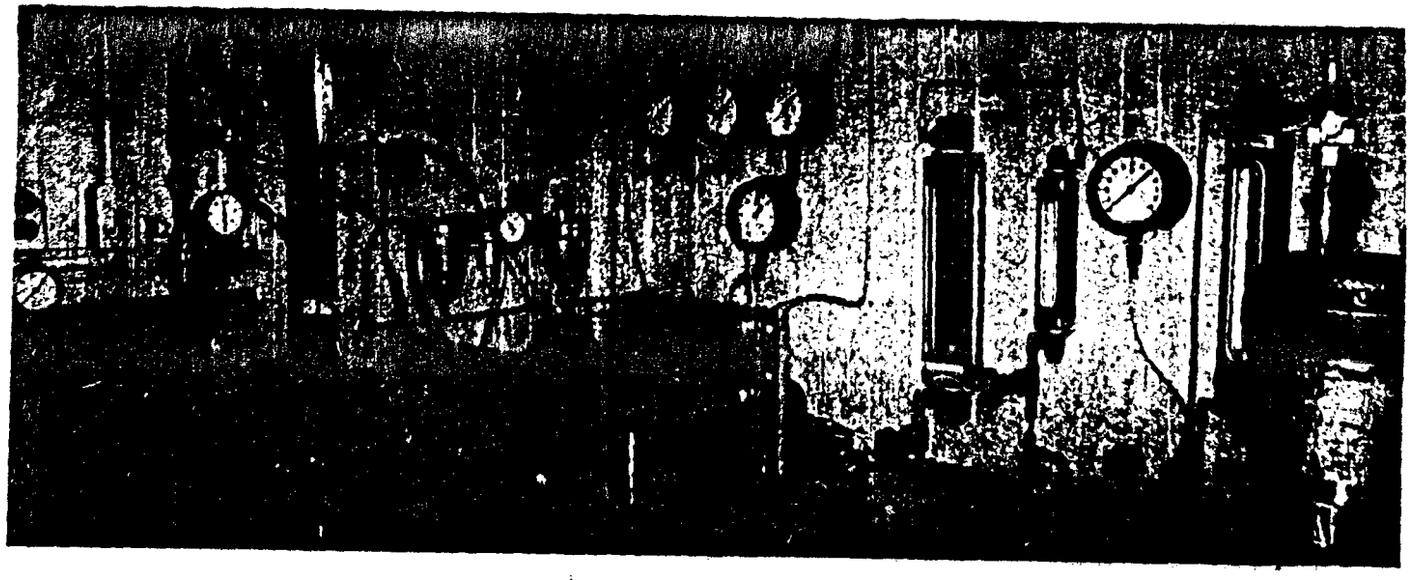

Figure 19. Picture of Test Rig

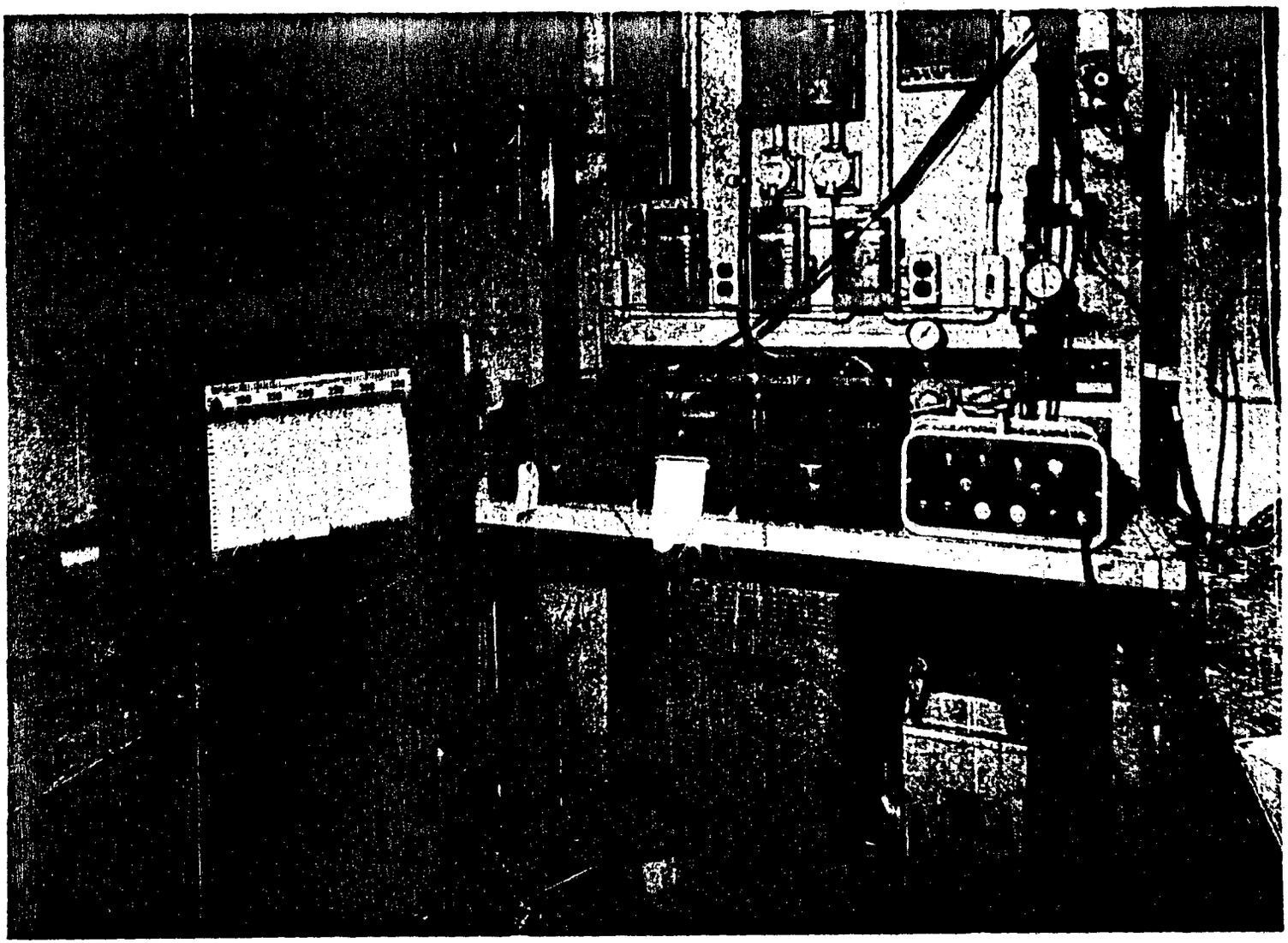

Figure 20. Picture of Instrumentation

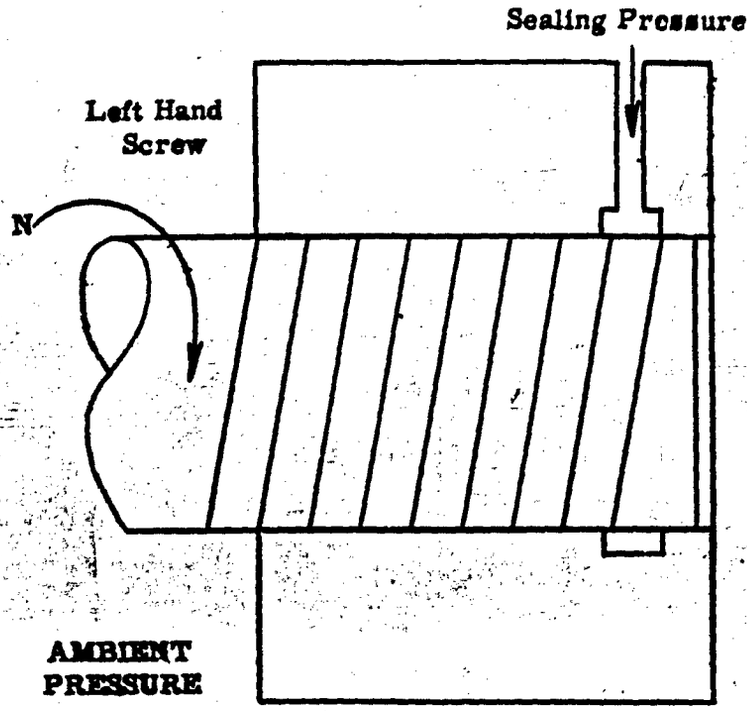

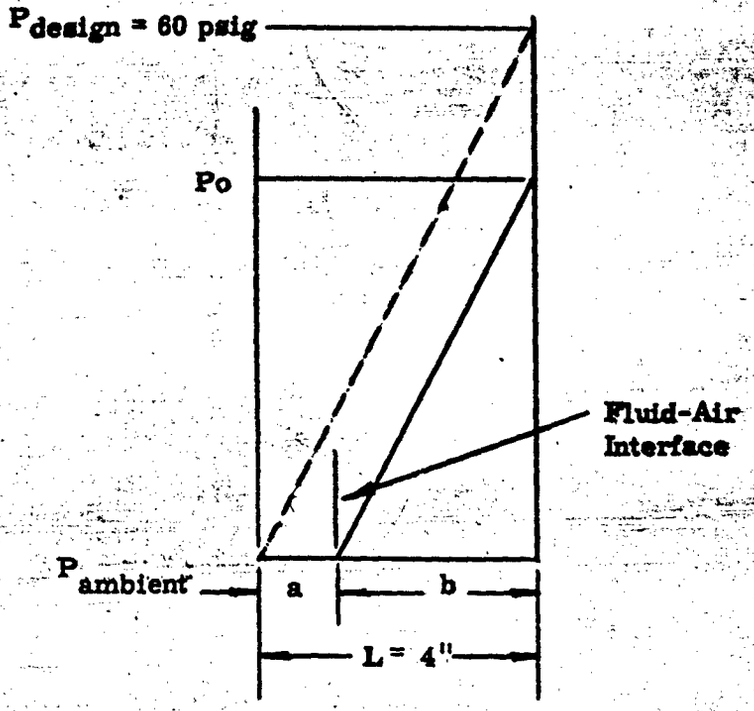

USE OF PRESSURE PROFILE TO DETERMINE LOCATION OF FLUID - AIR INTERFACE

Figure 21

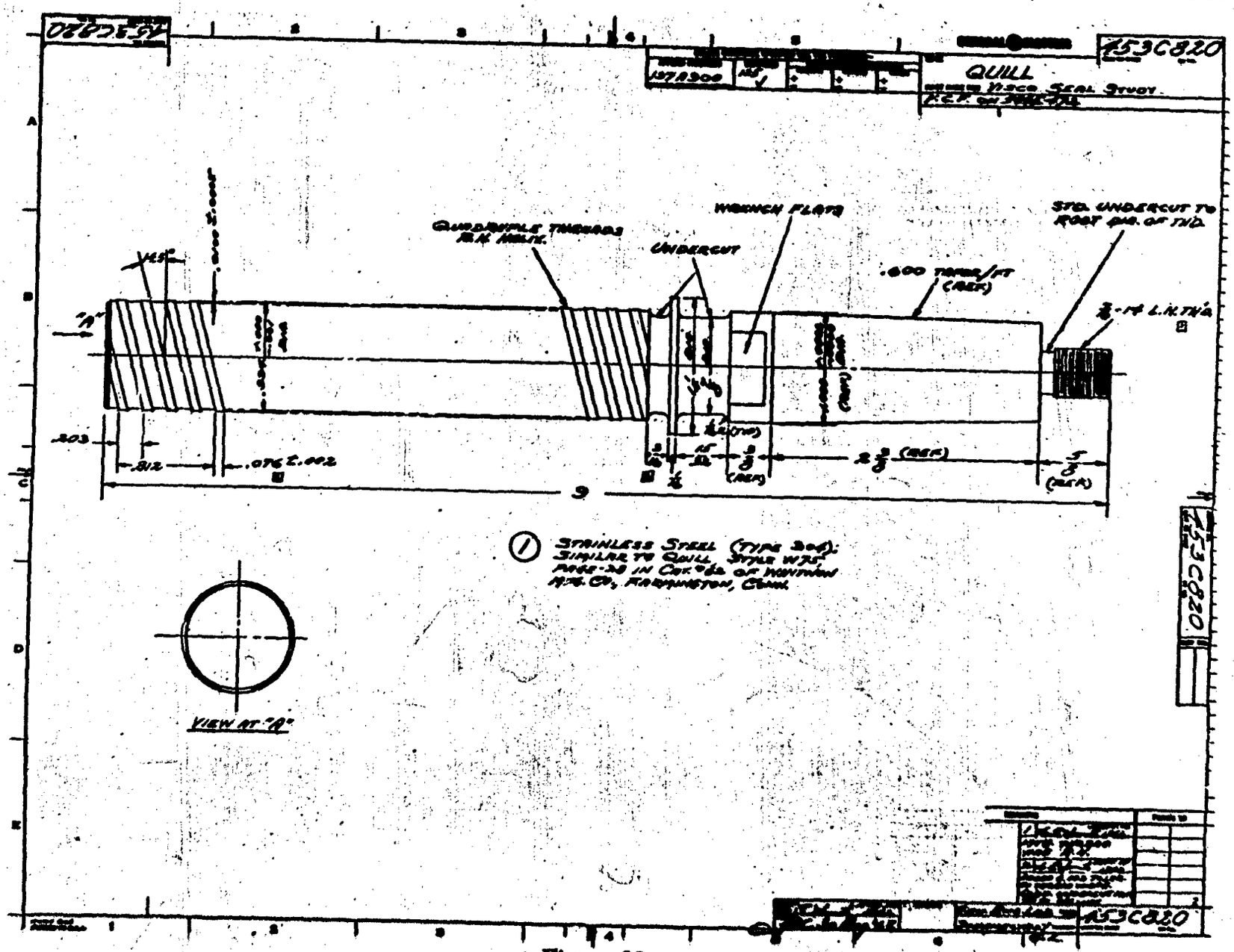

Figure 22

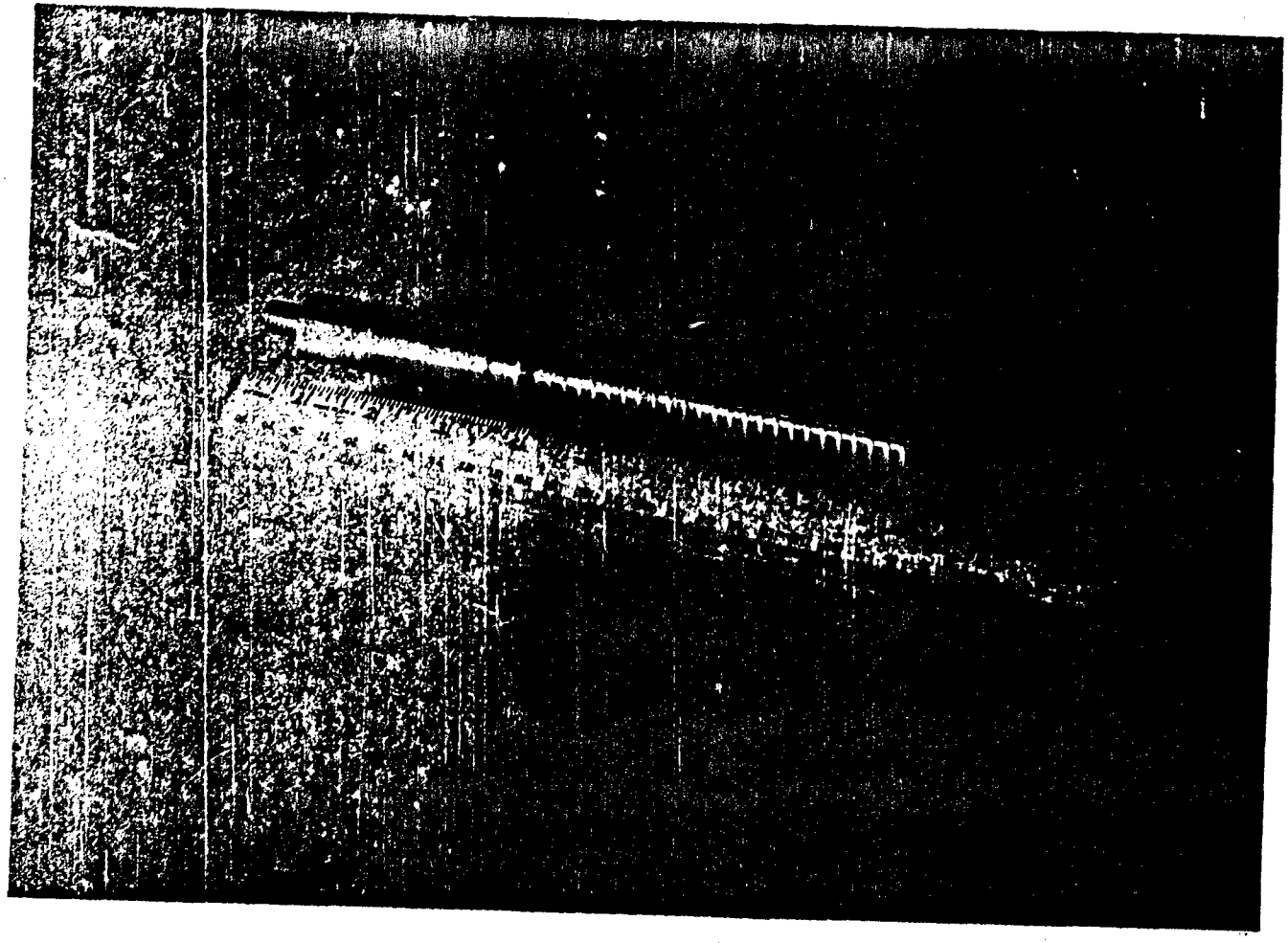

Figure 23. Picture of Test Quill

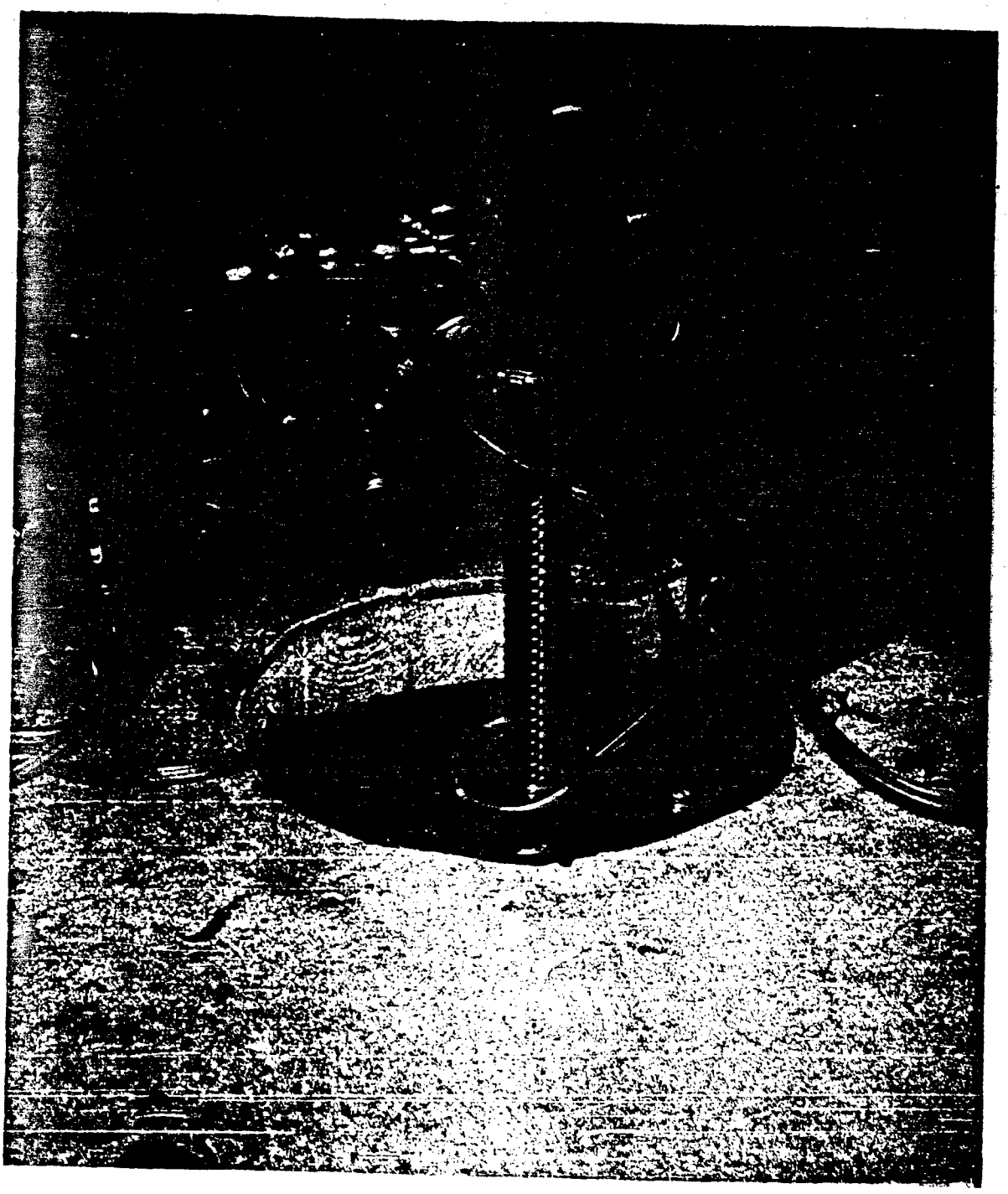

Figure 24. Picture of Screw Quill in Spindle

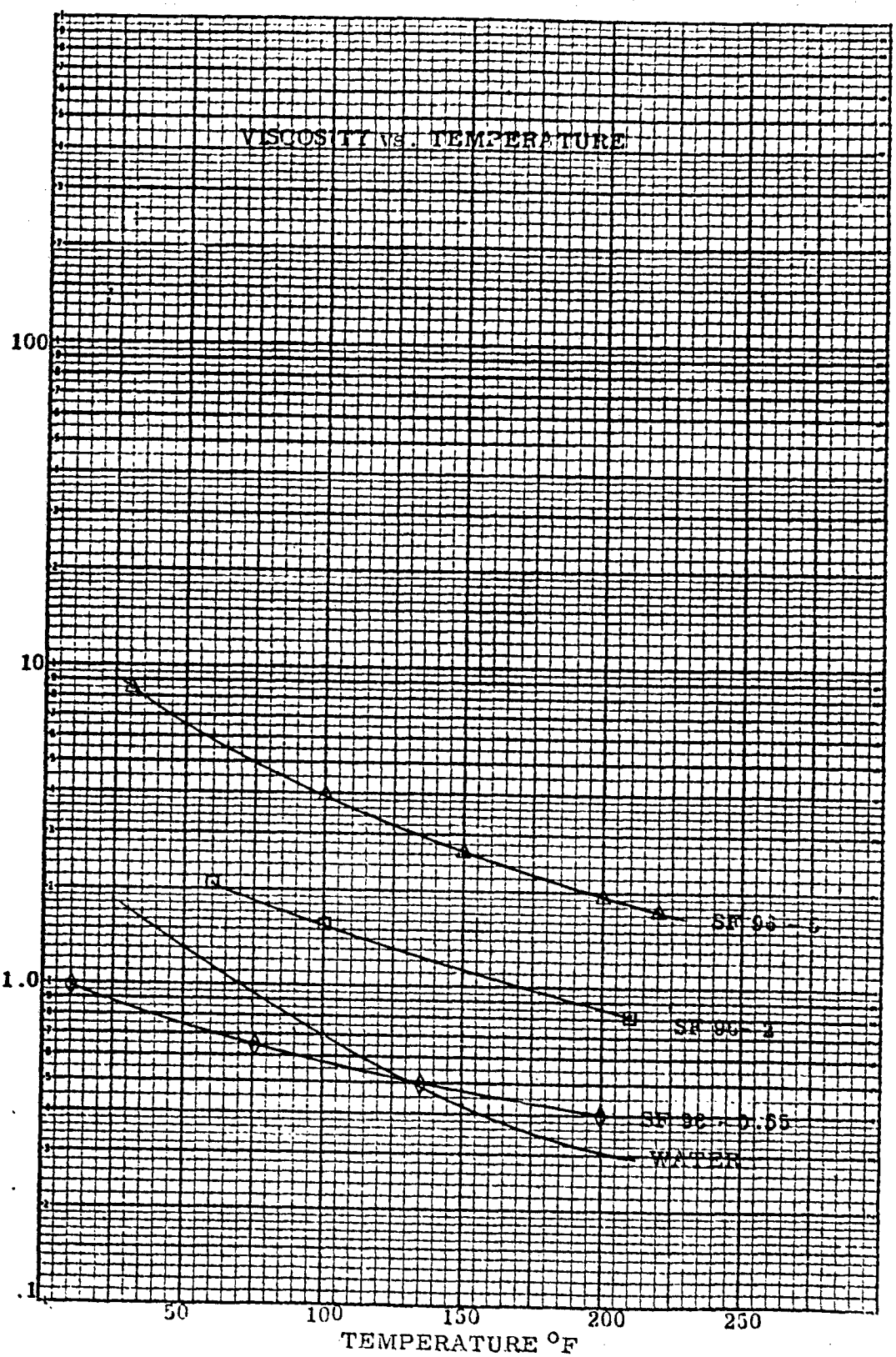
VISCOSITY vs. TEMPERATURE
VISCOSITY - CENTISTOKES
100
10
1.0
.1
50
100
150
200
250
TEMPERATURE °F
SF 96 - 5
SF 96 - 2
SF 96 - 0.65
WATER

Figure 25

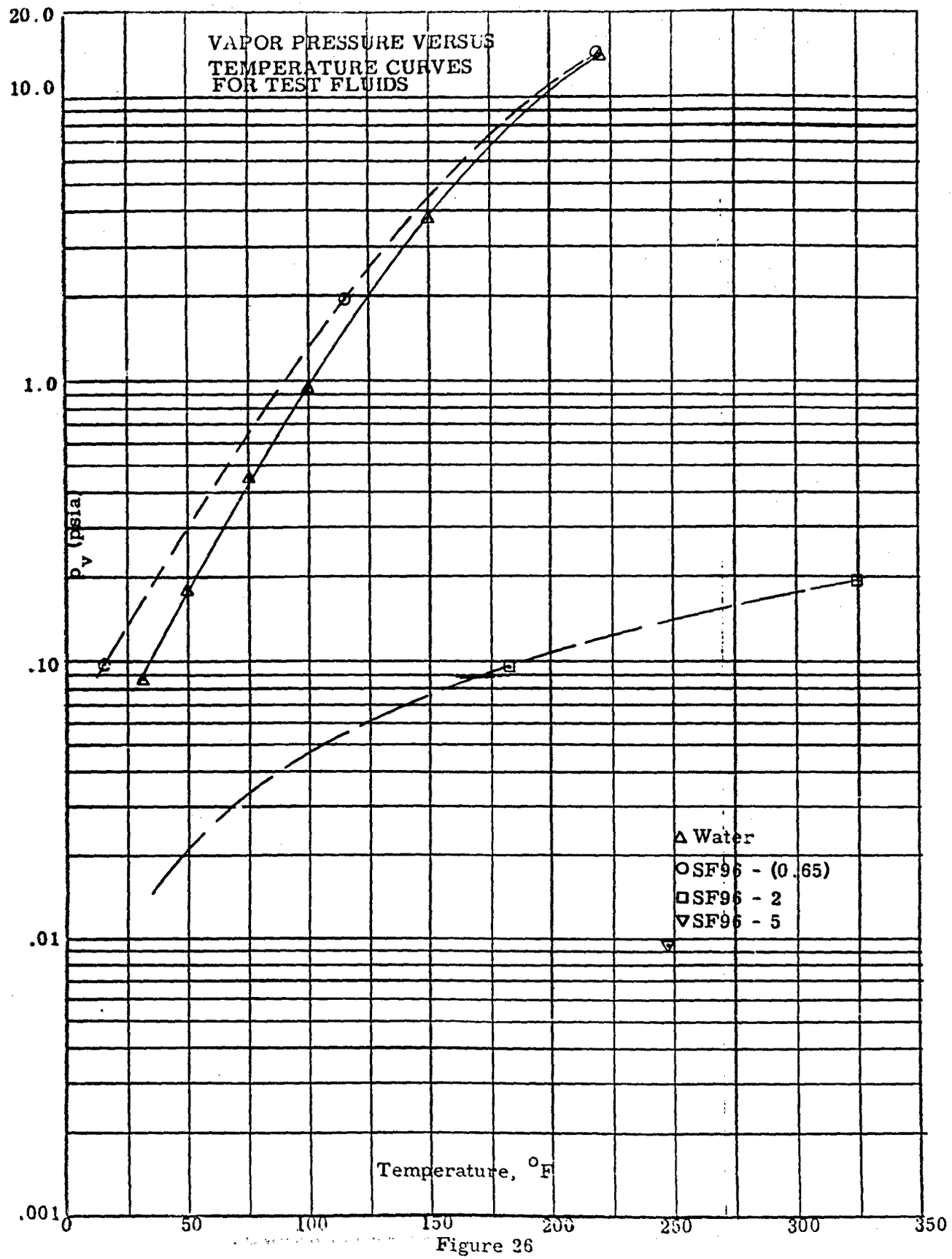
VAPOR PRESSURE VERSUS
TEMPERATURE CURVES
FOR TEST FLUIDS
20.0
10.0
1.0
.10
.01
.001
P_v (psia)
0
50
100
150
200
250
300
350
Temperature, °F
Water
SF96 - (0.65)
SF96 - 2
SF96 - 5

Figure 26

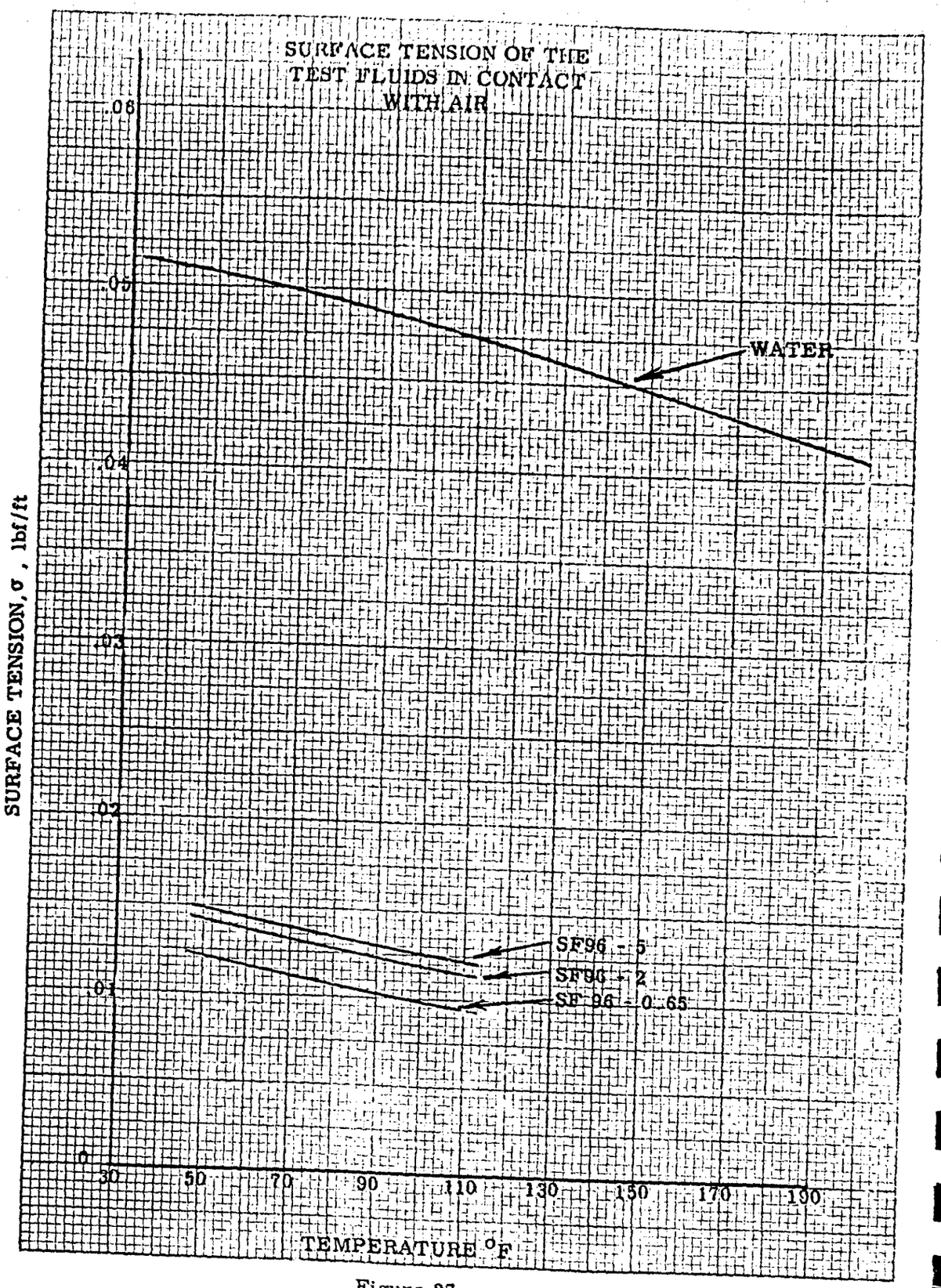

Figure 27

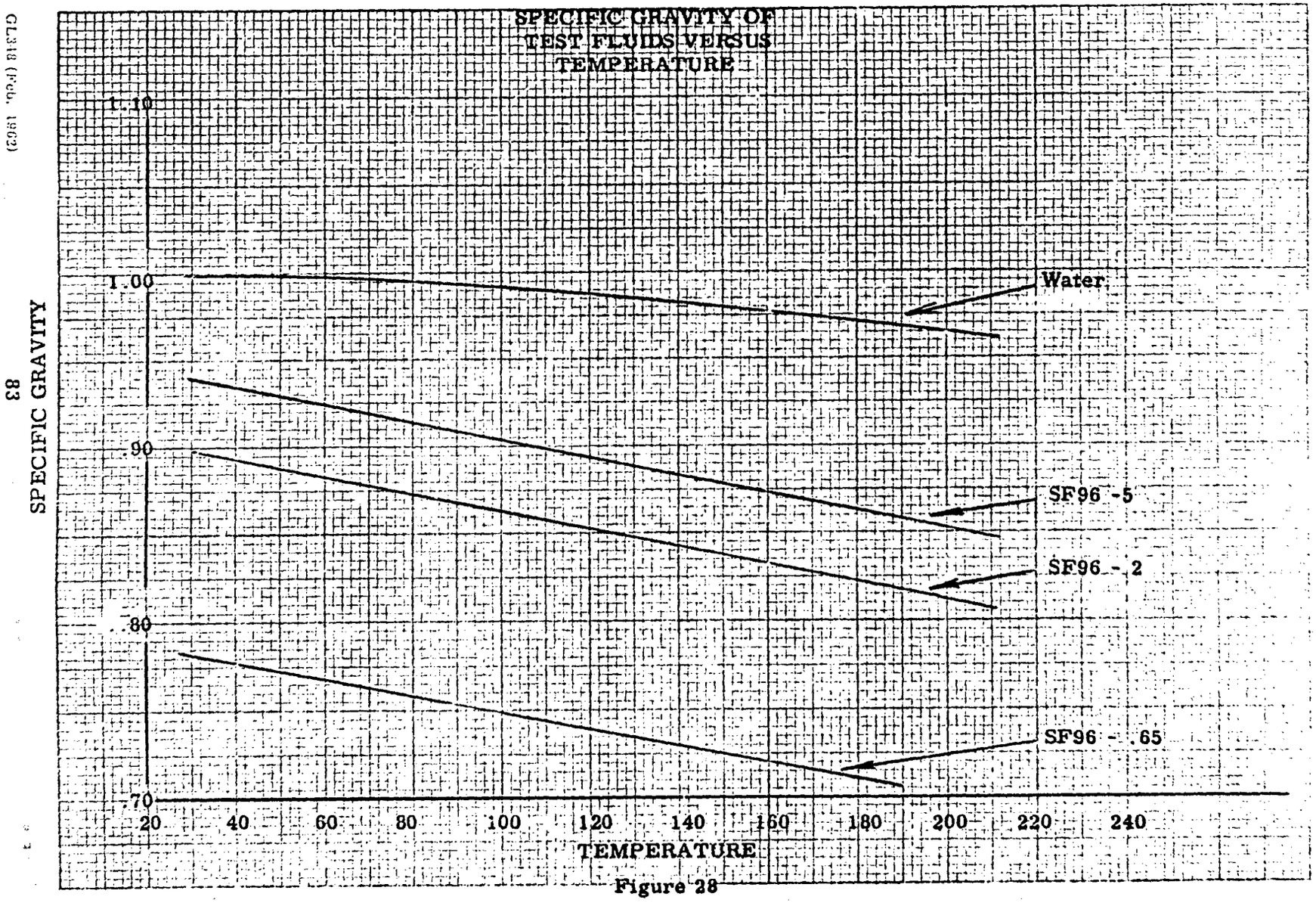

Figure 28

SUMMARY OF TEST RESULTS

Quill No. 1

Floating Sleeve h =.010

Test No.	Test Fluid	δ mils	N rpm	P psi	L in.	Measured Power h.p.
1-1	SF96-5	3.25	3980	15.05	2.86	----
1-2	SF96-5	3.25	4760	20.34	3.28	----
1-3	SF96-5	3.25	6240	25.74	3.15	----
1-4	SF96-5	3.25	4080	16.04	3.41	----
1-5	SF96-5	3.25	5660	20.54	2.90	----
1-6	SF96-5	3.25	5700	25.54	3.34	----
1-7	SF96-5	3.25	6940	30.54	3.18	----
1-8	SF96-0.65	3.50	4560	4.5	2.65	----
1-9	SF96-0.65	3.6	6680	6.54	3.0	-----
1-10	SF96-0.65	3.7	10360	10.24	2.70	-----
1-11	SF96-0.65	3.8	13460	13.14	2.60	-----
1-12	SF96-0.65	3.92	14940	15.44	2.50	-----
1-13	SF96-0.65	4.04	16560	18.24	2.48	-----
1-14	SF96-0.65	4.15	7080	6.14	3.20	-----
1-15	SF96-0.65	4.25	12160	10.44	2.61	-----
1-16	SF96-0.65	4.38	15400	15.64	2.57	-----
1-17	SF96-0.65	4.5	16840	20.44	2.70	-----
1-18	SF96-0.65	4.6	18760	22.94	2.57	-----
1-19	SF96-0.65	4.7	20420	25.64	2.65	-----

Figure 29

SUMMARY OF TEST RESULTS

Quill No. 1
Fixed Sleeve

δ = .0035 in.
h = .010 in.

Test No.	Test Fluid	N rpm	P psi	L in.	Measured Power h.p.
1-20	Distilled Water	5220	5.45	3.75	.0248
1-21	"	8560	10.05	2.80	.0405
1-22	"	11520	15.90	2.50	.0546
1-23	"	13600	20.55	2.42	.0645
1-24	"	15060	25.40	2.34	.0711
1-25	"	16340	30.40	2.31	.0775
1-26	"	6240	5.70	3.48	.0417
1-27	"	11780	15.65	2.51	.0906
1-28	"	17040	31.00	2.48	.114
1-29	"	17860	35.65	2.29	.111
1-30	"	19520	40.70	2.27	.141
1-31	"	20660	45.5	2.20	.159
1-32	"	21460	50.5	2.25	.166
1-33	"	23080	55.5	2.25	.189
1-34	"	24160	60.5	2.25	.197
1-35	"	27760	57.0	1.57	.227
1-36	"	29880	55.0	1.44	.244
1-37	"	31520	55.0	1.23	.257
1-38	"	18160	31.0	2.26	.140
1-39	"	5600	7.0	4.00	.0209

Figure 29 (cont'd)

SUMMARY OF TEST RESULTS

Quill No. 1

Fixed Sleeve δ = .0035 in.

h = .010 in.

Test No.	Test Fluid	N rpm	P psi	L in.	Measured Power h.p.
1-40	Distilled Water	16520	30.6	2.36	.0947
1-41	"	35000	56.8	1.21	.340
1-42	SF96-5	1360	5.3	4.00	.0087
1-43	"	3020	10.7	2.79	.0260
1-44	"	4520	15.5	2.53	.0441
1-45	"	6120	21.0	2.44	.0689
1-46	"	7780	26.0	2.37	.0877
1-47	"	9320	31.0	2.31	.1298
1-48	"	10700	36.1	2.28	.1490
1-49	"	11640	41.2	2.28	.1622
1-50	"	12700	46.2	2.27	.1881
1-51	"	13580	51.2	2.26	.2011
1-52	"	14320	55.8	2.24	.2122
1-53	"	15420	61.0	2.24	.2285
1-54	Distilled Water	5320	5.50	3.4	.0219
1-55	"	6580	6.42	3.22	.0174
1-56	"	7280	7.48	3.17	.0192
1-57	"	8240	8.48	2.96	.0218
1-58	"	8660	9.5	2.78	.0229
1-59	"	8680	10.3	2.70	.0293

Figure 29 (cont'd)

SUMMARY OF TEST RESULTS

Quill No. 1

Fixed Sleeve δ = .0035 in.

h = .010 in.

Test No.	Test Fluid	N rpm	P psi	L in.	Measured Power h.p.
1-60	Distilled Water	9520	11.8	2.63	.0321
1-61	"	10320	13.8	2.57	.0349
1-62	"	11132	15.9	2.49	.0376
1-63	"	12080	17.0	2.42	.0408
1-64	"	12840	20.4	2.39	.0434
1-65	"	13420	22.7	2.35	.0453
1-66	"	13880	25.5	2.34	.0574
1-67	"	14660	28.0	2.31	.0606
1-68	"	15220	30.4	2.30	.0629
1-69	"	16640	35.0	2.28	.0687
1-70	"	18060	39.9	2.25	.0745
1-71	"	19180	45.0	2.23	.0936
1-72	"	20440	50.3	2.20	.0845
1-73	"	22220	56.0	2.19	.1421
1-74	"	23080	60.4	2.17	.1294
1-75	"	31580	55.0	1.24	.2019
1-76	SF96-2	4680	5.4	3.62	.0214
1-77	"	5540	6.5	3.30	.0246
1-78	"	6340	7.3	3.20	.0281

Figure 29 (cont'd)

SUMMARY OF TEST RESULTS

Quill No. 1

Fixed Sleeve δ =.0035 in.

h =.010 in.

Test No.	Test Fluid	N rpm	P psi	L in.	Measured Power h.p.
1-79	SF96-2	7000	8.3	3.03	.0300
1-80	"	7700	9.3	2.89	.0330
1-81	"	8080	10.3	2.76	.0347
1-82	"	9060	12.1	2.67	.0389
1-83	"	9960	14.3	2.55	.0428
1-84	"	10620	16.4	2.49	.0456
1-85	"	11420	18.5	2.41	.0491
1-86	"	12240	20.5	2.39	.0528
1-87	"	12720	23.0	2.37	.0657
1-88	"	13480	25.5	2.35	.0756
1-89	"	14080	28.0	2.34	.0790
1-90	"	14620	30.5	2.32	.0820
1-91	"	16080	35.4	2.29	.0920
1-92	"	17040	40.3	2.27	.1032
1-93	"	18320	45.7	2.26	.1171
1-94	"	19080	50.5	2.25	.1496
1-95	"	20200	55.0	2.23	.1737
1-96	"	21140	60.3	2.21	.1817
1-97	"	31940	60.4	1.22	.2993

Figure 29 (cont'd)

SUMMARY OF TEST RESULTS

Quill No. 1

Fixed Sleeve δ = .0035 in.

h = .010 in.

Test No.	Test Fluid	N rpm	P psi	L in.	Measured Power h.p.
1-98	SF96-5	1940	5.6	3.6	.008
1-99	"	2420	6.0	3.42	.0112
1-100	"	2800	7.3	3.21	.0148
1-101	"	3640	8.6	3.02	.0192
1-102	"	4020	9.1	2.90	.0212
1-103	"	4420	10.5	2.77	.0234
1-104	"	5180	12.5	2.64	.0234
1-105	"	5400	14.4	2.59	.0382
1-106	"	5800	16.2	2.50	.0444
1-107	"	6200	18.5	2.48	.0474
1-108	"	6600	20.6	2.45	.0804
1-109	"	7080	22.6	2.43	.0628
1-110	"	7840	25.4	2.40	.0696
1-111	"	8820	28.0	2.38	.0886
1-112	"	9420	30.5	2.35	.0998
1-113	"	10840	35.5	2.34	.1148
1-114	"	12020	40.5	2.29	.1248
1-115	"	13040	45.5	2.28	.1696
1-116	"	14060	50.2	2.27	.2002

Figure 29 (cont'd)

SUMMARY OF TEST RESULTS

Quill No. 1

Fixed Sleeve δ =.0035 in.

h =.010 in.

Test No.	Test Fluid	N rpm	P psi	L in.	Measured Power h.p.
1-117	SF96-5	15500	55.5	2.26	.2206
1-118	"	16660	60.5	2.25	.2272
1-119	Distilled Water	5400	5.6	3.67	.0127
1-120	"	8660	10.5	2.82	.0229
1-121	"	10840	15.3	2.58	.0317
1-122	"	13020	19.8	2.40	.0380
1-123	"	14180	24.5	2.37	.0500
1-124	"	15860	29.2	2.32	.0654
1-125	"	17380	34.1	2.26	.1080
1-126	"	20060	44.2	2.28	.1427
1-127	"	23640	56.0	2.23	.2314
1-128	"	32020	47.4	3.32	.3224
1-131	SF 96-5	8380	19.9	2.44	.0769
1-132	"	7160	14.6	2.25	.0561
1-133	"	3480	10.0	2.77	.0159
1-134	"	1380	4.9	3.95	.0048
1-135	"	3540	10.3	2.82	.0130
1-136	"	5540	15.5	2.66	.0253
1-137	"	7020	15.6	2.31	.0374

Figure 29

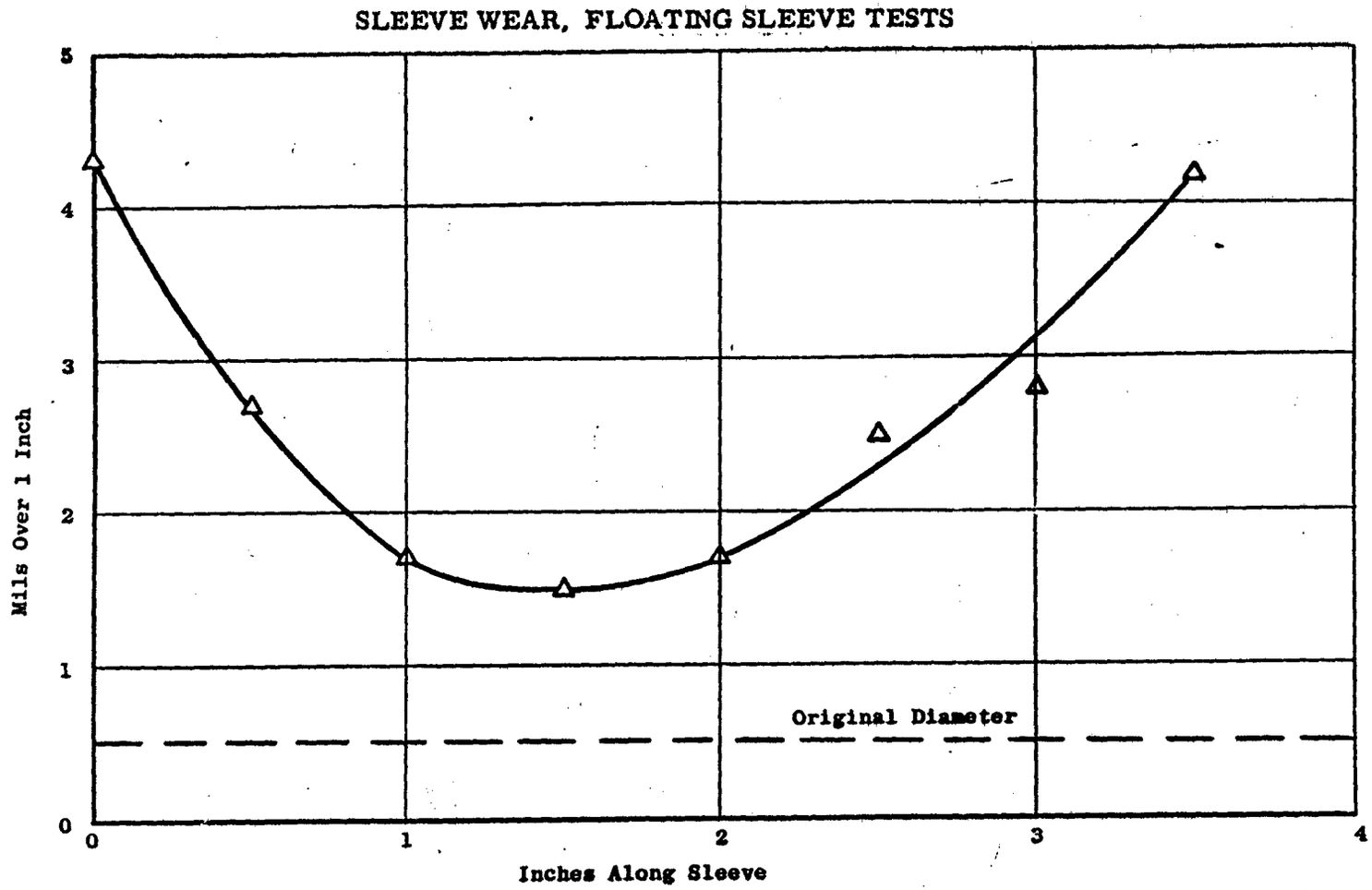

Figure 30, Screw Seal Wear.

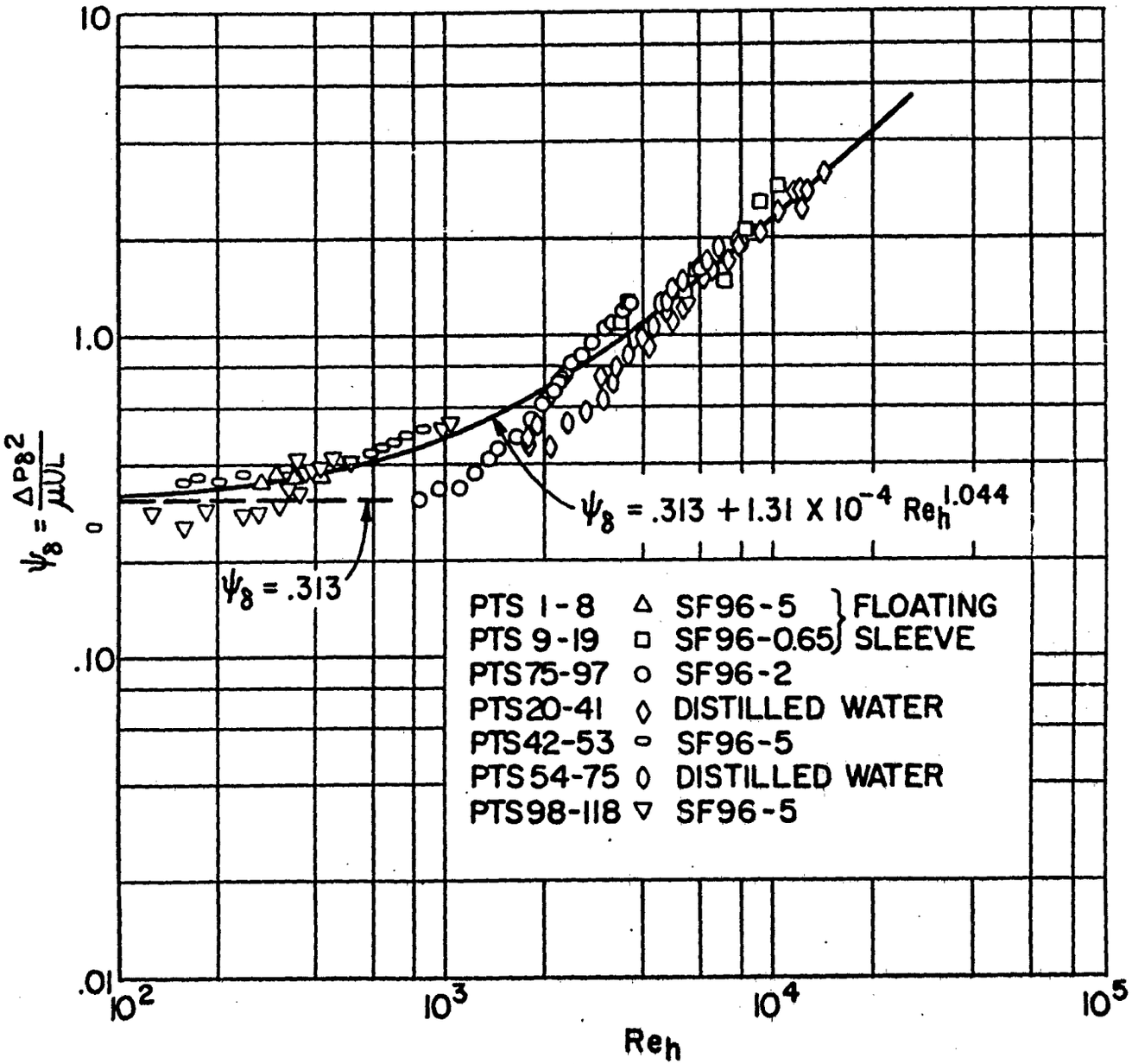

Figure 31

Sealing Coefficient Versus Reynolds Number

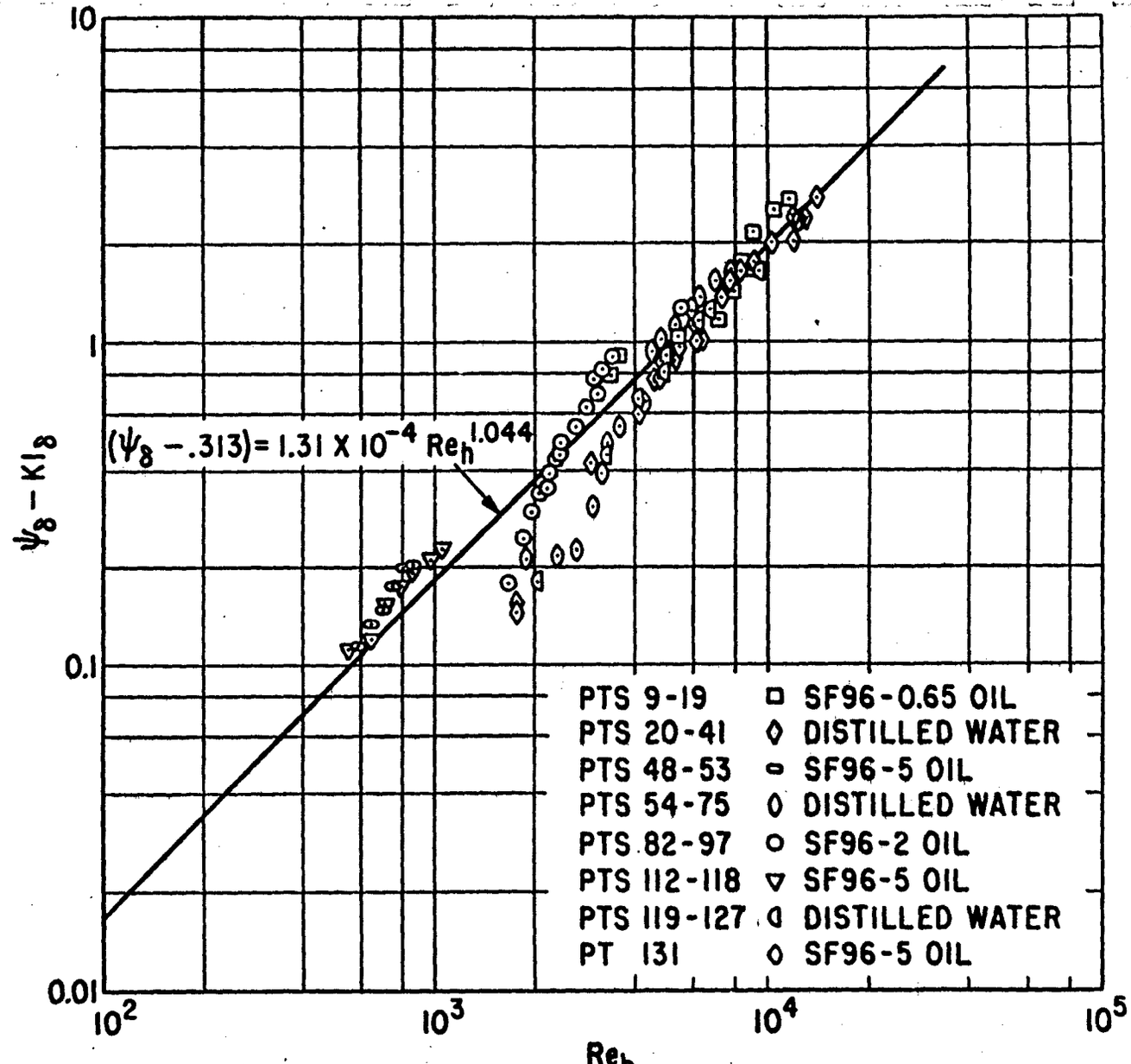

Figure 32

$\psi_\delta - K_{1_\delta}$ Versus Re_h

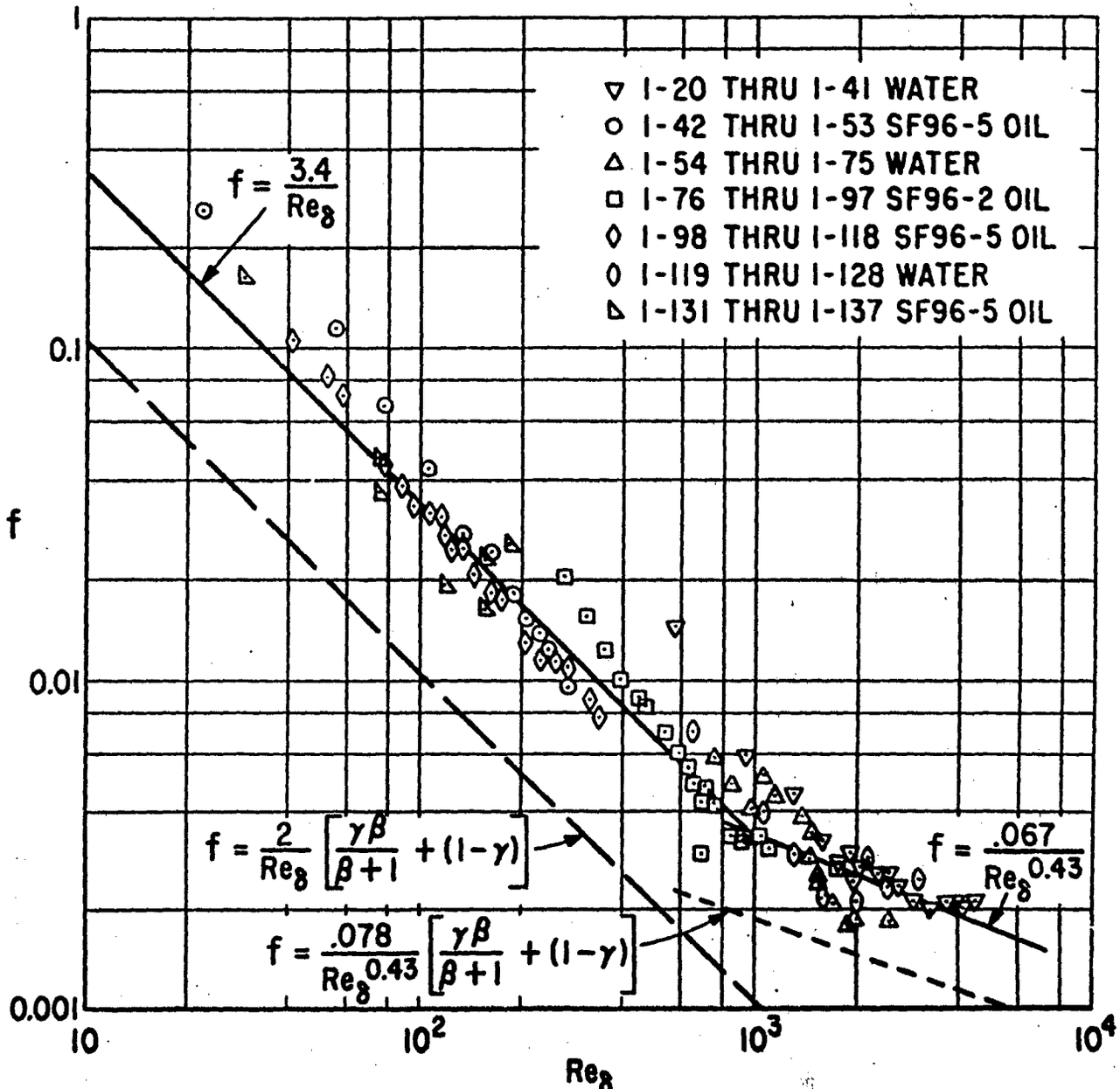

Figure 33

Friction Factor Versus Reynolds Number

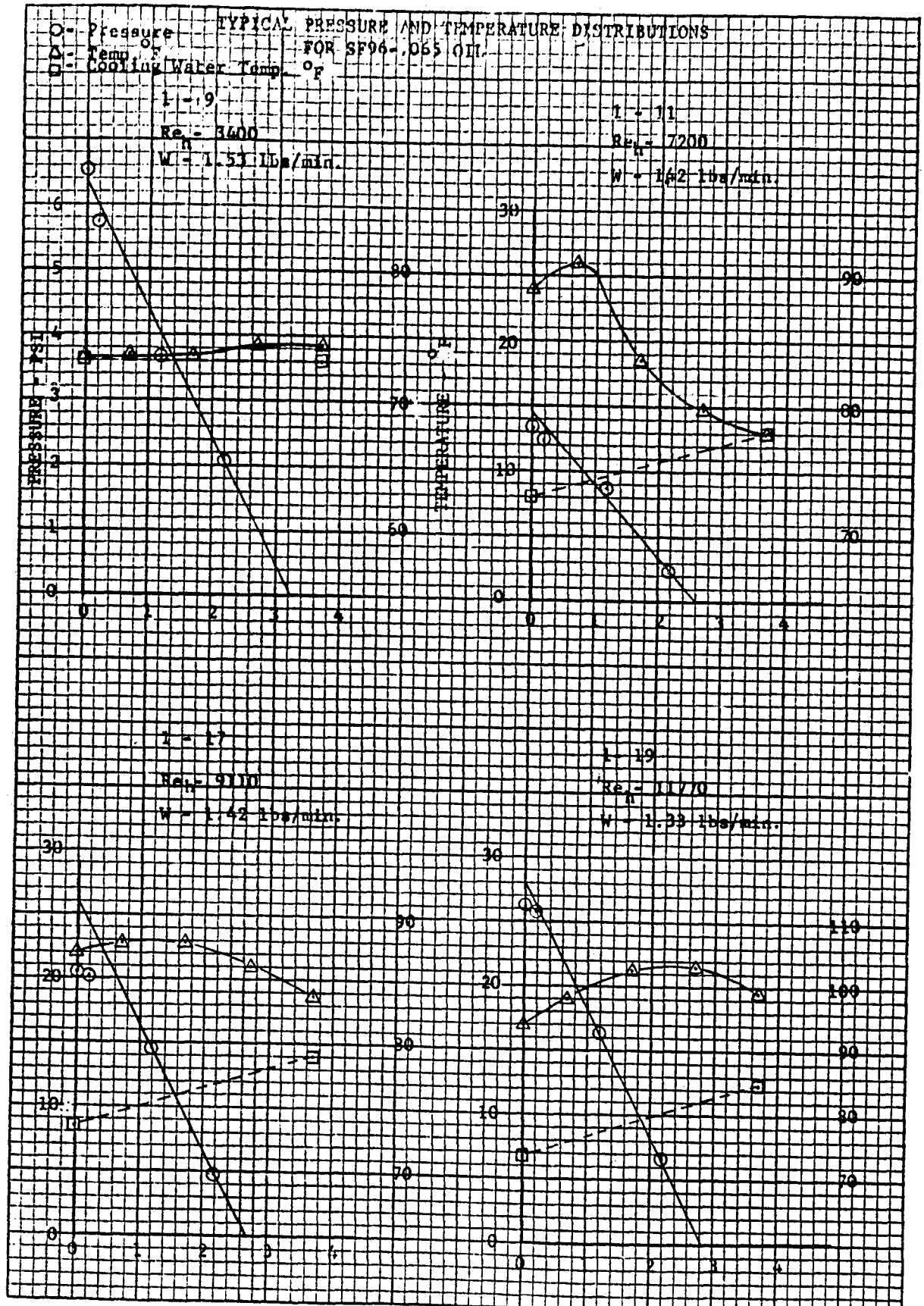
TYPICAL PRESSURE AND TEMPERATURE DISTRIBUTIONS FOR SF96-.065 OIL
O- Pressure
Δ- Temp. °F
□- Cooling Water Temp. °F
1 - 9
Re_h - 3400
W - 1.53 lbs/min.
1 - 11
Re_h - 7200
W - 1.42 lbs/min.
1 - 17
Re_h - 9110
W - 1.42 lbs/min.
1 - 19
Re_h - 11770
W - 1.33 lbs/min.
PRESSURE - PSI
TEMPERATURE °F

Figure 34

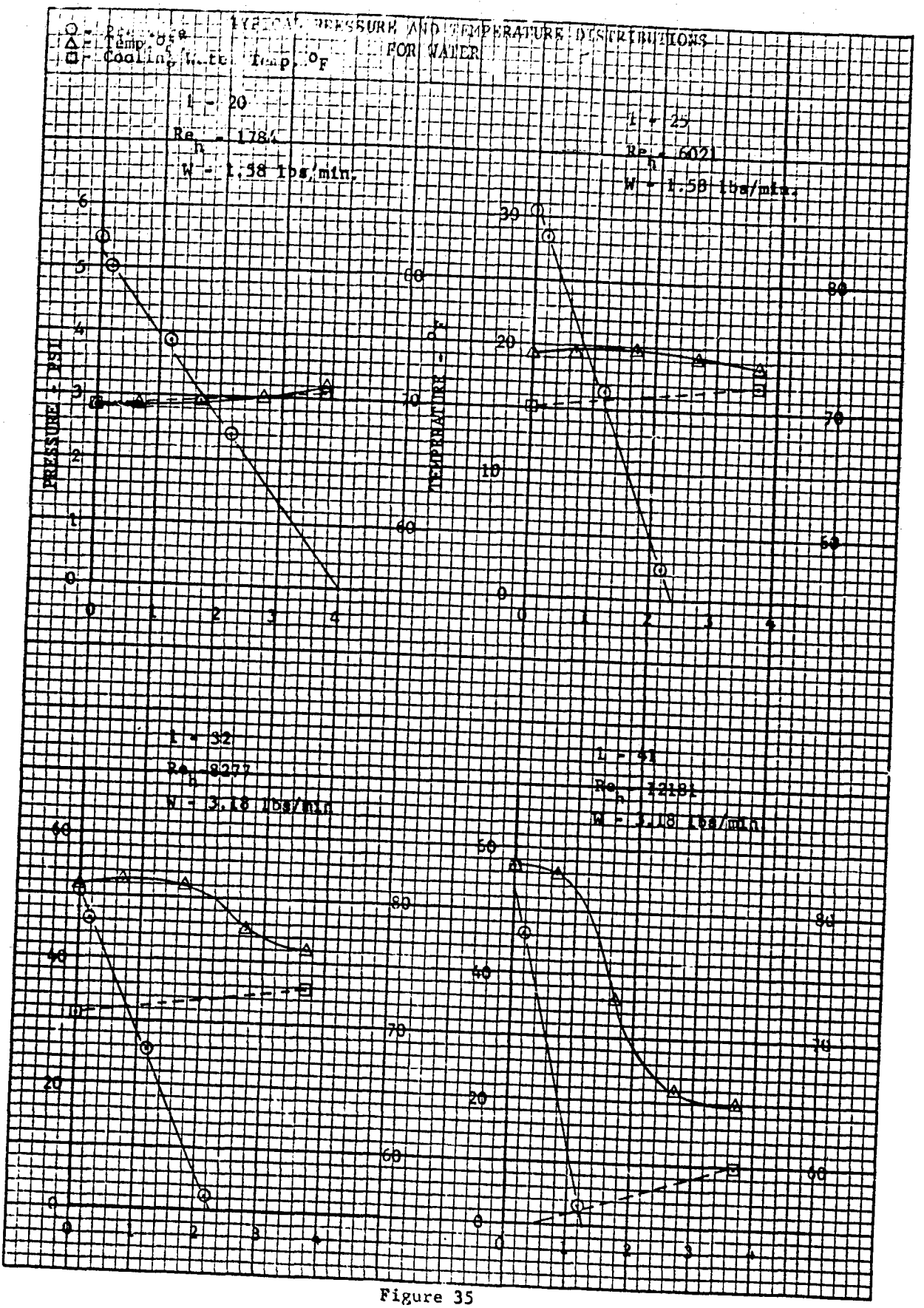
AXIAL PRESSURE AND TEMPERATURE DISTRIBUTIONS FOR WATER
○ - Pressure
△ - Temp. of
□ - Cooling Water Temp, °F
L = 20
Re_h = 1784
W = 1.58 lbs/min.
L = 25
Re_h = 6021
W = 1.58 lbs/min.
L = 32
Re_h = 8277
W = 3.18 lbs/min
L = 41
Re_h = 12181
W = 3.18 lbs/min
PRESSURE - PSI
TEMPERATURE - °F

Figure 35

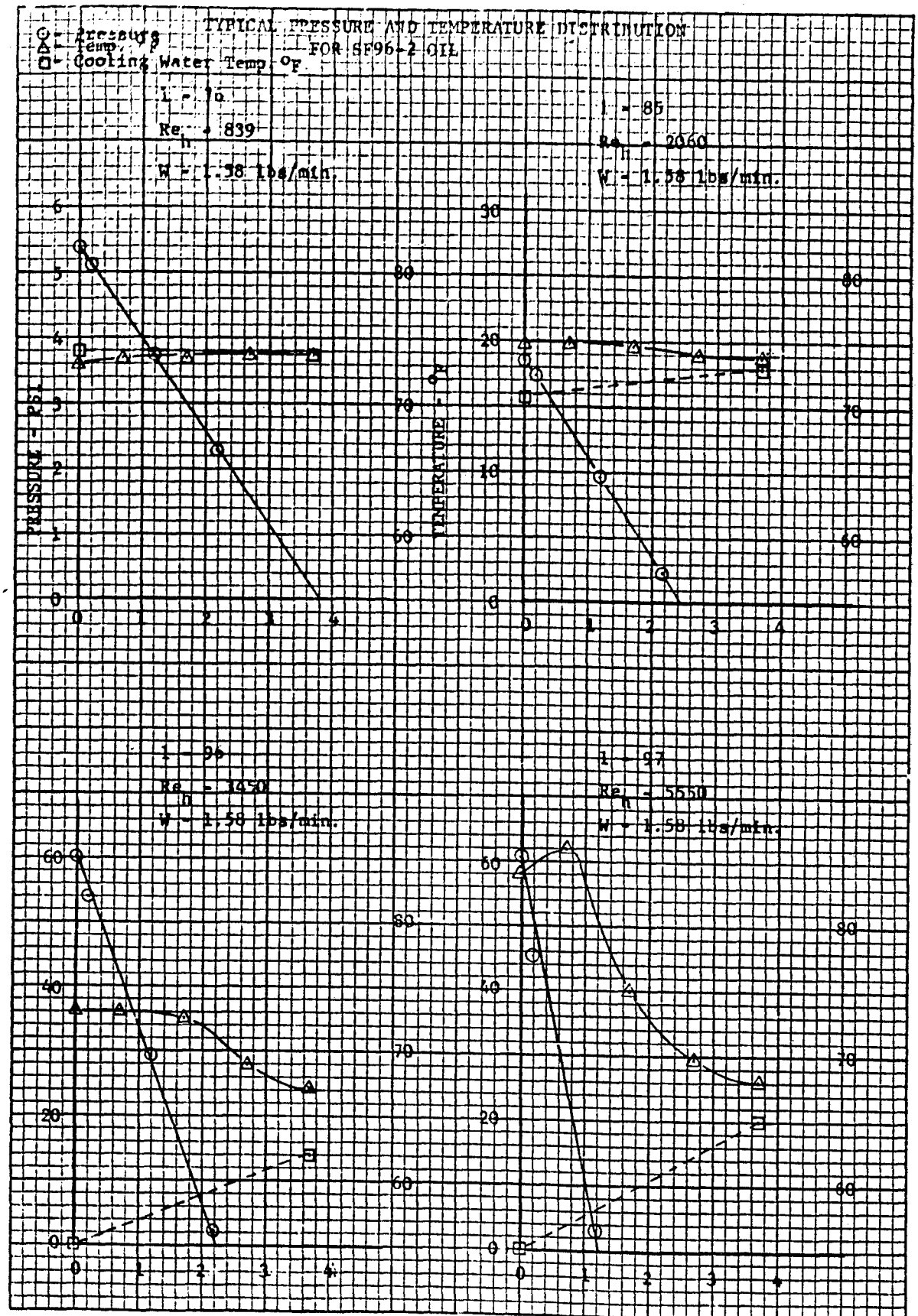
TYPICAL PRESSURE AND TEMPERATURE DISTRIBUTION
FOR SF96-2 OIL
○- Pressure
△- Temp.
□- Cooling Water Temp. °F
PRESSURE - PSI
TEMPERATURE - °F
L - 76
Re_h - 839
W - 1.58 lbs/min.
L - 85
Re_h - 2060
W - 1.58 lbs/min.
L - 96
Re_h - 3450
W - 1.58 lbs/min.
L - 97
Re_h - 5550
W - 1.58 lbs/min.

Figure 36

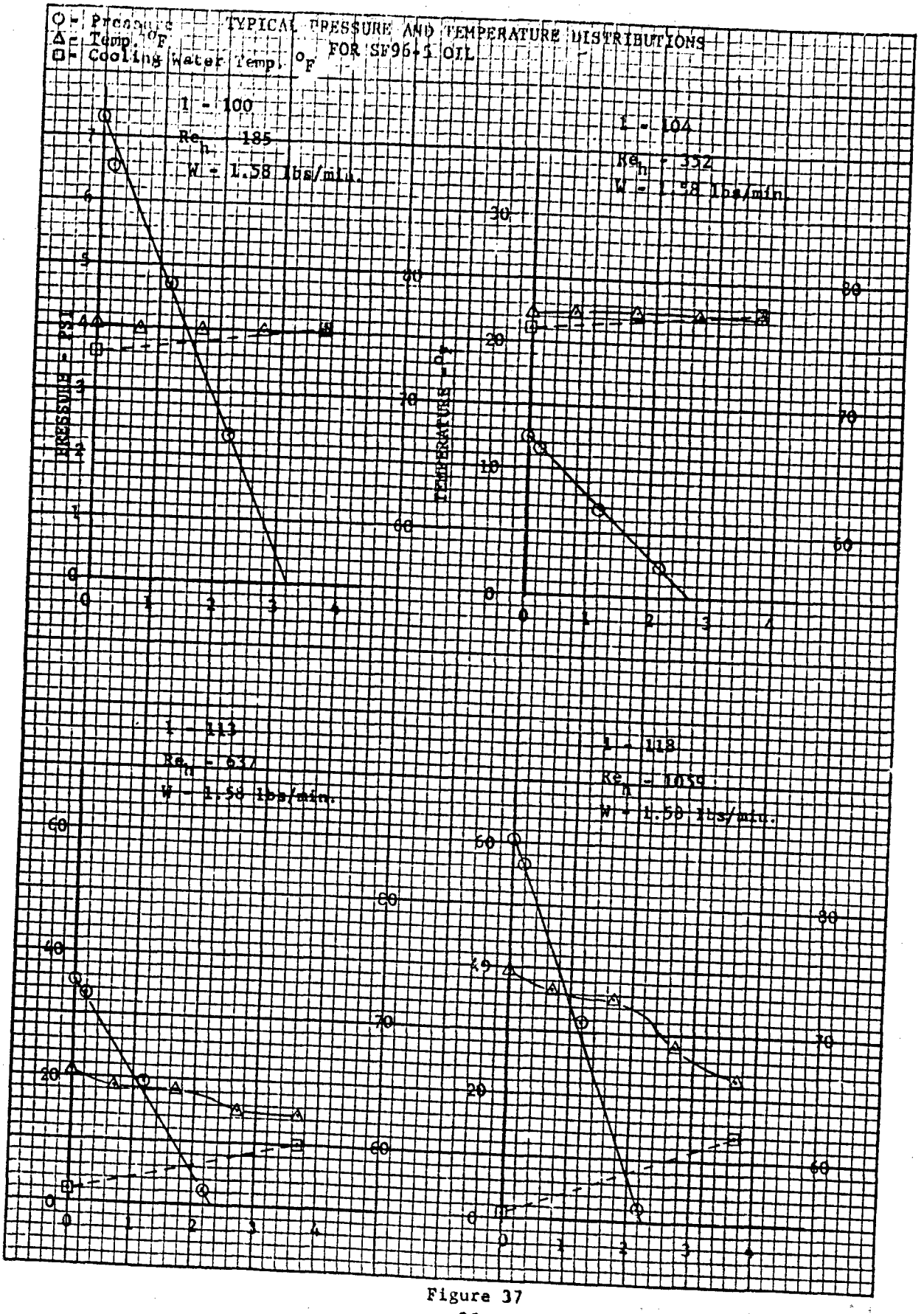
TYPICAL PRESSURE AND TEMPERATURE DISTRIBUTIONS FOR SF96-5 OIL
○ - Pressure, PSIG
△ - Temp. °F
□ - Cooling water temp. °F
1 - 100
Re_h - 185
W - 1.58 lbs/min.
1 - 104
Re_h - 352
W - 1.58 lbs/min.
1 - 113
Re_h - 637
W - 1.58 lbs/min.
1 - 118
Re_h - 1059
W - 1.58 lbs/min.
PRESSURE - PSIG
TEMPERATURE - °F

Figure 37

DISTRIBUTION LIST

Copies	Organization
1	ASD (ASRCNL-2, Mr. John Morris) Wright Patterson AFB, Ohio
1	ASD (ASNPFS-3, Mr. R. Ling) Wright Patterson AFB, Ohio
1	ASD (ASRCNL, Mr. G. A. Beane) Wright Patterson AFB, Ohio
2	ASD (ASRMFP-3, Mr. R. J. Smith) Wright Patterson AFB, Ohio
1	U.S. Atomic Energy Commission Office of Technical Information P.O. Box 62 Oak Ridge, Tennessee
1	Thompson Ramo Wooldridge Attn: Mr. Carl Nau 23555 Euclid Avenue Cleveland 17, Ohio
1	Rocketdyne Division North American Aviation Attn: Mr. R.B. Dillaway Department 584 6633 Canoga Park Boulevard Canoga Park, California
1	Technical Information Center Aerospace Corporation P.O. Box 95085 Los Angeles 45, California
11	ASTIA Arlington Hall Station Arlington 12, Virginia
1	Cleveland Graphite Bronze Division of Clevite Corporation Attn: Mr. E. James Vargo 17000 St. Clair Avenue Cleveland 10, Ohio

1 Battelle Memorial Institute
Attn: Mr. C. M. Allen
Columbus 10, Ohio

1 SSD (SSTRE, Capt. W. W. Hoover)
AF Unit Post Office
Los Angeles 45, California

1 Power Information Center
Moore School Building
200 South 33rd Street
Philadelphia 4, Pennsylvania

1 National Aeronautics and Space Administration
Lewis Research Center
Attn: Mr. Joseph Joyce
Space Electric Power Office
25000 Brookpark Road
Cleveland 35, Ohio

1 AiResearch Manufacturing Company
Attn: Mr. John Dennan
402 - 536th Street
Phoenix 34, Arizona

1 Sundstrand Aviation Corporation
Attn: Mr. K. Nichols
2480 West 70
Denver 21, Colorado

1 Aerojet - General Nucleonics
Attn: Mr. Paul Wood
Azusa, California

1 Pratt and Whitney Aircraft
Division of United Aircraft Corporation
Attn: Mr. Frederick A. Corwin
East Hartford, Connecticut

1 Mechanical Technology, Inc.
Attn: Mr. F. K. Orcutt
Albany Shaker Road
Latham, New York